



Analysis and development of a heat pump with air-to-air heat recovery system

António José Camossa Mendes Rebelo Barbosa

Supervisor at FEUP: Carlos Pinho

Supervisor at Bosch: Fernando Dias

Integrated Master in Mechanical Engineering

Faculty of Engineering of University of Porto

Porto, June 2018

[Blank Page]

“Coming together is a beginning, staying together is
progress, working together is success.”

Henry Ford

[Blank Page]

Abstract

The development of efficient solutions that ensure the quality of life of society, as well as the preservation of natural resources and low energy consumption is a challenge almost without comparison nowadays. Thus, with this project, it is expected to follow the main steps of the analysis and development of a compact solution that combines a heat recovery system and an air-to-air heat pump to ensure the mechanical ventilation within a residential using. The main variables that influence this solution are discussed in order to turn possible the modelling of the overall system, in which two ways of transferring heat are discussed: only sensible and both sensible and latent heats, and the main conclusions are presented. All the components are evaluated by applying several heat and mass transfer concepts and the overall system is analysed. The possibility of frost formation is also a phenomenon to take into account when an air-source heat pump is developed, its occurrence is studied and several measures are proposed in order to avoid it in the critical operation points. A functional sample is assembled, all the relevant steps are defined to evaluate the solution and the quality of the experimental results is analysed by doing an uncertainty analysis. This project was carried out in an industrial environment at Bosch Thermotechnology S.A. in Aveiro in the scope of the research and development of residential heat pumps.

Resumo

O desenvolvimento de soluções eficientes que garantam o bem-estar da sociedade, bem como a preservação de recursos naturais e baixo consumo energético é um desafio dificilmente equiparável na atualidade. Deste modo, neste trabalho é proposta a análise e desenvolvimento de uma solução compacta que combine um sistema de recuperação de calor incorporado na ventilação mecânica de uma habitação em conjunto com uma bomba de calor ar-ar. As principais variáveis que influenciam este processo são discutidas, de modo a sustentar o trabalho realizado e a permitir a posterior modelação global do sistema. Duas formas de recuperação de calor são discutidas: unicamente sensível e simultaneamente sensível e latente, e as principais vantagens e desvantagens de ambas as variantes são analisadas. Todos os componentes são avaliados através de conceitos de transferência de calor e de massa, quando aplicável, e o sistema é avaliado de uma forma global. A possibilidade de formação de gelo é também um fenómeno a ter em conta no desenvolvimento de bombas de calor que tenham ar como fonte de calor, a sua ocorrência é estudada e são propostas medidas para a evitar nos períodos críticos de utilização. Uma amostra funcional é montada e são realizadas as devidas medições de forma a avaliar a solução, sendo que é também realizada uma análise de incertezas de modo a avaliar os resultados obtidos experimentalmente. O trabalho é realizado nas instalações da Bosch Termotecnologia S.A. em Aveiro e inserido no âmbito da investigação e desenvolvimento de bombas de calor para a utilização no setor residencial.

Acknowledgments

I would like to express my gratitude to the people, who had a relevant impact for the achievement of this dissertation that represents an important step of my academic path.

In a first place, to my family, especially to my parents, Susana and Pedro, grandparents, Maria Elisa and José Luís, and brothers, Pedro and Mariana, who are the most responsible for the person I am and helped me to maintain a positive attitude to achieve my objectives. It is not possible to forget also the contribution of my uncles and cousins, who were available in the important moments.

To Gonçalo for the incredible positive memories and the power transmitted whenever he is reminded.

To my girlfriend Rita for her unconditional support, for all negative and positive shared moments during this important path in my life and for the affection transmitted during the last years.

A word of appreciation to Carlos Pinho, who accepted the coordination of the project at FEUP, for his dedication, the important contribute in this project from the beginning and all the support and the availability to discuss about the relevant subjects.

A special thanks to my colleagues at Bosch Thermotechnology in Aveiro for all contribution in my work, especially the continuous follow up by Eernando Dias and the important help with refrigerant circuit by Fábio Pereira, as well as the support of Pedro Moreira, Henrique Pinto, Pedro Assis and Ricardo Freitas, who were all the time opened to discuss and to help with any relevant subject to this project. The constructive discussions with Werner Hube, the personal support by David Pinho and the good environment created by all the team were very important to conclude this project.

To my old friends in Porto and the friendships developed at FEUP, who were all crucial for my personal and academic development.

To my all my Professors at FEUP, for all knowledge transmitted during the last years during the Integrated Master in Mechanical Engineering.

Index of Contents

1	Introduction	1
1.1	Bosch Thermotechnology S.A	1
1.2	Motivation	3
1.3	Objectives.....	7
1.4	Dissertation Outline.....	7
2	Literature Review	9
2.1	Heat Pump	9
2.1.1	Vapour Compression Cycle	9
2.1.2	Components	12
2.1.3	Refrigerant	16
2.1.4	Bosch Air-source Heat Pumps.....	18
2.2	Benchmark	19
2.3	Air-to-air Heat Exchangers	21
2.3.1	Heat Recovery Ventilation.....	24
2.3.2	Energy Recovery Ventilation.....	26
3	System Modelling.....	31
3.1	Functional Diagram.....	31
3.2	Technical Requirements and Specifications	32
3.3	Modelling	33
3.3.1	Membrane Based Enthalpy Exchanger.....	33
3.3.2	Evaporator.....	40
3.3.3	Condenser	47
3.3.4	Compressor	49
3.4	User Interface	50
4	Simulation and Results	52

4.1	Heat Recovery System	53
4.1.1	Heat Exchanger	53
4.1.2	Enthalpy Exchanger	56
4.2	Air-to-Refrigerant Heat Exchangers	60
4.2.1	Evaporator	60
4.2.2	Condenser	62
4.3	Compressor.....	64
4.4	Overall Solution	65
4.4.1	Heat Recovery Ventilation.....	67
4.4.2	Energy Recovery Ventilation.....	77
4.4.3	Comparison.....	87
5	Experimental Analysis.....	90
5.1	Piping/Ducting and Instrumentation Diagram	91
5.2	Climate Chamber.....	92
5.3	Measurement Devices	93
5.3.1	Temperature	93
5.3.2	Air Volume Flow Rate.....	95
5.4	Functional Sample.....	97
5.5	Refrigerant Charge	100
5.6	Test Points	102
5.7	Test Results	104
5.7.1	Refrigerant Charge and Insulation Analysis	104
5.7.2	Results Analysis.....	106
6	Conclusions and Future Work	110
6.1	Conclusions	110
6.2	Future Work	113
7	References	115

Appendix A	119
Appendix B.....	122
Appendix C.....	129

Index of Figures

Figure 1.1 – Total research and development costs [2].	1
Figure 1.2 – Entrance building of Bosch Thermotechnology S.A. in Aveiro.	2
Figure 1.3 – Most representative brands of Bosch Thermotechnology division [1].	3
Figure 1.4 - Distribution of final energy consumption (EU-28, 2015), based on tonnes of oil equivalent (%). Adapted from IEA [4].	4
Figure 1.5 – Final energy consumption in the residential sector by type of end-use (EU-28,2015). Adapted from IEA [4].	4
Figure 1.6 – Final energy consumption by type of end-use for the main energy products (EU-28,2015). Adapted from IEA [4].	5
Figure 1.7 – Consequences of humidity levels outside the optimum zone [6].	6
Figure 2.1 – Schematic representation of a heat pump circuit [10].	10
Figure 2.2 – Heat pump cycle representation in pressure-enthalpy diagram (Adapted from EES).	10
Figure 2.3 - Heat pump cycle representation in temperature-entropy diagram (Adapted from EES).	11
Figure 2.4 – Rolling-piston rotary compressor [10].	13
Figure 2.5 – Finned tube heat exchanger [13].	14
Figure 2.6 – Evolution of condensation and evaporation temperatures [13].	14
Figure 2.7 – Thermostatic expansion valve working with external pressure equalizer [9].	15
Figure 2.8 – Variation of saturation pressure with temperature.	17
Figure 2.9 - System solution for heating mode (Adapted from Nilan catalogue [20]).	20
Figure 2.10 – System solution for cooling mode (adapted from Nilan catalogue [20]).	20
Figure 2.11 – Principle solution of using air-to-air heat exchangers together with the air handling unit.	22
Figure 2.12 – Schematic representation of a heat exchanger.	22
Figure 2.13 – Representation of psychrometric evolution by passing through enthalpy exchanger (Adapted from ASHRAE [6]).	23

Figure 2.14 – Fixed plate heat exchanger (Adapted from ASHRAE Handbook) [6].	25
Figure 2.15 – Schematic representation of enthalpy exchanger during winter season.	27
Figure 2.16 – Schematic representation of enthalpy exchanger during summer season.	27
Figure 2.17 – Different transfer phenomena and barriers in MBEE [23].	28
Figure 2.18 – Energy wheel [14].	28
Figure 3.1 – Functional diagram of the solution.	31
Figure 3.2 – Representation of the flow arrangements in the heat exchanger.	34
Figure 3.3 – A schematic of heat-mass transfer analogy in a MBEE [25].	34
Figure 3.4 – Air flow over staggered tube arrangement [13].	41
Figure 3.5 – Staggered tube arrangement parameters [13].	41
Figure 3.6 – Adiabatic zones [28].	44
Figure 3.7 – User interface (input variables).	50
Figure 3.8 – User interface (output variables).	51
Figure 4.1 – Schematic representation of the main dimensions of the heat exchanger.	54
Figure 4.2 – Representation of a unity cell.	54
Figure 4.3 – Effectiveness as a function of volume flow rate in heat exchanger.	55
Figure 4.4 – Air Temperature at the outlet of heat recovery system as a function of outdoor air temperature and air volume flow rate [m^3/h].	56
Figure 4.5 – Dimensionless water content as a function of relative humidity	57
Figure 4.6 – Variation of the membrane permeability dimensionless parameter with relative humidity and material.	57
Figure 4.7 – Variation of the membrane permeability dimensionless parameter with relative humidity and intake air temperature.	58
Figure 4.8 – Effectiveness as a function of volume flow rate in enthalpy exchanger.	59
Figure 4.9 – Air temperature at the outlet of heat recovery system as a function of outdoor air temperature and air volume flow rate [m^3/h].	60
Figure 4.10 – Unity cell of the air-to-refrigerant heat exchangers.	60
Figure 4.11 - Analysis of the results obtained by different correlations for the evaporator.	62

Figure 4.12 - Analysis of the results obtained by different correlations for the condenser.	63
Figure 4.13 – Value of k as a function of evaporating temperature.....	65
Figure 4.14 – Diagram of the iterative process.	66
Figure 4.15 – Heat recovered as a function of the outdoor air temperature and air volume flow rate [m^3/h].....	68
Figure 4.16 – Power output as a function of the outdoor air temperature and air volume flow rate [m^3/h].....	68
Figure 4.17 – Sensible heat as a function of the outdoor air temperature and air volume flow rate [m^3/h].....	69
Figure 4.18 – COP as a function of outdoor air temperature and air volume flow rate [m^3/h].....	69
Figure 4.19 – COP of refrigerant cycle as a function of outdoor air temperature and air volume flow rate [m^3/h].....	70
Figure 4.20 – Discharge air temperature as a function of outdoor air temperature and air volume flow rate [m^3/h].....	70
Figure 4.21 – Supply air temperature as a function of outdoor air temperature and air volume flow rate [m^3/h].....	71
Figure 4.22 – Power output as a function of the air volume flow rate and frequency.	71
Figure 4.23 – Sensible heat as a function of the air volume flow rate and frequency.....	72
Figure 4.24 – Coefficient of performance (COP) as a function of the air volume flow rate and frequency.	72
Figure 4.25 – Discharge air temperature as a function of the air volume flow rate and frequency.	73
Figure 4.26 – Recovered heat as a function of outdoor air temperature and air volume flow rate [m^3/h] for cooling mode.	73
Figure 4.27 – Cooling power output as a function of the outdoor air temperature and air volume flow rate [m^3/h].....	74
Figure 4.28 – Sensible heat as a function of the outdoor air temperature and air volume flow rate [m^3/h].....	74

Figure 4.29 – <i>EER</i> as a function of the outdoor air temperature and air volume flow rate [m ³ /h].	75
Figure 4.30 – Discharge air temperature as a function of the outdoor air temperature and air volume flow rate [m ³ /h].....	75
Figure 4.31 – Cooling power output as a function of the air volume flow rate and frequency.	76
Figure 4.32 – Sensible heat as a function of the air volume flow rate and frequency.....	76
Figure 4.33 – <i>EER</i> as a function of the air volume flow rate and frequency.	77
Figure 4.34 – Recovered heat as a function of the outdoor air temperature and air volume flow rate [m ³ /h].....	77
Figure 4.35 – Latent recovered heat as a function of the outdoor air temperature and air volume flow rate [m ³ /h].....	78
Figure 4.36 – Power output as a function of the outdoor air temperature and air volume flow rate [m ³ /h].....	78
Figure 4.37 – Sensible heat as a function of the outdoor air temperature and air volume flow rate [m ³ /h].....	79
Figure 4.38 – <i>COP</i> as a function of the outdoor air temperature and air volume flow rate [m ³ /h].	79
Figure 4.39 – <i>COP</i> of the refrigerant cycle as a function of the outdoor air temperature and air volume flow rate [m ³ /h].....	80
Figure 4.40 – Discharge air temperature as a function of the outdoor air temperature and air volume flow rate [m ³ /h].....	80
Figure 4.41 – Supply air temperature as a function of the outdoor air temperature and air volume flow rate [m ³ /h].....	81
Figure 4.42 – Power output as a function of the air volume flow rate and frequency.	81
Figure 4.43 – Sensible heat as a function of the air volume flow rate and frequency.....	82
Figure 4.44 – <i>COP</i> as a function of the air volume flow rate and frequency.....	82
Figure 4.45 – Discharge air temperature as a function of the air volume flow rate and frequency.	83

Figure 4.46 – Recovered heat as a function of the outdoor air temperature and air volume flow rate [m ³ /h].	83
Figure 4.47 – Latent recovered heat as a function of the outdoor air temperature and air volume flow rate [m ³ /h].	84
Figure 4.48 – Cooling power output as a function of the outdoor air temperature and air volume flow rate [m ³ /h].	84
Figure 4.49 – Sensible heat as a function of the outdoor air temperature and air volume flow rate [m ³ /h].	85
Figure 4.50 – <i>EER</i> as a function of the outdoor air temperature and air volume flow rate [m ³ /h].	85
Figure 4.51 – Discharge air temperature as a function of the outdoor air temperature and air volume flow rate [m ³ /h].	86
Figure 4.52 – Cooling power output as a function of the air volume flow rate and frequency.	86
Figure 4.53 – Sensible heat as a function of the air volume flow rate and frequency.	87
Figure 4.54 – <i>EER</i> as a function of the air volume flow rate and frequency.	87
Figure 5.1 – Piping/Ducting and Instrumentation Diagram.	92
Figure 5.2 – User interface of the climate chamber.	93
Figure 5.3 – Electrical resistance of the different sensors.	94
Figure 5.4 – Calibration curve of the air volume flow rate measurement.	95
Figure 5.5 – Volume flow rate measurement device.	96
Figure 5.6 – Pressure differential transducer.	96
Figure 5.7 – Evaporator, compressor and expansion valve.	97
Figure 5.8 – Fixed speed rotary compressor.	97
Figure 5.9 – Connection between condenser and the other components.	98
Figure 5.10 – Heat Recovery Ventilation system.	98
Figure 5.11 – Duct connection between refrigerant boxes, HRV and climate chamber.	99
Figure 5.12 – Electrical connections.	99

Figure 5.13 – Discharge air temperature as a function of air volume flow rate and outdoor air temperature.	102
Figure 5.14 – Insulation analysis for low volume flow rate.	105
Figure 5.15 – Insulation analysis for high volume flow rate.	105
Figure 5.16 – Sensible effectiveness of the HRV.	106
Figure 5.17 – Sensible effectiveness of the evaporator.	107
Figure 5.18 – Power output of the overall solution from experimental analysis (separated points) and modelling (connected by a line).	108
Figure 5.19 – COP of the overall solution from experimental analysis (separated points) and modelling (connected by a line).	108
Figure 5.20 – Discharge air temperature from experimental analysis (separated points) and modelling (connected by a line).	109
Figure B.1 – Electrical circuit of the NTC sensor.	123
Figure B.2 – Systematic uncertainty of temperature as a function of measured temperature.	125
Figure B.3 – Systematic uncertainty of volume flow rate as a function of the difference of pressure.	126

Index of Tables

Table 2.1 – Comparison between different refrigerants	18
Table 2.2 – Technical specifications (Adapted from Nilan catalogue [20])	21
Table 2.3 – Comparison of air-to-air heat recovery devices [10].....	26
Table 2.4 – Comparison of air-to-air energy recovery devices [10]	29
Table 3.1 – List of components	32
Table 3.2 – Nusselt number and friction factor as a function of cross section [13]	36
Table 3.3 – Constants of equation (3.25) for the tube bank [13]	42
Table 3.4 – Constants of equation (3.25) depending on N_L for $N_L < 20$ [13].....	42
Table 3.5 – Verified range of boiling correlations [10].....	46
Table 3.6 – Verified range of condensing correlations [10, 33].....	48
Table 4.1 – Input variables of the heat exchanger	55
Table 4.2 – Output dimensions of the geometry of the heat exchanger	55
Table 4.3 – Input variables of the enthalpy exchanger.....	58
Table 4.4 – Output variables of the geometry of the enthalpy exchanger.....	59
Table 4.5 – Dimensions of the evaporator.....	60
Table 4.6 – Geometric output variables of the evaporator	61
Table 4.7 – Properties of the evaporator refrigerant side	61
Table 4.8 – Properties of the condenser refrigerant side	63
Table 4.9 – Dimensioning data of the compressor	64
Table 4.10 – Temperature and relative humidity ranges	67
Table 4.11 – Outdoor air conditions for variable speed analysis during heating mode (HRV)	71
Table 4.12 – Outdoor air conditions for variable speed analysis during cooling mode (HRV)	75
Table 4.13 – Comparison during heating mode	88
Table 5.1 – Temperature and Relative Humidity ranges of the climate chamber	93
Table 5.2 – Sensors specific values [38]	94

Table 5.3 – Correspondence between sensors name and variant	95
Table 5.4 – Refrigerant charge distribution.....	100
Table 5.5 – Air-to-air test conditions [42].....	102
Table 5.6 – Minimum values of volume flow rate	103
Table 5.7 – Values of volume flow rate and difference of pressure to be measured by the manometer	103
Table 5.8 – Location of insulation.....	104
Table A.1 –Parameters of air thermophysical and transport properties	119
Table A.2 – Parameters of evaporating temperature properties	121
Table A.3 – Parameters of condensing temperature properties.....	121
Table B.1 – Systematic uncertainties of influence variables of temperature	124
Table C.1 – Test results for outdoor air temperature equal to 2 °C.....	129
Table C.2 – Test results for outdoor air temperature equal to 7 °C.....	129
Table C.3 – Test results for outdoor air temperature equal to 12 °C.....	130
Table C.4 – Random uncertainties of the measurements for outdoor air temperature equal to 2 °C	130
Table C.5 – Random uncertainties of the measurements for outdoor air temperature equal to 7 °C	131
Table C.6 – Random uncertainties of the measurements for outdoor air temperature equal to 12 °C	131

Abbreviations

BDS	Beyond Degree Scenario
<i>COP</i>	Coefficient of Performance
DS	Degree Scenario
EATR	Exhaust Air Transfer Ratio
EER	Energy Efficiency Ratio
EES	Engineering Equations Solver
ERV	Energy Recovery Ventilation
GWP	Global Warming Potential
HE	Heat Exchanger
HRV	Heat Recovery Ventilation
HVAC	Heating, Ventilation and Air Conditioning
MBEE	Membrane Based Enthalpy Exchanger
<i>NTU</i>	Number of Transfer Units
<i>NTU_L</i>	Number of Mass Transfer Units
ODP	Ozone Depletion Potential

Nomenclature

Symbol	Unit	Description
<i>a</i>	[-]	Dimensionless longitudinal pitch
<i>A</i>	[m ²]	Area
<i>A_{ch}</i>	[m ²]	Channel cross section area
<i>A_{transfer}</i>	[m ²]	Heat transfer area
<i>b</i>	[-]	Dimensionless transversal pitch
<i>B</i>	[-]	Systematic uncertainty

b_l	[m]	Length
Bo	[-]	Boiling number
c_p	[J/(kg°C)]	Specific heat capacity
C	[W/°C]	Heat capacity rate
C_{sf}	[-]	Shape factor
Co	[-]	Shah's convection number
d	[m]	Diameter
D	[m ² /s]	Mass diffusivity
D_h	[m]	Hydraulic diameter
D_{w-m}	[m ² /s]	Water diffusivity in membrane
f	[-]	Friction factor
F_a	[-]	Arrangement factor
Fr	[-]	Froude number
G	[kg/(m ² s)]	Mass flux
h	[J/kg]	Specific enthalpy
h_c	[W/(m ² °C)]	Heat convective coefficient
h_m	[kg/(m ² s)]	Mass convective coefficient
J_g	[-]	Dimensionless vapour velocity
k	[W/(m°C)]	Thermal conductivity
l	[m]	Heat exchanger dimension
Le	[-]	Lewis number
m_{ref}	[kg]	Refrigerant mass
\dot{m}	[kg/s]	Mass flow rate
N_{ch}	[-]	Number of channels

N_L	[-]	Number of lines
Nu	[-]	Nusselt number
p	[Pa]	Pressure
P	[-]	Random uncertainty
P_{ch}	[m]	Channel cross section perimeter
Pr	[-]	Prandtl number
q_c	[J/kg]	Specific refrigeration effect
q_h	[J/kg]	Specific heat output
\dot{Q}_c	[W]	Cooling power
\dot{Q}_h	[W]	Heating power
r	[m]	Radius
R	[W/m ²]	Thermal resistance
R_e	[Ω]	Electrical resistance
s	[m]	Heat exchanger dimension
S_T	[m]	Transverse pitch
S_L	[m]	Longitudinal pitch
Sh	[-]	Sherwood number
T	[°C, K]	Temperature
U	[-]	Global uncertainty
\dot{V}	[m ³ /s]	Volume flow rate
v	[m/s]	Cross section velocity
x	[-]	Quality (i.e., mass fraction of vapour)
w_c	[J/kg]	Specific work input
\dot{W}_c	[W]	Working power

α	[m ² /s]	Thermal diffusivity
δ	[m]	Wall thickness
δ_{X_i}	[-]	Uncertainty of the variable X_i
ε	[-]	Effectiveness
ε_L	[-]	Latent effectiveness
ε_S	[-]	Sensible effectiveness
ε_T	[-]	Total effectiveness
η_{is}	[-]	Isentropic efficiency
η_f	[-]	Fin efficiency
η_s	[-]	Finned surface efficiency
θ	[kg/m]	Moisture uptake
μ	[Pa·s]	Dynamic viscosity
ρ	[kg/m ³]	Density
ρ_e	[Ω /m]	Electrical resistivity
ν	[m ² /s]	Kinematic viscosity
ϕ	[-]	Relative humidity
ψ	[-]	Dimensionless membrane permeability
ω	[kg/kg]	Moisture content

1 Introduction

This project is carried out in the scope of the Dissertation for the Master in Mechanical Engineering Degree at the Faculty of Engineering of the University of Porto. The work is developed within an industrial and business environment at Bosch Thermotechnology S.A., at the Aveiro plant, and it is integrated in a research and development work carried out by the team of heat pump appliances. The principal objective is to develop an efficient solution, including the integration of a heat recovery system within a compact mechanical ventilation heat pump appliance. In the next subsections, the framework of the project is defined as well as the main objectives.

1.1 Bosch Thermotechnology S.A.

The origins of Bosch Group date back to 1886 when Robert Bosch (1861-1942) set up the “Workshop for Precision Mechanics and Electrical Engineering” in Stuttgart and nowadays the company may be divided in four main business sectors: Mobility Solutions, Industrial Technology, Consumer Goods and Energy and Building Technology [1]. The basis of the company’s strategy and future is its innovative strength as can be seen in the 62,500 employees associates in research and development at the 125 locations across the world. This strategy is verified by looking at Figure 1.1, in which the research and development costs of the Bosch Group are represented as a percentage of the sales revenue and its value is approximately constant and equal to 10% between 2012 and 2016.

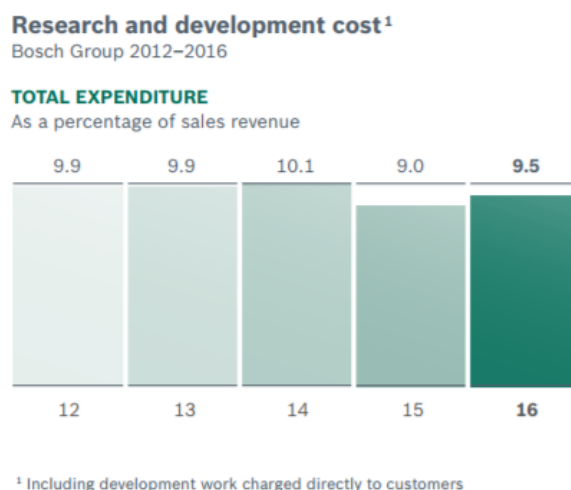


Figure 1.1 – Total research and development costs [2].

With more than 4,000 associates (as per 31st December, 2016), Bosch is one of the largest industrial employers in Portugal and the company is represented by Bosch Car Multimedia

Portugal in Braga, Bosch Security Systems in Ovar and finally Bosch Thermotechnology in Aveiro. The entrance building of the Bosch Thermotechnology S.A. in Aveiro is presented in Figure 1.2.



Figure 1.2 – Entrance building of Bosch Thermotechnology S.A. in Aveiro.

In the year of 1977, Bosch Thermotechnology S.A. started its activity under the name of “Vulcano Termodomésticos SA” by transferring the technology used by Robert Bosch Company in water heaters manufacturing. Because of the higher quality of the products and the sales strategy, the influence in the national market increased and the company was acquired by the Bosch Group in 1988, who transferred competence and equipment to Portugal and Bosch Thermotechnology S.A. is now the center of competence of Robert Bosch for hot water solutions in the Thermotechnology unit. In 2011, the company started the development and production of heat pumps for domestic use, being followed by the production of electrical appliances for water heating, which was the last step in terms of products range expansion until now. With more than 1,100 employees, the Bosch’s Thermotechnology division in Aveiro is a global leader in development of central heating and domestic hot water solutions and is responsible for develop and manufacture boilers, heat pumps and water heaters, which are exported to more than 30 countries around the world. Hereby, Bosch Thermotechnology produces under different brands, such as Buderus, Junkers, Worchester and Vulcano, as it is presented in Figure 1.3.



Figure 1.3 – Most representative brands of Bosch Thermotechnology division [1].

In 2016, a second R&D building was constructed in Aveiro and it represents an investment of 25 million euros by 2020. The main objective of this building is to develop technologies for more sustainable homes, focused on connectivity, energy efficiency and sustainable resource management. Thus, the present study was developed inside the new building in the scope of the activities of research and development for heat pump appliances.

1.2 Motivation

The requirements of energetic efficiency of the different existing processes are continuously increasing due to the scarcity of resources, the destruction of the ozone layer and other negative environmental impacts connected to waste heat and gaseous emissions. A substantial shift in energy sector trends is now considering the influence of energy security, energy poverty, air quality and climate changes by the incorporation of the environmental risks in their plans [3]. For these reasons, the investment towards renewable energy sources and energy efficiency is increasing, so that the improvements and cost reductions in these technologies are making them competitive when compared with traditional fossil fuel sources [3]. In this subsection, the impact of the heating, ventilation and air conditioning systems, HVAC, in the energy consumption of the buildings is analysed and the main challenges for the new developments, in which this project is included, are presented.

Firstly, it is important to know the distribution of energy consumption within the different activities and the European Union segment is now analysed. In Figure 1.4, this parcelling is presented and it is directly concluded that the energy spent in households or residential sector represent a high value of 25.4% of the final energy consumption¹.

¹ Final energy consumption is the total energy consumed by end users and it excludes the energy used by the energy sector, including for deliveries and transformation.

1. Introduction

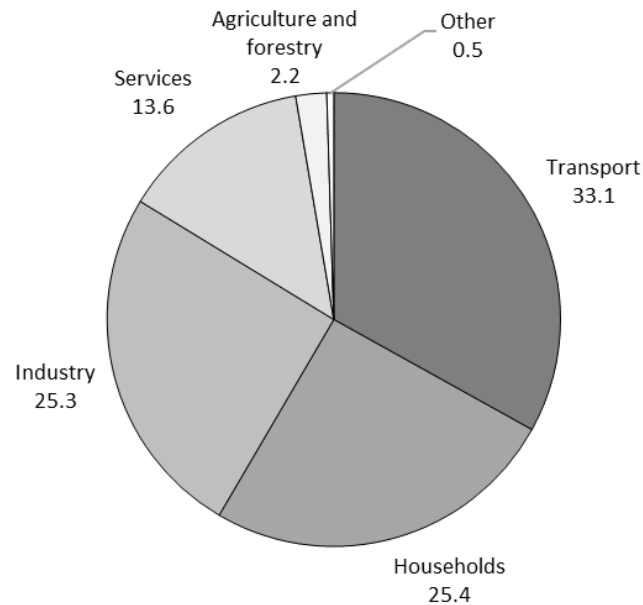


Figure 1.4 - Distribution of final energy consumption (EU-28, 2015), based on tonnes of oil equivalent (%)². Adapted from IEA [4].

Secondly, Figure 1.5 shows the distribution of energy consumption in the residential sector by type of end-use and the main use of energy is for heating homes (64.7%), followed by water heating (13.9%) and lighting and appliances (13.8%).

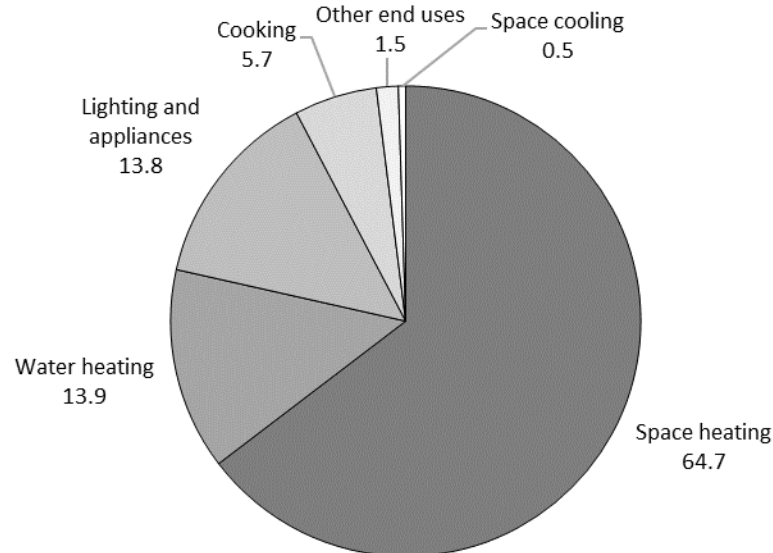


Figure 1.5 – Final energy consumption in the residential sector by type of end-use (EU-28,2015). Adapted from IEA [4].

Thirdly, the distribution of final energy consumption by type of end-uses for the main energy products is presented in Figure 1.6, in which is possible to verify that energy consumptions are

² Note: figures do not sum to 100.0% due to rounding [3].

largely dependent on fossil fuels, such as gas and petroleum products, and this dependency has to be reduced because of resources scarcity and environment requirements [3].

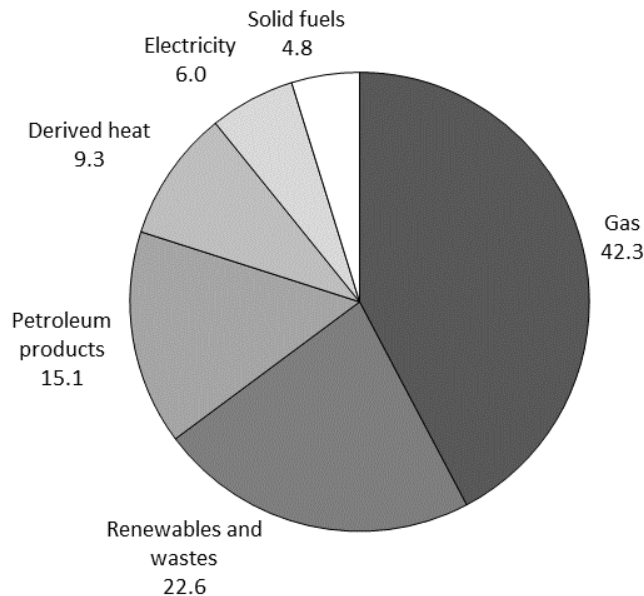


Figure 1.6 – Final energy consumption by type of end-use for the main energy products (EU-28,2015). Adapted from IEA [4].

In order to reduce the dependence of the fossil fuels, there are different strategies and scenarios which were developed using a combination of forecasting and development of feasible pathways to a desired long-term outcome, such as 2 °C Scenario (2DS) or Beyond 2°C Scenario (B2DS) [3]. Both set out a quick decarbonisation pathway in line with international policy goals. The rising share of renewables in electricity supply turns the electric heat pumps into an important role in heat decarbonisation by using energy from a supposed useless environment in terms of energy, such as ground, air or water source. For example, with a B2DS perspective, the natural gas demand in buildings can be reduced by as much as 80 % by 2060 compared to today, by shifting the demand to efficient, renewable and integrated solutions (heat pumps and district energy, for example) [3]. These objectives may be considered by the majority as an impossible dream, but the challenge of developing solutions with higher energy efficiency to avoid its wasting with lower gas emissions is, without any doubt, the key for the future.

On the other hand, with the increase of low energy consumption requirements and the consequent dramatic increase of the air tightness of modern buildings, the lack of indoor air quality (IAQ) must be avoided. Poor IAQ may be caused by numerous factors, such as humidity, odours, chemicals and pollutant emissions from people [5, 6]. More specifically, high levels of CO₂ lead to unhealthy and even dangerous living conditions. For example, in the short term, a badly ventilated building is highly connected with undesirable effects, such as coughing,

1. Introduction

sneezing, fatigue and headaches. Lately, these poor indoor air conditions may lead to more critical consequences, such as allergic and asthma symptoms, lung cancer, chronic obstructive pulmonary disease and cardiovascular disease [7]. Therefore, the dilution of these pollutants is an important step to reduce its concentration and it can be easily ensured with the installation of a mechanical ventilation system that guarantees a certain inlet air volume flow as a function of indoor pollutants concentration.

On the other hand, not only the renovation of indoor air guarantees its quality in terms of health needs, but also the indoor air humidity represents high importance to avoid for example mould and mites formation. Consequently, according to ASHRAE [6], in Figure 1.7 is presented a representation of the consequences of having relative humidity outside an optimum zone in which those effects have a minimum value. Thus, a precise control of indoor relative humidity, ideally between 30 and 60 %, is the key to obtain indoor air conditions that promote higher thermal comfort and finally lead to an increase of the performance and satisfaction of the people [8].

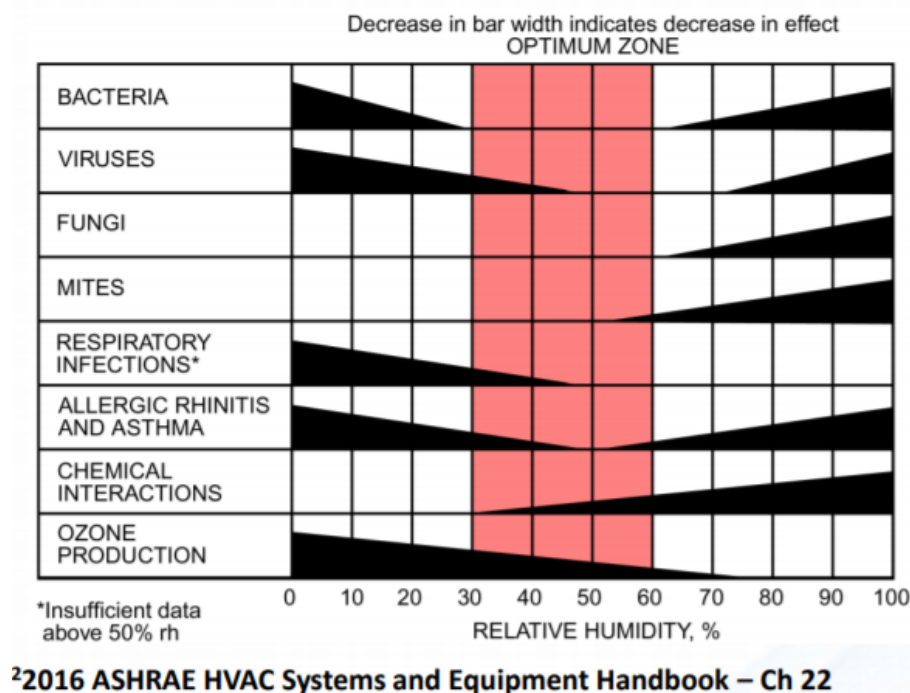


Figure 1.7 – Consequences of humidity levels outside the optimum zone [6].

In conclusion, with the higher requirements of energy wasting and consumption and the actual policies of reducing greenhouse gas emissions, the integration of energy efficient solutions ensuring the indoor air quality may be considered a challenge that can have a positive impact due to its high efficiency and consequently reduction of energy consumptions. Therefore, heat recovery is a method that is increasingly used to reduce the heating and cooling demands, by

transferring energy from the exhaust air to the incoming fresh air during winter season, whereas during the cooling season, the exhaust cooler air may be used to reduce the incoming air temperature.

1.3 Objectives

In order to develop an integrated solution of a heat and mass recovery system incorporated in a mechanical ventilation heat pump, the principal objectives are the dimensioning, assembly and test the functional sample of the appliance, with respect to the applicable norms. In a final step, the feasibility of the solution will be evaluated.

The main objectives are presented in the following list:

- State of the art and benchmark of the technical solutions available in the market;
- Definition and analysis of the requirements and technical specifications;
- Pre-dimensioning of the refrigerant circuit;
- Modelling of the overall circuit;
- Selection of the components;
- Assembly of a functional sample;
- Conduct test plan;
- Uncertainty analysis;
- Analysis of the results and conclusions.

1.4 Dissertation Outline

Looking forward to the next sections, this dissertation is divided in four main chapters. Firstly, a review of the literature is presented in which a state of the art is conducted: general and energy concepts regarding heat pumps (circuits, components, directives, indicators of performance), actual state of air source heat pumps within Bosch developments, use of heat pumps integrated with mechanical ventilation (benchmark included), discussion about different types of heat or energy recovery systems, e.g. counter flow heat exchanger, membrane based heat and mass exchanger and wheels desiccant heat and mass exchanger. After this, the functional solution is proposed, the requirements and specifications are defined and the complete circuit is modelled. A functional sample is assembled and all the steps are described. Finally, the tests are performed for all test points that are considered important for the evaluation of the performance of the appliance and the appropriate conclusions and the improvement suggestions are discussed. In the appendixes, the properties of the fluids are presented as well as the analysis of uncertainty and test results.

1. Introduction

[Blank page]

2 Literature Review

A brief analysis about the state of the art of the development of residential heat pumps to guarantee heating, ventilation and air conditioning is an important step to understand the next possible improvements and researches regarding this theme. In a first section, a theoretical presentation of a typical heat pump circuit is performed to describe the main components, norms, directives and indicators of performance that are necessary to evaluate the performance of this type of appliance. After this, the state of the art regarding Bosch air source heat pumps is defined by analysing the last solutions developed inside the company. In the second place, a benchmark analysis is done in which the existing solutions in market are presented. To conclude this section, the air-to-air heat exchangers are described and divided in its different ways of transferring energy, such as sensible or latent recovery systems.

2.1 Heat Pump

A heat pump is a refrigerating machine that extracts energy from a low temperature heat source and rejects heat to a high temperature source, such as air or water, by working through a thermodynamic cycle. During winter, its useful effect is the rejected heat, whereas in summer, the heat extraction is the desired effect. According to the types of thermal energy sources from which the refrigerant absorbs heat, the heat pump systems are divided into two categories: air-source and water-source [9]. During the following subsections, heat pump theoretical fundamentals are presented, such as vapour compression cycle, components and refrigerant.

2.1.1 Vapour Compression Cycle

As illustrated in Figure 2.1, a typical vapour compression cycle is basically composed of the following components: evaporator, compressor, condenser and expansion valve. Starting at the exit of the evaporator, saturated, or even super-heated, refrigerant vapour passes through the compressor raising its temperature and pressure [9]. The high temperature super-heated vapour is cooled in the condenser and enters into the liquid-vapour region. At the outlet of the heat exchanger, the refrigerant at a liquid-vapour state, or at saturated or even as sub-cooled liquid region is expanded by passing through the expansion valve, in which its temperature and pressure decrease, ideally without enthalpy change, reaching a liquid-vapour state. Finally, it passes in the evaporator, extracting energy from a lower temperature source, becomes saturated, or even super-heated, and then the cycle re-starts.

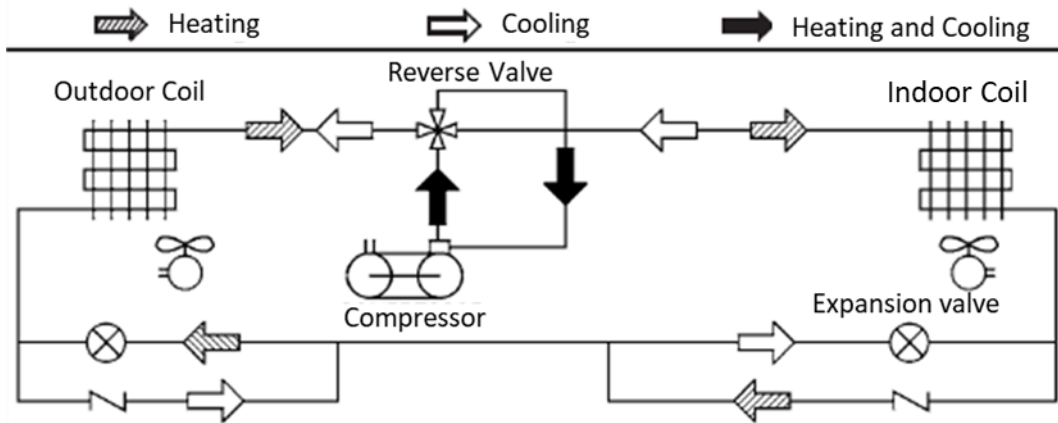


Figure 2.1 – Schematic representation of a heat pump circuit [10].

The basic vapour compression cycle evolutions can be plotted in the pressure-enthalpy, $p - h$, and temperature-entropy, $T - s$, diagrams as can be seen in Figure 2.2 and Figure 2.3, respectively. To perform this representation, an adiabatic expansion, an isentropic compression and no pressure drop through heat exchangers (evaporator and condenser) were assumed, as well as neither subcooling or superheating. In the $T - s$ diagram, the Carnot cycle is also represented as the ideal one working between two constant temperatures and the corresponding characteristic points are identified by the “c” subscript.

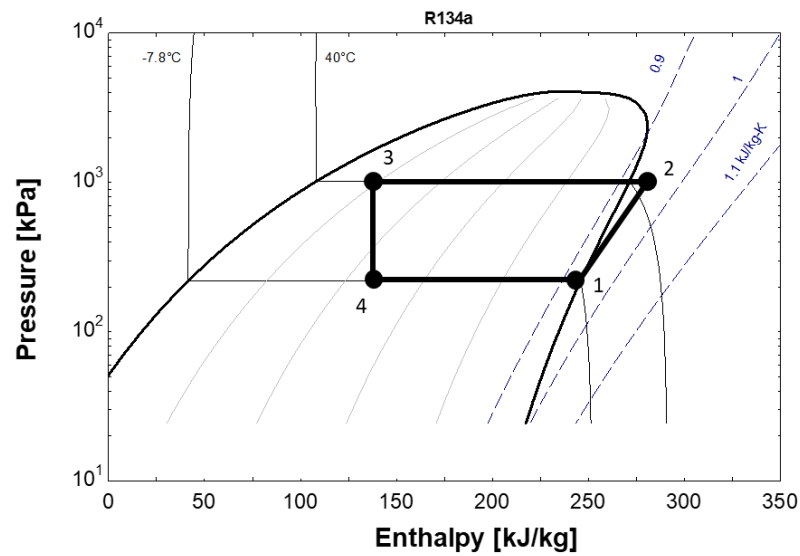


Figure 2.2 – Heat pump cycle representation in pressure-enthalpy diagram (Adapted from EES).

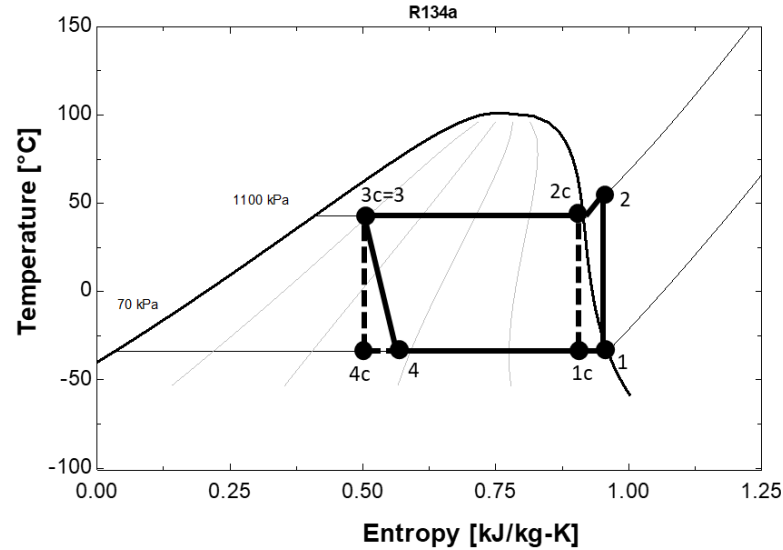


Figure 2.3 - Heat pump cycle representation in temperature-entropy diagram (Adapted from EES).

The real cycle differs from the ideal due to non-isentropic expansion and compression and the pressure drop through both heat exchangers, but in Figure 2.3 only the non-ideal expansion is considered. Additionally, in order to ensure a complete vapour compression, i. e. there is no liquid at the inlet of the compressor, few degrees of superheat exist at the compressor outlet. During heating mode, the heat output of the cycle, q_h , and the compression work input, w_c , both per unit mass of the flowing refrigerant, are calculated by the following expressions:

$$q_h = \frac{\dot{Q}_h}{\dot{m}_R} = h_2 - h_3 \text{ [kJ/kg]} \quad (2.1)$$

$$w_c = \frac{\dot{W}_c}{\dot{m}_R} = h_2 - h_1 \text{ [kJ/kg]} \quad (2.2)$$

where

h_1, h_2 and h_3 are the specific enthalpy of the different points and

\dot{m}_R is the refrigerant mass flow rate.

Regarding the cooling mode, the refrigeration effect, q_c , is then obtained:

$$q_c = \frac{\dot{Q}_c}{\dot{m}_R} = h_1 - h_4 \text{ [kJ/kg]} \quad (2.3)$$

The performance of the cycle is evaluated by dividing the desired output (heat output or refrigeration effect) by the energy consumption (compression work). For the heating mode, the Coefficient of Performance, COP , is evaluated, whereas in cooling mode, the Energy Efficiency Ratio, EER , is calculated [9].

$$COP = \frac{q_h}{w_c} = \frac{h_2 - h_3}{h_2 - h_1} \quad (2.4)$$

$$EER = \frac{q_c}{w_c} = \frac{q_h - w_c}{w_c} = COP - 1 \quad (2.5)$$

Lately, the procedure to evaluate the performance of the solution and its coefficients is presented accordingly to the standards.

2.1.2 Components

During this subsection, a brief analysis of each component of the compression vapour cycle is performed, such as compressor, evaporator or condenser and expansion valve, in which its function is explained and the different available types are presented.

Compressor

The compressor may be considered the heart of a vapour compression refrigerant cycle, due to its capacity of raising the fluid pressure and providing energy to circulate the refrigerant [9]. Regarding the characteristics of the compression process, this component is classified as either positive displacement, or volumetric, and non-positive displacement compressor, when increase of vapour refrigerant pressure is caused by reducing the internal volume of the compression chamber through mechanical work applied to the compressor or by converting kinetic energy into static pressure, respectively. The main non-positive displacement compressor used in refrigeration systems is the centrifugal compressor, whereas the other compressor's variant may be mainly subdivided in four categories: reciprocating, scroll, screw and rotary compressors [9]. In addition, the rotary and reciprocating compressors are the most adequate in terms of power capacity required to this project [11, 12].

The compressors are also divided in terms of the driving connection between the compressor and the electric motor: hermetic, semi hermetic and open compressors. In a hermetic compressor, both components are sealed and welded in the same housing [9] and it leads to lower refrigerant leakage and to cool the motor by the suction vapour flowing through the motor windings, which causes a cheaper and smaller assembly between these components, whereas the process of repairing and maintenance is not easily realized. On the other hand, the semi hermetic compressor main advantage over the previous is the accessibility for repair or for regular maintenance, maintaining the other features. In an open compressor, the components are evolved in two separate housings and this solution needs shaft seals to minimize refrigerant leakage.

In terms of performance, compressors are evaluated by several parameters, such as:

- Volumetric efficiency, which is defined as the quotient between the actual volume of suction vapour at suction pressure with the theoretical volume displacement of

compressor. This value is influenced by compression ratio, clearance volume, which affect the re-expansion gas volume, heating effects and fluid leakage;

- Motor efficiency, which is defined as the relation between power input to compressor shaft and to motor, respectively;
- Mechanical efficiency: which is defined as the quotient between the work delivered to fluid and to compressor shaft, respectively;
- Isentropic efficiency, which is defined as the relation between the real refrigerant enthalpy difference by passing through compressor and the ideal in which an isentropic process is occurs [9].

In addition, in Figure 2.4 a fixed-vane rotary compressor is presented, which is characterized by high volumetric efficiency due to its small clearance volume leading to low re-expansion losses. This variant is commonly used in air conditioning and small heat pump applications [9].

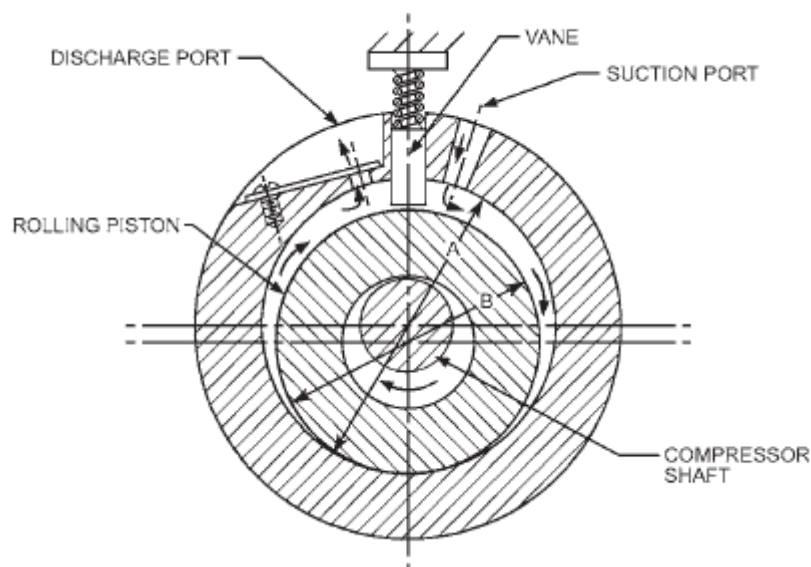


Figure 2.4 – Rolling-piston rotary compressor [10].

Evaporator and Condenser

The heat exchangers in which evaporation and condensation of refrigerant fluid occur are other important components that have to be considered when a vapour compression cycle is desired and they are classified as air or liquid source depending on the medium or substance that participates in heat transfer as thermal energy source or sink. In this case, considering that heat transfer process occurs mainly by convective phenomena and refrigerant transfers heat with airstreams, which have typically low convective coefficients, the mainly used type of these heat exchangers is finned tube geometry. Therefore, a minimum convective coefficient is ensured by an arrangement of tubes in which two-phase refrigerant flows and the surface, which

participates in heat transfer, is increased by adding fins. The tubes and fins are usually made of copper and aluminium, respectively [10]. Figure 2.5 shows an example of the mentioned heat exchanger variants, which also may be defined as compact heat exchangers, due to its dense arrays of finned tubes or plates. Typically, flow passages associated with compact heat exchangers are small ($D_h \leq 5 \text{ mm}$) and the flow is laminar [13].

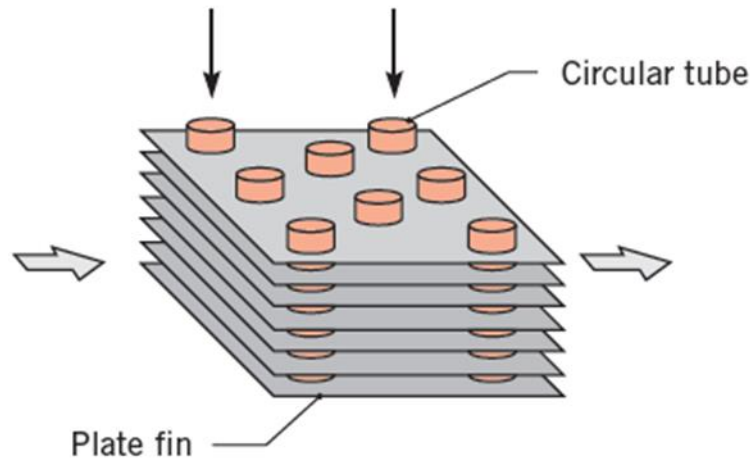


Figure 2.5 – Finned tube heat exchanger [13].

Regarding temperature evolution through heat exchanger, Figure 2.6 presents the typical evolution of airside temperature for both phase change phenomena. It is important to refer that the temperature of the refrigerant is considered constant and no subcooled or superheated fluid is taken into account within this analysis.

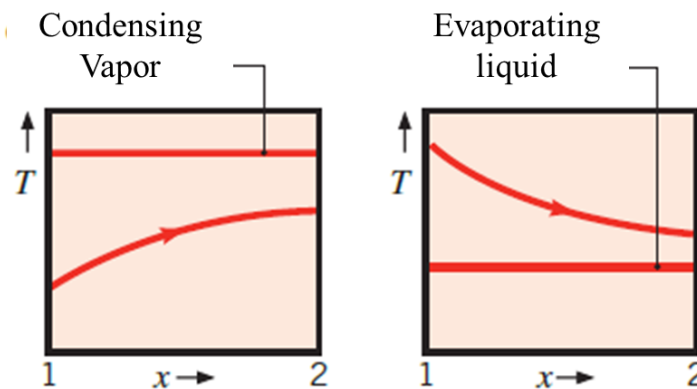


Figure 2.6 – Evolution of condensation and evaporation temperatures [13].

When the refrigerant evaporation occurs, the formation of water condensates has to be considered, i.e., this amount of water has to be drained out, due to the effect of cooling the airstream until its temperature reaches the dew point point [10]. If the airstream temperature is below frosting point, ice will be deposited in the fins and the presence of this state of water has to be avoided because it leads to: partial or full blockage of air flow passages, increase in

pressure drop through the exchanger or decrease in air flow rate, increase in electric fans power consumption, decrease in the heat transfer rate between the two airstreams and decrease of supply air temperatures [14].

Expansion Valve

The expansion system is the remaining component of the refrigerant circuit and these refrigerant flow control devices include thermostatic expansion valves, electric expansion valves, float valves, capillary tubes and multiple orifices. By passing through this component, the refrigerant at condensing pressure is throttled to evaporating pressure and the flow passing at the evaporator is controlled to ensure the necessary refrigeration load [9, 12, 15].

The thermostatic expansion valves are the most widely used expansion devices within the use of this type of refrigerant systems, in which the refrigerant flow rate is regulated according to the desired degree of super-heat of vapour refrigerant leaving the evaporator. Figure 2.7 shows the working principle of a thermostatic expansion valve with external equalizer, in which the main components are disposed, such as diaphragm, external equalizer connecting tube, sensing bulb, valve pin and spring.

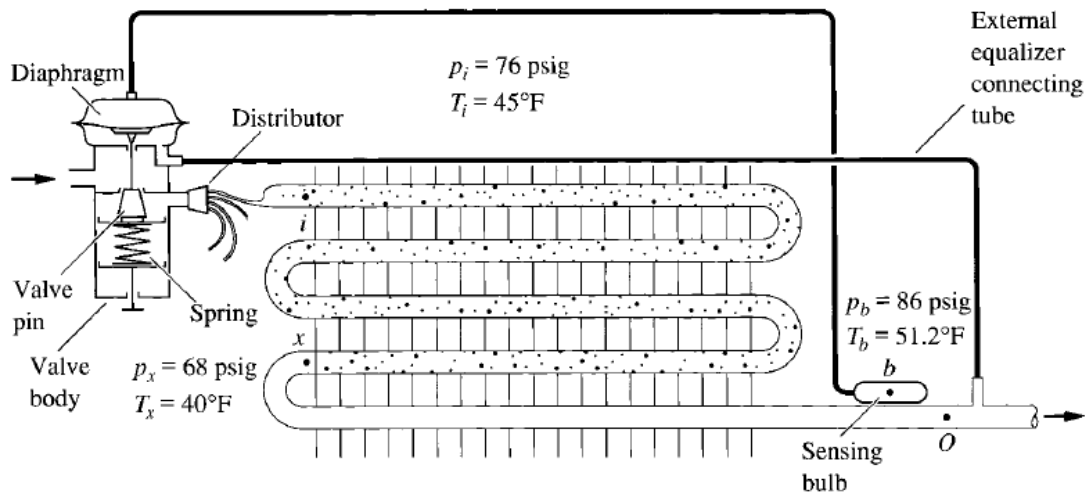


Figure 2.7 – Thermostatic expansion valve working with external pressure equalizer [9].

Basically, the degrees of super-heat are defined as a result of the equilibrium forces caused by the following pressures:

$$f(p_b) = f(p_i) + f(p_{spr}) \quad (2.6)$$

where

p_b is the saturation pressure at a temperature equal to the sum of superheated degrees and evaporation temperature,

p_i is the saturation pressure at evaporation temperature and

p_{spr} is the pressure by the compression of the spring.

Consequently, the equilibrium of these three values defines not only the evaporation temperature, but also the degrees of super-heat. The electric expansion valves could also be used and this variant has the following advantages when compared to the thermostatic version: more precise temperature control, superheat control under fluctuating head pressure and more energy-efficient. However, this type of expansion device is more complex and the cost is higher [9].

2.1.3 Refrigerant

The refrigerant is the primary working fluid used to absorb heat at a low pressure and low temperature and to release heat at a high pressure and high temperature. These heat transfer phenomena occur mainly while the refrigerant phase is changing, i.e., evaporation during heat absorption and condensation during heat delivery. In general, when choosing a refrigerant for heat pump applications, there are several parameters to be taken into account and they are divided into three main categories: thermodynamics, chemistry and physics. Thus, ideally the refrigerant will [9, 10, 15, 16, 17, 18]:

- Operate between certain evaporation and condensation pressures, to avoid air infiltration into the system (evaporation pressure higher than atmospheric) and to minimize the pipe and component's weight (modest condensation pressure);
- Have a low freezing point, in order to avoid freezing inside any installation component;
- Have high latent heat of vaporization, which causes high heating and cooling capacities per mass unit;
- Be non-flammable, in order to avoid fire or explosion risks;
- Be non-toxic, for health and safety reasons;
- Be stable against the materials of the components, in order to avoid the wearing of the components;
- Be detectable, to avoid leakages thus minimizing recharging costs;
- Have low viscosity and high thermal conductivity, to reduce pressure drops and to maximize as much as possible the heat transfer process;
- Be environmentally friendly;
- Have high density, so that the volume flow rate at the compressor inlet is reduced and then the work input is lower.

Considering the different requirements previously presented, in practice the selection of a refrigerant represents a compromise between thermodynamic performance and environmental

questions. Regarding these environment requirements, there are two parameters which also turn possible the comparison among different refrigerants. The first one is the Ozone Depletion Potential (ODP), which represents the impact of a certain chemical substance in ozone depletion when compared with the impact of the same mass of R-12 refrigerant (the ODP value for R-12 is assumed to be equal to 1). The other measure is the Global Warming Potential (GWP), which represents the mass of CO₂ needed to absorb the same amount of radiation absorbed by a certain substance within a period of time (the GWP value for CO₂ is assumed to be equal to 1).

Regarding heat pump application, until 1980's the R22 was the main used refrigerant in residential air conditioning and heating appliances, but it had to be replaced, due to its high ODP. Therefore, nowadays there are other refrigerants with lower impact on the ozone layer that are used within heat pumps dedicated to heat water or air, such as R134a, R407C, R410a and CO₂. In Figure 2.8, the variation of saturation pressure with temperature is presented for the referred refrigerants.

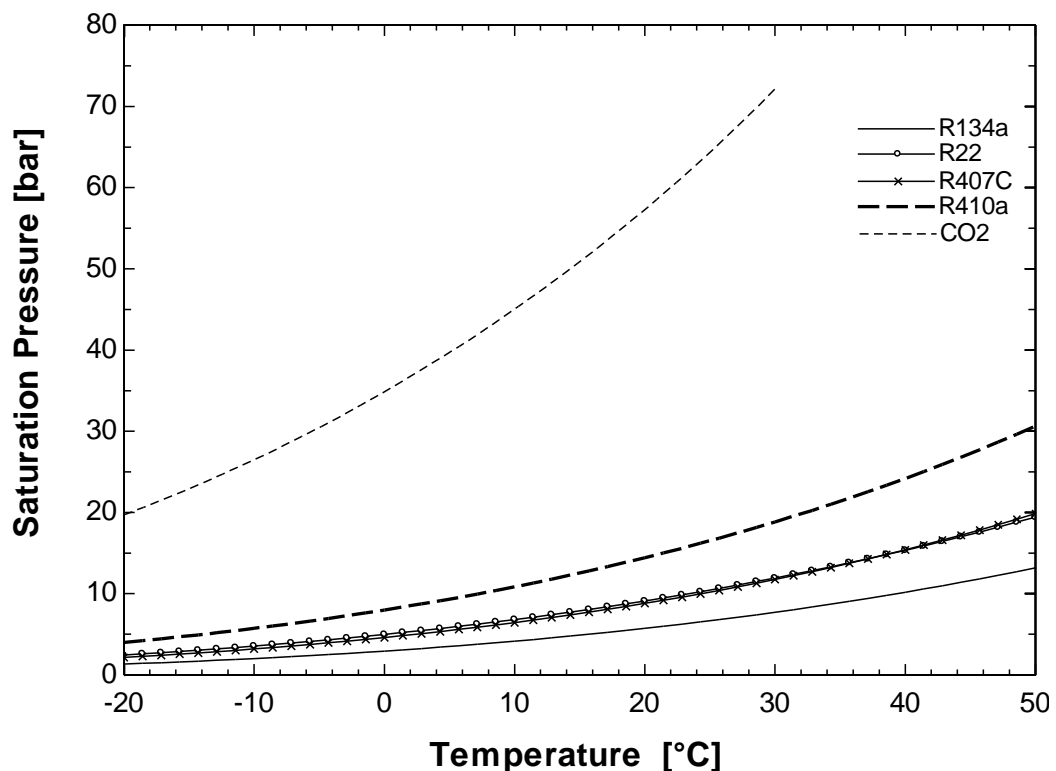


Figure 2.8 – Variation of saturation pressure with temperature.

In Table 2.1, the ODP, GWP, density at 0 °C ($x=1$) and latent heat of vaporization at 0 °C is presented for the different refrigerants [19].

2. Literature Review

Table 2.1 – Comparison between different refrigerants

Refrigerant	ODP	GWP	$\rho_{0^\circ\text{C},x=1}[\text{kg/m}^3]$	$h_{lv,0^\circ\text{C}}[\text{kJ/kg}]$
R22	0.05	1700	21.2	205.0
R134a	0	1300	14.4	198.6
R407C	0	2000	19.7	209.3
R410a	0	2088	30.6	221.4
CO ₂	0	1	97.6	230.9

R134a is used as a refrigerant for medium sized or large heat pump system. When compared to R407a and R410a, its GWP is lower and its temperature at critical point is higher, but its density is lower, which causes higher investment costs, because the compressor is bigger. On the other hand, R407c and R410a are commonly used in small to medium sized heat pump systems and R410a is more applied in low temperature heat pump systems, due to its lower critical temperature (71 °C). CO₂ is a natural refrigerant and it is used in supercritical cycles (pressure higher than critical pressure), which means that condensation process occurs within a range of temperatures and its circuit working pressure is very high and then the robustness requirements of the components are higher. Considering air as the other working fluid in both heat exchangers (evaporator and condenser) and its lower heat capacity, it is important to use one refrigerant with high temperature at critical point in order to turn possible relevant values of heat transfer, i.e., to transfer the same amount of energy to airstream compared to water, the outlet air temperature has to be higher which implies that the condensing temperature becomes higher. Therefore, the R134a refrigerant is the more adequate working fluid due to its higher temperature at critical point, lower working pressures and lower GWP.

2.1.4 Bosch Air-source Heat Pumps

In order to evaluate the actual state of developments inside the company, it is important to establish the applications, which are based in the same working principles of the presented solution. Therefore, air-source heat pumps are analysed and this variant may be divided in two groups: air-to-air heat pumps divided in indoor and outdoor units, which are connected by refrigerant pipes (also called split units) and exhaust air-to-water heat pump, in which the exhaust air passes through the evaporator of the refrigerant circuit, while the heat pump delivers energy to heating up water for different uses (central heating and/or domestic hot water).

Basically, this project concentrates on a solution that results in a combination of both variants. The evaporator side is equivalent to the exhaust air side of the air-to-water solution, while the

condenser side is equivalent to the indoor air side of the air-to-air solution. Considering the same amount of energy involved within the working conditions of the air-to-water solution (both solutions work with exhaust air), the main components of its circuit, such as evaporator and compressor, are defined as a base for the development of the new solution and the hypothesis of using them may be turned real, due to the similarity of both cases.

2.2 Benchmark

The analysis of the existing solutions in the market is an important step to evaluate the state of the art and potential improvements. Therefore, during this subsection a combined solution of heat recovery and heat pump created by Nilan is presented, including its relevant technical specifications [20].

The “Combi 302 Polar Top” solution developed by Nilan includes both active and passive heat recovery plus comfort cooling and heating within an air-to-air system solution. By other words, a passive heat recovery implies that sensible energy is recovered with low energy consumption and the active heat recovery is ensured by using a heat pump system that uses, as heat source, the remaining outlet air energy to provide heat for heating. The incorporation of a heat recovery system means that no moisture transfer occurs and the supply air absolute humidity, during heating mode, remains constant. In Figure 2.9 and Figure 2.10, the system solutions for both heating and cooling modes are presented, respectively, as well as the nomenclature used (Figure 2.9). These representations were obtained by consulting the catalogue [20]. As it is shown in Figure 2.9, when the outdoor air conditions are those that imply frost formation, an electrical pre-heating element is used to avoid its formation. Despite this inefficient use of energy, in contrary with the typical defrost modes, the refrigerant cycle is not inverted, which increases the global efficiency of the process because the heat consumption due to this process becomes useful. During summer season, if the outdoor air conditions are better outside than inside, the fresh airstream has a possibility of by-passing the counter flow heat exchanger, in order to avoid the heating up of this airstream and the corresponding energy consumption.

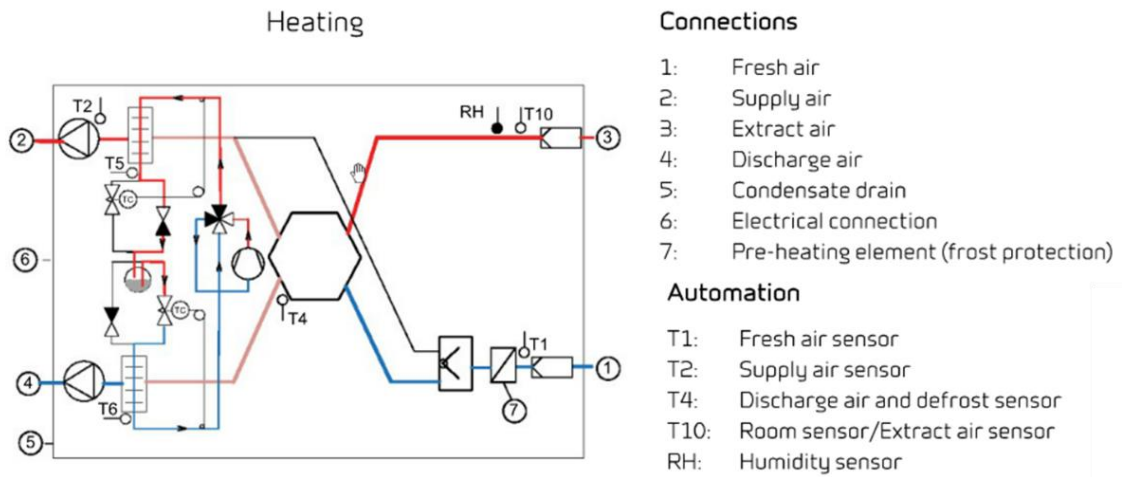


Figure 2.9 - System solution for heating mode (Adapted from Nilan catalogue [20]).

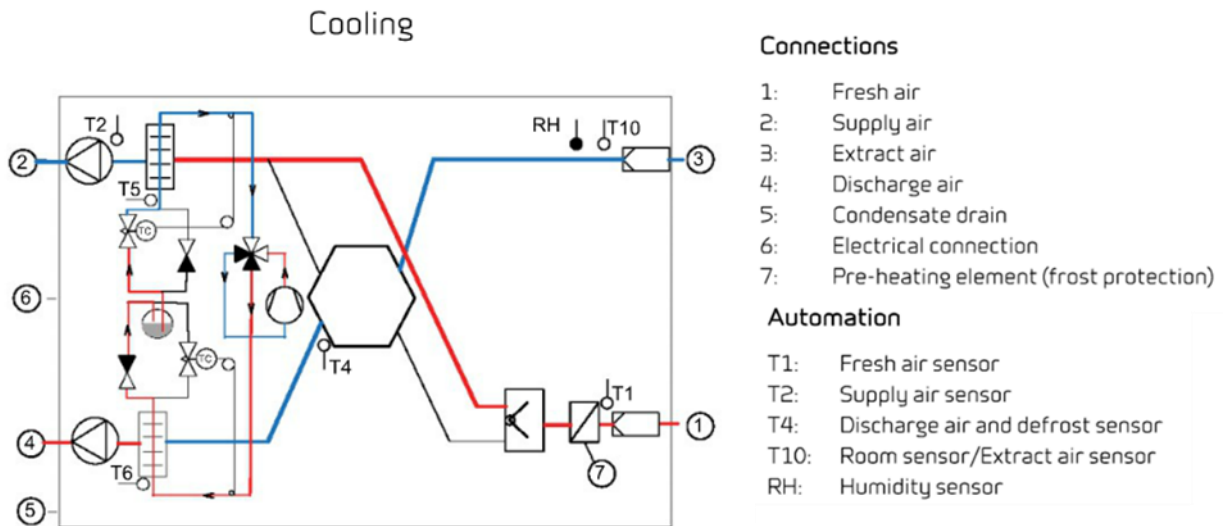


Figure 2.10 – System solution for cooling mode (adapted from Nilan catalogue [20]).

Regarding technical specifications, the catalogue of the solution was consulted and this information is presented in Table 2.2.

Table 2.2 – Technical specifications (from Nilan catalogue [20])

Dimensions	900 × 604 × 808 mm	Refrigerant filling	2 kg
Weight	85 kg	External leakage	< 0.54 %
Heat loss casing	32 W /-32 W	Internal leakage	< 1.71 %
Heat exchanger type	Counterflow heat exchanger	Supply voltage	230 V (± 10%), 50/60 Hz
Compression type	Piston compressor	Max. input/power	2.1 kW / 9.2 A
Fan type	EC, constant volume	Tightness class	IP31
Filter Class	Standard G4	Standby power	3.2 W
Duct connections	Φ 160 mm	Power consumption preheating element	1.2 kW
Refrigerant	R134a	Ambient temperature	-20 / +40 °C

2.3 Air-to-air Heat Exchangers

In HVAC systems, the air-to-air heat exchangers usage is increasing due to its advantages in terms of reducing energy consumptions. Thus, in order to recover the energy spent to ensure indoor air quality by mechanical ventilation, these devices may be considered as an efficient solution. In Figure 2.11, the principle solution of application of this technology is presented, in which a process of transferring energy (sensible or latent) between airstreams coming from bathrooms or kitchens and outdoors is performed. A supplementary fresh air heating or cooling process is also needed to guarantee the desired discharge conditions and a minimum filter class may be required when there is a direct contact between both airstreams in order to avoid migration of particles [21], but this supplied energy from the energy sources, e.g. heat pump or gas appliance, may be reduced with the installation of these air-to-air heat exchangers.

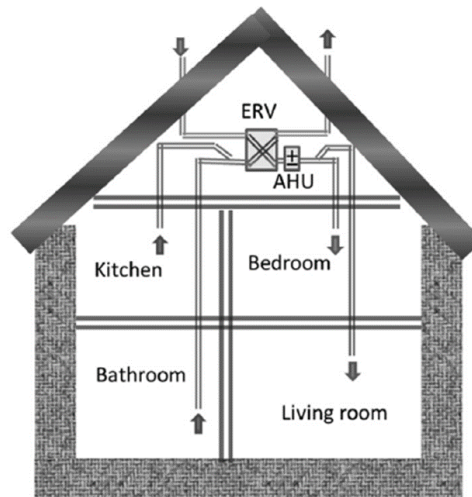


Figure 2.11 – Principle solution of using air-to-air heat exchangers together with the air handling unit.

There are several classifications of heat or energy exchangers, based on operation (moving or static parts) and others (e.g. heat exchangers when only sensible heat is recovered and energy exchangers when both sensible and latent heat exchange takes place) [21]. In this section, the heat and energy recovery ventilation systems are distinguished and analysed and then the advantages and disadvantages of both solutions are discussed in order to evaluate its performance and feasibility.

Firstly, in order to evaluate the effectiveness of the process, in Figure 2.12 a schematic representation of the heat exchanger airstreams (1 and 2) is presented.

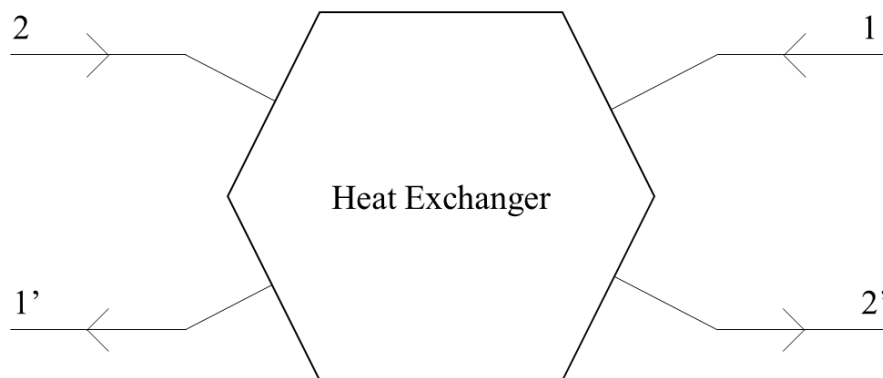


Figure 2.12 – Schematic representation of a heat exchanger.

Secondly, due to these two different ways of transferring energy (sensible and latent), it is important to define the parameters that evaluate the effectiveness of each process. Basically, the performance of the energy transfer is assessed by its effectiveness ε , defined as

$$\varepsilon = \frac{\text{actual transfer}}{\text{maximum possible transfer between airstreams}} \quad (2.7)$$

Considering adiabatic process, sensible, latent and total effectiveness, respectively ε_S , ε_L and ε_T , are obtained by the following expressions [9]:

$$\varepsilon_S = \frac{\dot{m}_1 \cdot c_{p1}}{\min(\dot{m}_1 \cdot c_{p1}; \dot{m}_2 \cdot c_{p2})} \cdot \frac{|T_1 - T_{1'}|}{|T_1 - T_2|} = \frac{\dot{m}_2 \cdot c_{p2}}{\min(\dot{m}_1 \cdot c_{p1}; \dot{m}_2 \cdot c_{p2})} \cdot \frac{|T_{2'} - T_2|}{|T_1 - T_2|} \quad (2.8)$$

$$\varepsilon_L = \frac{\dot{m}_1}{\min(\dot{m}_1; \dot{m}_2)} \cdot \frac{|\omega_1 - \omega_{1'}|}{|\omega_1 - \omega_2|} = \frac{\dot{m}_2}{\min(\dot{m}_1; \dot{m}_2)} \cdot \frac{|\omega_{2'} - \omega_2|}{|\omega_1 - \omega_2|} \quad (2.9)$$

$$\varepsilon_T = \frac{\dot{m}_1}{\min(\dot{m}_1; \dot{m}_2)} \cdot \frac{|h_1 - h_{1'}|}{|h_1 - h_2|} = \frac{\dot{m}_2}{\min(\dot{m}_1; \dot{m}_2)} \cdot \frac{|h_{2'} - h_2|}{|h_1 - h_2|} \quad (2.10)$$

where

\dot{m}_1 and \dot{m}_2 are the mass flow rates of each airstream,

c_{p1} and c_{p2} are the average constant pressure specific heat capacity of each airstream,

T_1 , T_2 , $T_{1'}$, and $T_{2'}$, are the temperature of the different points,

ω_1 , ω_2 , $\omega_{1'}$, and $\omega_{2'}$, are the absolute humidity of the different points, and

h_1 , h_2 , $h_{1'}$, and $h_{2'}$, are the specific enthalpy of the different points.

To evaluate these different parameters, a psychrometric chart is now analysed. Thus, in Figure 2.13 the evolution of both air streams are schematically represented and the values to quantify the respective effectiveness are presented.

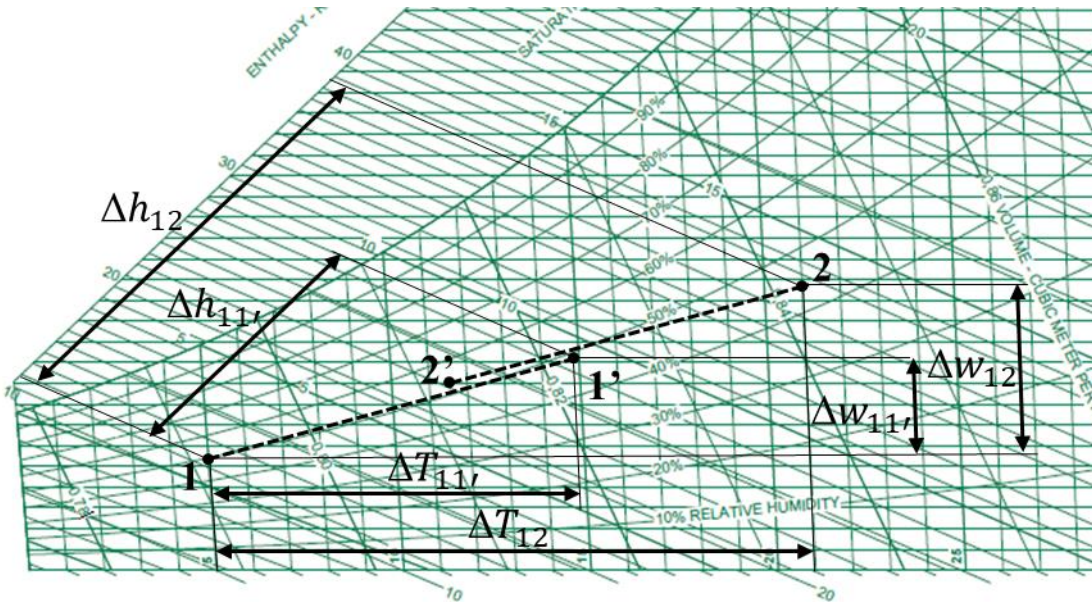


Figure 2.13 – Representation of psychrometric evolution by passing through enthalpy exchanger (Adapted from ASHRAE [6]).

In addition, both sensible and latent effectiveness may be expressed as a function of the variables presented in the following equation, by applying the heat-mass transfer analogy:

$$\varepsilon_S = f(NTU, C_{min}, \text{Flow arrangement}) \quad (2.11)$$

$$\varepsilon_L = f(NTU_L, \dot{V}_{min}, \text{Flow arrangement}) \quad (2.12)$$

where

NTU and NTU_L are the number of heat and mass transfer units, respectively,

C_{min} is the minimum heat capacity rate and

\dot{V}_{min} is the minimum volume flow rate.

The different types of recovery ventilation provide a balanced, i.e., the volume flow rate is considered the same for both inlet and outlet ducts, and measured the necessary amount of fresh air which comes into the house to cycle out pollutants, while also transferring energy (sensible or latent) from the exhausted indoor airstream with the incoming air. The relevance of its use has high dependency on the outdoor air conditions and, for example, with extreme outdoor conditions, such as very low and high temperatures during winter and summer season, respectively, the importance of its use becomes higher, due to the increase of the potential energy savings. On the other hand, in mild climates, the using of these technologies may not be cost effective. In the next subsections, air-to-air heat exchangers are distinguished regarding to its main objective and principle solution and the most relevant solutions are presented. Finally, both solutions are compared in order to evaluate its advantages and disadvantages.

2.3.1 Heat Recovery Ventilation

A recovery system is called heat recovery ventilation system (HRV) when only sensible heat is transferred, whereas moisture is not transferred, which causes a shortage of moisture inside homes during winter season and an excess of humidity during summer season. Consequently, the humidity amount is not controlled and it may lead to healthy problems or premature wear of building materials as it was mentioned in Section 1.2. In addition, a lack of moisture control leads to higher energy consumptions in both winter and summer seasons, due to ensure the needs of adding/removing latent heat to/from home. Despite this, and considering that the amount of indoor air humidity remains between an acceptable range, high efficient sensible heat recovery systems are considered a good solution to reduce the energy consumption of the residential market, due to its high sensible effectiveness.

There are different existing technologies, such as fixed plate, heat wheel, heat pipe, and run-around coil loop. In Figure 2.14 a fixed plate heat exchanger is presented, in which the supply and exhaust air pass through adjacent channels in cross-flow configuration. Another arrangement types are commonly used, such as parallel or counter-flow, and the surfaces are made of an impermeable material, e.g. aluminium.

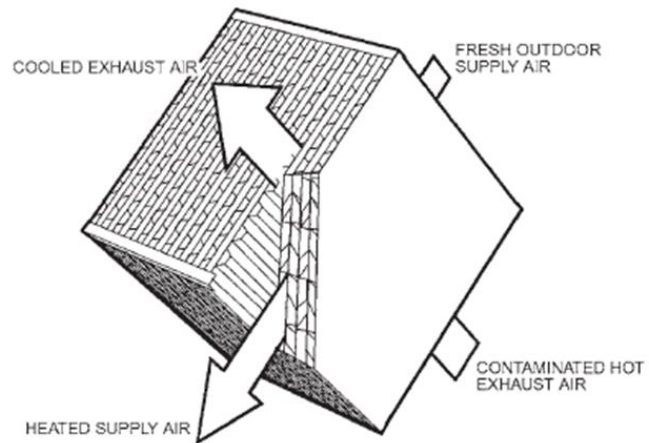


Figure 2.14 – Fixed plate heat exchanger (Adapted from ASHRAE Handbook) [6].

In Table 2.3, the main distinctive characteristics are presented in order to distinguish the different solutions.

2. Literature Review

Table 2.3 – Comparison of air-to-air heat recovery devices [10]

	Fixed Plate	Heat Wheel	Heat Pipe	Run-around Coil Loop
Airflow arrangements	Counterflow Cross-flow	Counterflow Parallel flow	Counterflow Parallel flow	-
Equipment size range, L/s	>25	25 to 35000	<50	>50
Sensible Effectiveness, %	50 to 80	50 to 85	45 to 65	45 to 65
Advantages	No moving parts; Low pressure drop; Easily cleaned.	Compact large sizes; Easily cleaned.	No moving parts.	Exhaust airstream can be separated from supply air.
Limitations	Large size at higher flow rates.	Some EATR ³ with purge.	Effectiveness limited by pressure drop and costs; Few suppliers.	Predicting performance requires accurate simulation model.

2.3.2 Energy Recovery Ventilation

A recovery system is called energy recovery ventilation system (ERV) when both sensible and latent heats are transferred, and then moisture is transferred between the airflows, from the higher amount to the lower as well as sensible heat [22]. Considering the moisture transfer

³ EATR is the Exhaust Air Transfer Ratio which represents the percentage of exhaust air that is transferred into fresh air

capacity of these devices, it is important to divide its analysis between the two working modes: heating and cooling. During the next analysis, only the moisture content is taken into account. During a typical winter season (heating mode), warm and wet exhaust air transfers moisture to the cold and dry fresh incoming air, increasing its temperature and absolute humidity. When the internal latent gain loads are low, ventilation process is directly related with a loss of humidity, which can be reduced by introducing an enthalpy heat exchanger, internal moisture remains between acceptable values and an external humidification is avoided. In Figure 2.15, these processes are schematically represented.

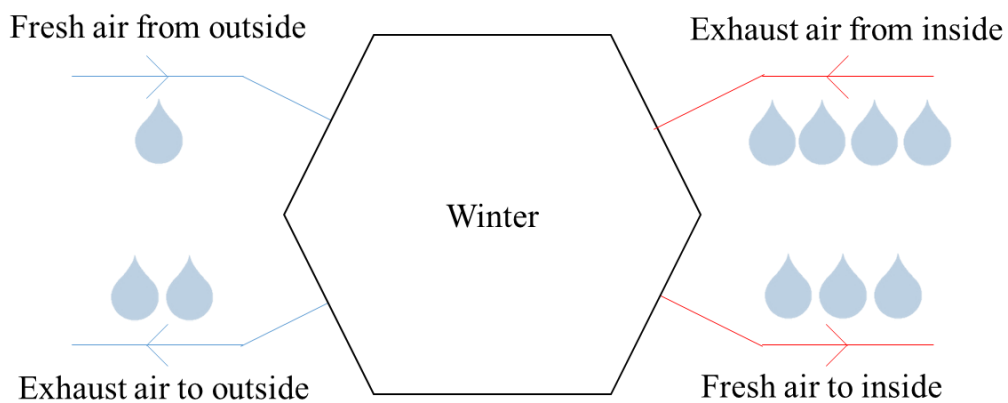


Figure 2.15 – Schematic representation of enthalpy exchanger during winter season.

During a typical summer season, the cold and dry exhaust airstream receives both heat and moisture from the warm and wet fresh incoming air, which reduces its absolute humidity and temperature and then decreases the additional cooling demand. It is particularly relevant when latent internal loads have a big impact on the overall cooling loads and then air needs to be cooled and dehumidified.

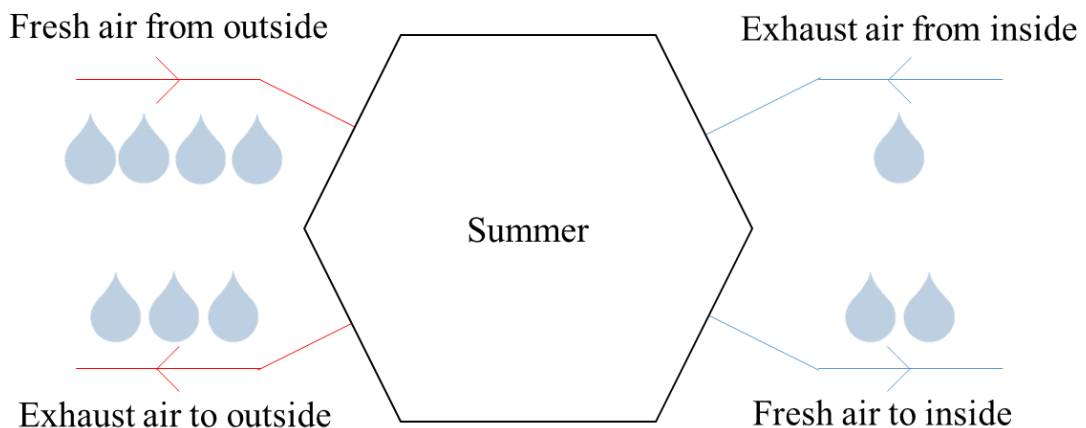


Figure 2.16 – Schematic representation of enthalpy exchanger during summer season.

Within the previous analysis, the worst typical cases of the different working modes were covered, but the situations when outdoor air conditions are better than indoors, e.g. lower temperature and humidity during summer nights, have to be considered to ensure that no energy wasting occurs.

Regarding membrane based enthalpy exchangers, moisture transfer occurs without transferring gases, odours and dirt, the membranes are antimicrobial, i.e., resistant against mould and bacteria, and are washable with water, which leads to a long operating life. The air leakage is also low, avoiding migration of particles. In Figure 2.17, a schematic representation of this energy recovery mechanism is presented.

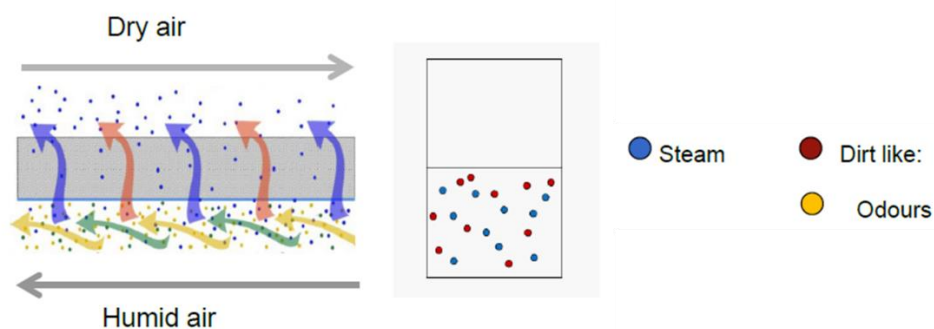


Figure 2.17 – Different transfer phenomena and barriers in MBEE [23].

Regarding energy wheel recovery devices, Figure 2.18 shows its principle of working, in which both heat and mass are transferred while the wheel rotates, which leads to high total effectiveness and to particles migration between the airstreams.

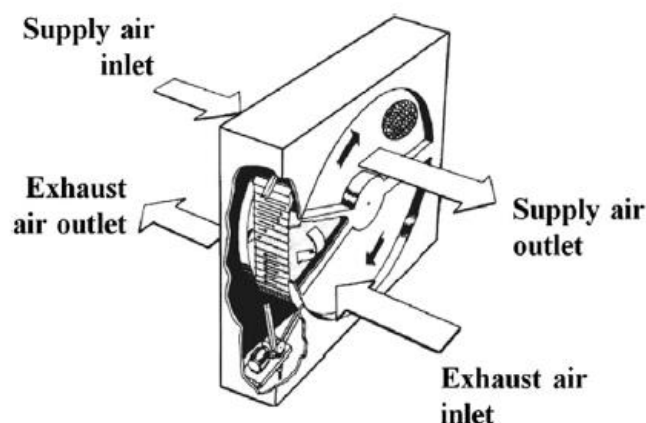


Figure 2.18 – Energy wheel [14].

Table 2.4 shows a comparison between the principle of air-to-air energy recovery devices in terms of its airflow arrangement, equipment size, sensible and latent effectiveness, and advantages and limitations.

2. Literature Review

Table 2.4 – Comparison of air-to-air energy recovery devices [10]

	Membrane Plate	Energy Wheel
Airflow arrangements	Counterflow Cross-flow	Counterflow Parallel flow
Equipment size range, L/s	>25	25 to 35000
Sensible Effectiveness, %	50 to 75	50 to 85
Latent Effectiveness, %	50 to 72	50 to 85
Advantages	No moving parts; Low air leakage; Moisture/ mass transfer.	Moisture/ mass transfer; Compact large sizes.
Limitations	Few suppliers; Long-term maintenance and performance unknown.	Some EATR without purge; Moving parts.

As can be observed in Table 2.4, in which energy wheels and membrane plate variants of transferring energy are compared, the use of the first one represents a gain of total effectiveness, both sensible and latent, and the capacity of using this device with higher volume flows. The main advantages of the membrane-based devices are the lower air leakage and exhaust air transfer ratio (EATR) and no moving parts. By analysing also the existing suppliers, the energy

wheels are more used within commercial applications, due to its higher complexity, i.e., the higher the complexity, the higher the costs, which makes this variant more relevant when the energy consumptions reach a minimum value, whereas in residential application, the membrane plate is considered more suitable [24].

Additionally, there is another way to guarantee moisture transferring which is not based on wall or membrane water permeability, in contrast with the other solutions presented in this section. It is a normal heat exchanger (without transfer moisture), in which a determined amount of water condensates and is accumulated. After reaching a certain level, a change of a valve position switches the airstream location and then the mass transfer phenomena occurs. It is expected that this solution may have several problems, such as transfer of dust and particles, which decreases the fresh incoming air quality, and freezing phenomena due to condensation below water freezing point.

When enthalpy and heat exchangers are compared, there is also another important phenomenon to take into account: frost formation tendency. The lower sensible effectiveness and the existence of moisture transfer imply a higher exhaust air outlet temperature and a continuous decrease of its dew point temperature without water condensation. Therefore, the energy recovery systems are more suitable to avoid frost formation inside the heat exchanger and the defrost operation mode is required for lower outdoor air temperatures.

3 System Modelling

In this section, the main components of the system are firstly presented within a functional diagram, in which each position is defined as well as the two airstream paths. It is also important to define the main components of the refrigerant circuit and the connections between both circuits. After, the most important technical requirements and specifications are presented, especially in terms of heat transfer and volume flow ranges. Then, the referred components are modelled by applying several heat and mass transfer concepts, in which boundary conditions and simplifying assumptions are considered. The analysis of the components starts in the heat and mass exchanger and ends in the refrigerant phase change heat exchangers, i.e., condenser and evaporator, in which both air and refrigerant sides are analysed.

3.1 Functional Diagram

In order to perform the modelling of the overall solution, the definition of a functional diagram becomes an obligatory step. In Figure 3.1, the main components are presented, their location is defined and two separated fluid circuits are analysed, air and refrigerant. The evaporator and the condenser ensure the connection between both parts, by using two air-to-refrigerant heat exchangers, as presented in Section 2.1.

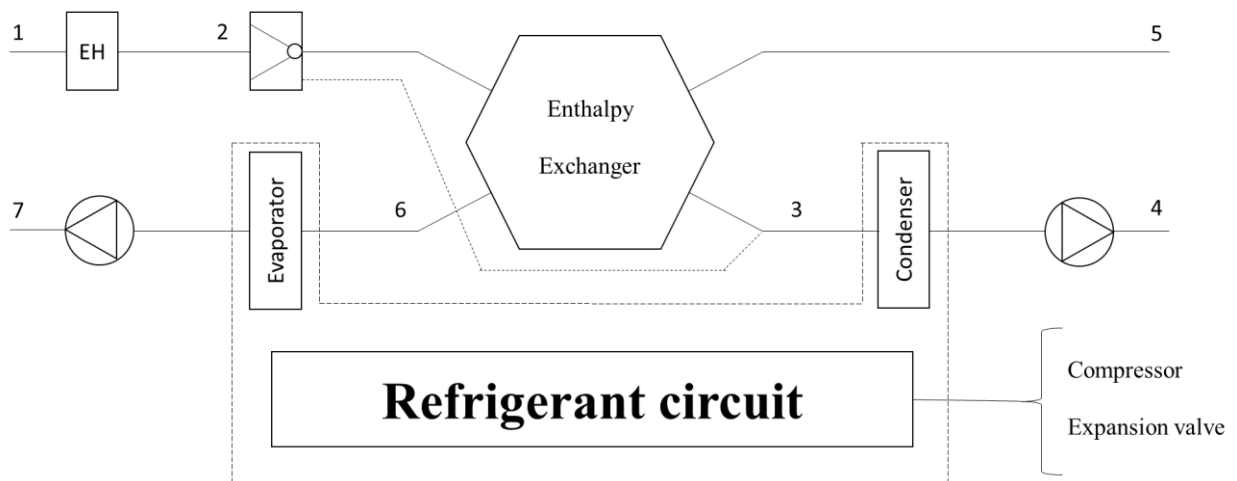


Figure 3.1 – Functional diagram of the solution.

In Table 3.1, a list of the required components is presented as well as the selection of those needed for a thermal modelling of the overall system. The using of the electrical heater, EH, is justified by the possibility of frost formation in the evaporator, which has to be avoided, but this component is not thermal modelled because its thermal performance is assumed constant, independent of the flow rate and based on the Joule effect.

3. System Modelling

Table 3.1 – List of components

Circuit	Component	Quantity	Thermal modelling
Air	Electrical Heater	1	No
	Damper	1	No
	Enthalpy Exchanger	1	Yes
	Fan	2	No
Air & Refrigerant	Evaporator	1	Yes
	Condenser	1	Yes
Refrigerant	Compressor	1	Yes
	Expansion Valve	1	No

3.2 Technical Requirements and Specifications

In this section, the main technical requirements and specifications in terms of volume flow rate range and heating or cooling output are defined. Regarding fresh air requirements and considering that it is expected to introduce this solution in the Swedish market, the minimum airflow value has to respect the legislation of this country. Therefore, the Swedish Building Code, BFS 2014:3-BBR 21, addresses requirements related to hygiene, health and environment and defines that ventilation systems shall be designed for air flux rates higher than $0.35 \text{ l}/(\text{s}\cdot\text{m}^2)$ in the cases of new buildings. Thus, for a residential use of floor areas between 60 and 200 m^2 , the airflow range is approximately $75\text{-}250 \text{ m}^3/\text{h}$ [5].

Considering the heating mode as a critical operation point, due to frost formation tendency, the power output of the compressor has to be dimensioned for the case of maximum flow rate and minimum outdoor air temperature from which water condensates starts freezing inside the evaporator. For the other conditions, the system has a wide range of working principle, in which it can work to transfer the maximum power output as possible, fixed speed compressor, or a compressor frequency input may be controlled in order to avoid undesired situations, such as frost formation due to low volume flow rate of air.

3.3 Modelling

After defining the functional diagram and the main technical requirements and specifications of the integration of an air-to-air enthalpy exchanger into a heat pump circuit, a thermal analysis of each component is now performed in order to evaluate not only the performance of the overall solution but also the influence of several dimensioning parameters. Firstly, considering each airstream path, the heat recovery system is modelled and, considering the analysis presented in Section 2.3, a membrane based enthalpy exchanger, MBEE, is selected, in which both heat and mass transfer processes are evaluated by considering the specifications of the component. Secondly, both air and refrigerant sides of air-to-refrigerant heat exchangers (evaporator and condenser) are analysed and finally the compressor closes the entire cycle. It is important to analyse these components by considering heat and mass transfer concepts as well as thermodynamic equilibrium.

Naturally, due to resources limitation, the main components of the circuit will be re-used from the samples, which are assembled regarding to the air-to-refrigerant actual developments inside the company. Considering the lower energy consumptions of this project solution, it is expected that it may cause an over dimensioning, especially in compressor dimensioning. The development of a user-friendly interface becomes now an important step to evaluate different scenarios in terms of flow rates, outdoor and indoor air conditions and fundamentally the analysis of the influence of different heat exchangers dimensioning parameters.

It is important to refer that all components modelling consists in a first geometry analysis in which symmetry conditions are defined and makes possible to represent the system in only one cell. Consequently, this symmetry implies an adiabatic condition and the overall system coefficients and parameters are obtained by multiplying the results for single cells by the number of cells.

3.3.1 Membrane Based Enthalpy Exchanger

When both heat and mass transfer processes occur at the same time, these phenomena are analysed by applying the well-known convective-mass transfer analogy in which the heat convective coefficients are firstly obtained, considering the flow conditions inside the channels, and after the mass transfer parameters are calculated by using dimensionless parameters, such as Lewis and Sherwood numbers. After this step, and considering the same transfer coefficients, the effectiveness-Number of Transfer Units method, $\varepsilon - NTU$, allows the calculation of the overall efficiency for all different flow patterns in terms of heat transfer. Figure 3.2 shows the different arrangements within the use of the selected component.

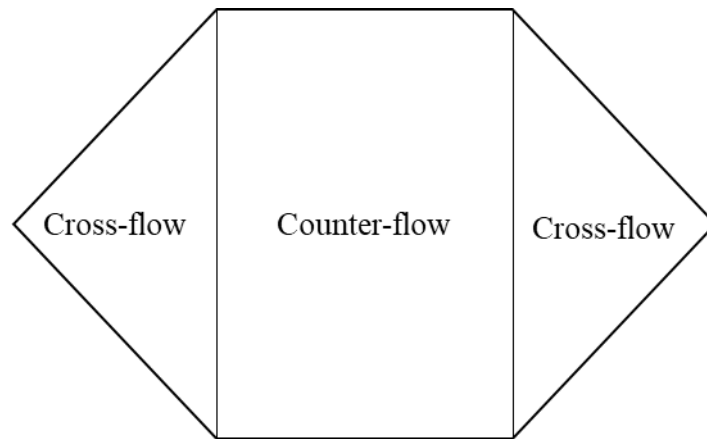


Figure 3.2 – Representation of the flow arrangements in the heat exchanger.

The mass transfer analysis is performed by applying the heat-mass transfer analogy in which heat convection is replaced by moisture convection, whereas heat conduction is replaced by moisture diffusion. Figure 3.3 shows the schematic representation of the referred analogy.

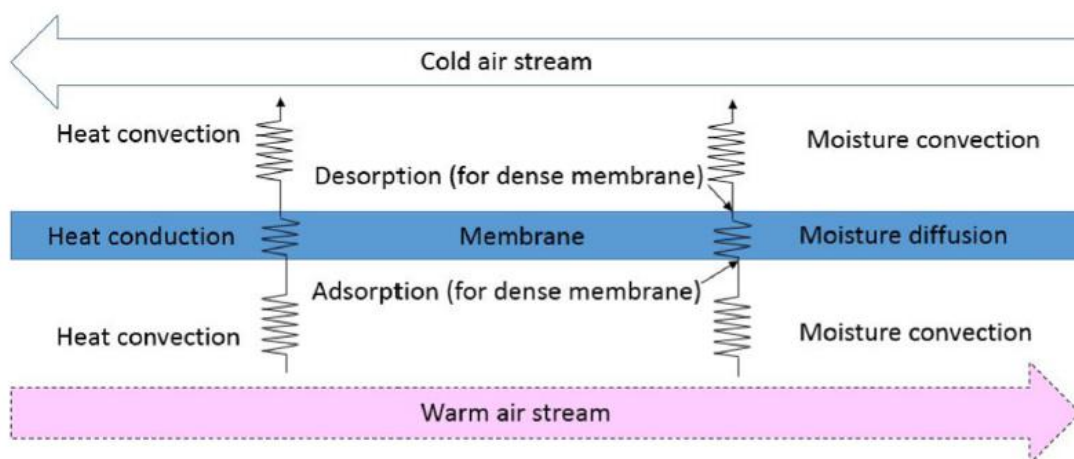


Figure 3.3 – A schematic of heat-mass transfer analogy in a MBEE [25].

Primarily, the procedure to obtain the overall heat transfer coefficient is presented, in which the system is analysed in terms of heat transfer perspective and the main heat transfer phenomena. After obtaining the convective heat transfer coefficient, the correspondent moisture convection coefficient is determined by applying the Chilton-Colburn analogy.

Heat transfer analysis

Overall heat transfer coefficient

A precise analysis of the heat exchanger is an important step to understand the main simplifications and the basic geometric restrictions, allowing the determination of the desired global heat transfer coefficient and then to evaluate heat transfer rates. When two fluid streams are transferring heat through a separating conductive wall, the use of reo-electrical analogy is

recommended, in which the resistance of all heat transfer mechanisms may be compared as an electrical resistance within an electric circuit. Therefore, the overall heat transfer coefficient, U , may be expressed as,

$$\frac{1}{UA} = R_{conv,1} + R_{cond,wall} + R_{conv,2} = \frac{1}{h_{c1} \cdot A_1} + \frac{\delta}{k_{wall} \cdot A} + \frac{1}{h_{c2} \cdot A_2} \quad (3.1)$$

where

$R_{conv,1}$, $R_{conv,2}$ are the convective resistances of each fluid stream,

$R_{cond,wall}$ is the conductive resistance of the wall,

δ and k_{wall} are the wall thickness and conductivity, respectively,

h_{c1} and h_{c2} are the convective coefficients of each fluid stream, and

A_1 and A_2 are the heat transfer surface area of each fluid stream.

From equation 3.1, only the convective coefficients are considered unknown for a given heat exchanger. Therefore, the procedure to obtain these parameters is now described. Firstly, due to the fact that the geometry of the channels is not circular, the hydraulic diameter, D_h , is calculated as a function of the channel cross section area, A_{ch} , and perimeter, P_{ch} ,

$$D_h = \frac{4 \cdot A_{ch}}{P_{ch}} \quad (3.2)$$

It is now possible to obtain Reynolds number Re , and then define the flow regime,

$$Re = \frac{v \cdot D_h}{\nu} \quad (3.3)$$

where

v is the fluid flow velocity inside the channel and

ν is the kinematic viscosity of the fluid.

The fluid flow velocity v , is obtained as

$$v = \frac{\dot{V}_{ch}}{A_{ch}} = \frac{\dot{V}_{tot}}{N_{ch} \cdot A_{ch}} \quad (3.4)$$

where

\dot{V}_{ch} and \dot{V}_{tot} are the channel and total volume flow and


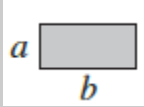
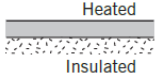

N_{ch} is the number of channels.

Considering a laminar regime ($Re < 2300$), it is possible to obtain the Nusselt number as a function of the cross section for fully developed laminar flow, as well as friction factor f . This information is presented in Table 3.2, in which there are two different values for Nusselt

3. System Modelling

number, depending on the border condition, i.e., constant flow rate or wall temperature, respectively.

Table 3.2 – Nusselt number and friction factor as a function of cross section [13]

Cross Section	b/a	<i>Nu</i>		
		$(q''_s \approx const)$	$(T_s \approx const)$	(fRe)
	-	4.36	3.66	64
	1.0	3.61	2.98	57
	1.43	3.73	3.08	59
	2.0	4.12	3.39	62
	3.0	4.79	3.96	69
	4.0	5.33	4.44	73
	8.8	6.49	5.60	82
	∞	8.23	7.54	96
	∞	5.39	4.86	96
	-	3.11	2.49	53

Additionally, for the same fluid with similar heat capacities, the quasi counter-flow heat exchanger represents the constant surface heat transfer rate border condition to obtain the Nusselt number Nu . Considering the typical high value of ratio b/a , the value of the Nusselt number is equal to 8.23. After defining this non-dimensional number (Nu), the convective coefficient is easily calculated by using the following equation:

$$Nu = \frac{h_c \cdot D_h}{k_f} \Rightarrow h_c = \frac{k_f \cdot Nu}{D_h} \quad (3.5)$$

ε -NTU analysis

After defining the convective coefficients, the Number of Transfer Units, NTU , is calculated and then it is possible to obtain the effectiveness of the process depending on the flow arrangement. Therefore, the NTU is defined as

$$NTU = \frac{UA}{C_{min}} \quad (3.6)$$

For a cross flow arrangement, the sensible effectiveness correlation, $\varepsilon_{s,cross}$, is defined as [13]

$$\varepsilon_{s,cross} = 1 - \exp \left\{ \frac{NTU_{cross}^{0.22}}{\frac{C_{min}}{C_{max}}} \left[\exp \left(-\frac{C_{min}}{C_{max}} NTU_{cross}^{0.78} \right) - 1 \right] \right\} \quad (3.7)$$

where NTU_{cross} is calculated for the cross-flow arrangement section of the heat exchanger. Similarly, for a counter-flow arrangement, the sensible effectiveness correlation, $\varepsilon_{s,count}$, is defined as [13]

$$\varepsilon_{s,count} = \frac{1 - \exp \left[-NTU_{count} \left(1 - \frac{C_{min}}{C_{max}} \right) \right]}{1 - \frac{C_{min}}{C_{max}} \exp \left[-NTU_{count} \left(1 - \frac{C_{min}}{C_{max}} \right) \right]} \quad (3.8)$$

where NTU_{count} is calculated for the counter-flow arrangement section of the heat exchanger. Considering also the combinations of different flow arrangements, the overall sensible effectiveness, ε_s , is obtained as a function of the previously determined parameters [13]:

$$\varepsilon_s = \frac{\varepsilon_{s,cross} \cdot A_{cross} + A_{count} \cdot \varepsilon_{s,count}}{A_{cross} + A_{count}} \quad (3.9)$$

Mass transfer analysis

Overall mass transfer coefficient

After defining the convective coefficients, the procedure to obtain the mass transfer coefficients is explained, through the use of the heat-mass analogy to determine the desired parameters. The overall mass transfer coefficient, U_m , is defined as

$$\frac{1}{U_m A} = R_{m,1} + R_{diff,wall} + R_{m,2} = \frac{1}{h_{m,1} A_1} + R_{diff,wall}(\delta, D_{w-m}, A) + \frac{1}{h_{m,2} A_2} \quad (3.10)$$

where

$R_{m,1}$ and $R_{m,2}$ are the mass convective resistances,

$R_{diff,wall}$ is the wall permeability resistance,

D_{w-m} is the diffusivity of water in membrane, and

$h_{m,1}$ and $h_{m,2}$ are the mass convective coefficients.

While in the thermal conductive analysis, the properties of the wall are constant and independent of the intake air conditions, the mass transfer process through the membrane is more complex and the diffusivity of water in the membrane D_{w-m} , is not constant but a function

of the membrane material and intake air properties, and this component has to be analysed separately [21, 26]. The moisture mass flow rate through the membrane is defined as

$$\dot{m}_w = \frac{(w_s - w_{ms})}{R_{diff,wall}} = \frac{D_{wm}}{\delta} (\theta_{me} - \theta_{ms}) \quad (3.11)$$

where

w_s and w_{ms} are the moisture content in supply airstream and the moisture at the membrane in supply air side.

θ_{me} and θ_{ms} are the moisture uptake in membrane in the exhaust and supply air, respectively.

The moisture uptake is defined as [21, 26]

$$\theta = \frac{w_{max}}{1 - C + \frac{C}{\phi}} \quad (3.12)$$

where

w_{max} is the maximum water uptake of membrane material,

C is the shape factor of the material and

ϕ is the air relative humidity.

The moisture uptake in the exhaust airstream is written as [21, 26]

$$\theta_{me} = \theta_{ms} + \left. \frac{\partial \theta}{\partial \phi} \right|_{ms} \Delta \phi = \theta_{ms} + \left. \frac{\partial \theta}{\partial \phi} \right|_{ms} (\phi_{ms} - \phi_{me}) \quad (3.13)$$

The moisture flow rate is written by substituting equation 3.13 into equation 3.11 as follows [21, 26]

$$\dot{m}_w = \frac{D_{wm}}{\delta} \left(\left. \frac{\partial \theta}{\partial \phi} \right|_{ms} \right) (\phi_{ms} - \phi_{me}) \quad (3.14)$$

The differentiation of equation 3.12 gives [21, 26]

$$\left(\frac{\partial \theta}{\partial \phi} \right) = \frac{w_{max} C}{\left(1 - C + \frac{C}{\phi} \right)^2 \phi^2} \quad (3.15)$$

Considering the relation between moisture content and relative humidity defined in Appendix A, the moisture diffusive resistance is expressed as [21, 26]

$$R_{diff,wall} = \frac{\delta}{D_{wm}} \frac{10^6}{\exp\left(\frac{5294}{T}\right) \cdot \left(\frac{\partial \theta}{\partial \phi} \right)} = \frac{\delta}{D_{wm}} \frac{10^6 \cdot \left(1 - C + \frac{C}{\phi} \right)^2 \phi^2}{\exp\left(\frac{5294}{T}\right) \cdot w_{max} C} = \frac{\delta}{D_{wm}} \psi \quad (3.16)$$

where ψ is a dimensionless parameter which reflects the effect of operating conditions on the membrane mass diffusivity resistance. Considering the mass diffusivity of water in air, the Lewis number is defined as

$$Le = \frac{\alpha}{D_{w-a}} \quad (3.17)$$

where

α is the air thermal diffusivity and

D_{w-a} is the water diffusivity in air.

Secondly, the Sherwood number is defined as

$$Sh = \frac{h_m \cdot D_h}{D_{w-a}} \quad (3.18)$$

Finally, considering the Chilton-Colburn analogy [25], when the Nusselt, Lewis and Sherwood numbers are known, the mass convective coefficient is then obtained [13, 26, 27]:

$$Sh = Nu \cdot Le^{-\frac{1}{3}} \Leftrightarrow \frac{h}{h_m} = \frac{k \cdot Le^{-\frac{1}{3}}}{D_{w-a}} \quad (3.19)$$

ε_L - NTU_L analysis

Similarly, it is possible to obtain the correlation between the effectiveness and the Number of Transfer Units regarding to the mass transfer phenomena. Therefore, the Number of Transfer Units NTU_L , is obtained by equation 3.20

$$NTU_L = \frac{U_m A}{\dot{V}_{min}} \quad (3.20)$$

where \dot{V}_{min} is the minimum volume flow of both fluid streams. For a cross flow arrangement, the latent effectiveness correlation, $\varepsilon_{L,cross}$, is defined as

$$\varepsilon_{L,cross} = 1 - \exp \left\{ \frac{NTU_{L,cross}^{0.22}}{\frac{\dot{V}_{min}}{\dot{V}_{max}}} \left[\exp \left(-\frac{\dot{V}_{min}}{\dot{V}_{max}} NTU_{L,cross}^{0.78} \right) - 1 \right] \right\} \quad (3.21)$$

where $NTU_{L,cross}$ is calculated for the cross-flow arrangement section of the heat exchanger. Similarly, for a counter-flow arrangement, the sensible effectiveness correlation, $\varepsilon_{L,count}$, is defined as

$$\varepsilon_{L,count} = \frac{1 - \exp\left[-NTU_{L,count}\left(1 - \frac{\dot{V}_{min}}{\dot{V}_{max}}\right)\right]}{1 - \frac{\dot{V}_{min}}{\dot{V}_{max}} \exp\left[-NTU_{L,count}\left(1 - \frac{\dot{V}_{min}}{\dot{V}_{max}}\right)\right]} \quad (3.22)$$

where $NTU_{L,count}$ is calculated for the counter-flow arrangement section of the heat exchanger. Considering also the combination of different flow arrangements, the overall latent effectiveness, ε_L , is obtained as a function of the parameters previously calculated [13]:

$$\varepsilon_L = \frac{\varepsilon_{L,cross} \cdot A_{cross} + A_{count} \cdot \varepsilon_{L,count}}{A_{cross} + A_{count}} \quad (3.23)$$

After defining the outlet conditions of both airstreams, the thermal performance analysis of the air-to-refrigerant heat exchangers becomes an important step. Therefore, in the next sections, the evaporator and the condenser are defined in terms of dimensioning analysis.

3.3.2 Evaporator

The evaporator heat transfer process may be divided in two fluid flow sides: air and refrigerant. The overall heat transfer coefficient is defined as

$$\frac{1}{UA} = R_{conv,air} + R_{cond,wall} + R_{conv,ref} = \frac{1}{h_{air}A_{air}} + \frac{\delta}{k_{wall} \cdot A} + \frac{1}{h_{ref}A_{ref}} \quad (3.24)$$

Considering that frost formation is one of the most avoidable phenomena that occur within the use of heat pump appliances, the evaporator is firstly analysed. Therefore, this analysis is divided in two, considering both fluid streams passing through the heat exchanger. Thus, the air side of this component is firstly defined.

Air side

Regarding the air-to-refrigerant heat exchangers, the fin and tube variant is the most used, due to low air convective coefficients, which decrease the overall effectiveness of the heat transfer process. Generally, these heat exchangers are composed of continuous plate fins disposed in parallel with a determined tube layout, whether in inline or as staggered configuration, with a clear better performance for the staggered layout [9, 28, 29]. Using a staggered arrangement of tubes, the flow across these banks of tubes is represented in Figure 3.4.

3. System Modelling

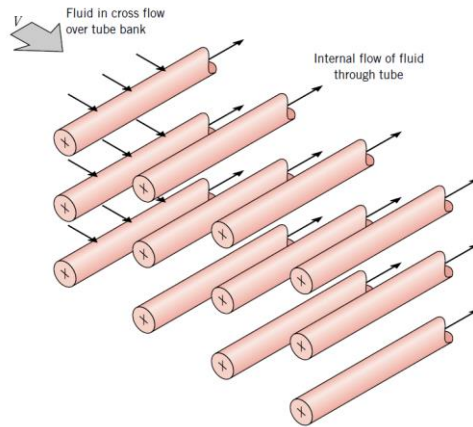


Figure 3.4 – Air flow over staggered tube arrangement [13].

Basically, this configuration is characterized by the tube diameter d , as well as the spacing between tube centers measured in both directions: transverse pitch, S_T , and longitudinal pitch S_L . These three parameters, as well as the air flow velocity, are especially important in boundary layer separation effect and in wake interactions, which consequently influence convection heat transfer [13]. Figure 3.5 shows the representation of these variables.

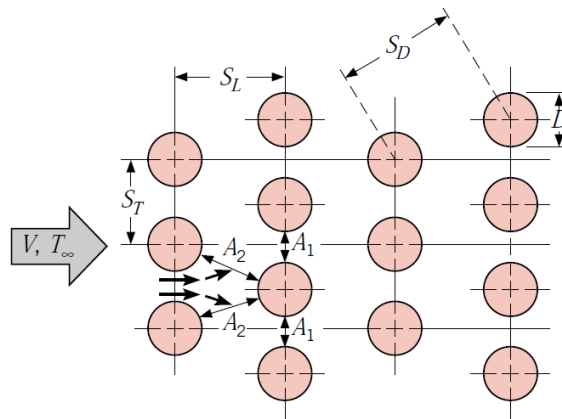


Figure 3.5 – Staggered tube arrangement parameters [13].

After doing an analysis about the geometry, the desired average heat transfer coefficient for the entire tube bank is obtained by looking to the work developed by Zukauskas who proposed a correlation the following [13]

$$Nu_D = C_1 \cdot C_2 \cdot Re_{D,max}^m \cdot Pr^{0.36} \cdot \left(\frac{Pr}{Pr_s}\right)^{\frac{1}{4}}, \quad \begin{cases} 0.7 \leq Pr \leq 500 \\ 10 \leq Re_{D,max} \leq 2 \times 10^6 \end{cases} \quad (3.25)$$

where

C_1 , C_2 e m are constants that are dependent on the air flow conditions,

$Re_{D,max}$ is the Reynolds number based on the maximum fluid velocity and

Pr and Pr_s are the Prandlt number evaluated at different conditions.

3. System Modelling

It is important to refer that all properties are evaluated at the arithmetic mean of the fluid inlet and outlet temperatures, except Pr_s , which is evaluated at surface arithmetic mean temperature. The properties are defined in Appendix A. The $Re_{D,max}$ depends on the plane in which the maximum fluid velocity occurs, and it is given by

$$Re_{D,max} = \frac{v_{max} \cdot D}{\nu}, v_{max} = \begin{cases} \frac{S_T}{S_D - D} v, & S_D < \frac{S_T + D}{2} \\ \frac{S_T}{S_T - D} v, & S_D \geq \frac{S_T + D}{2} \end{cases} \quad (3.26)$$

In Table 3.3, the values of C_1 and m are given for the defined range of $Re_{D,max}$, whereas Table 3.4 shows the C_2 values if there are 20 or fewer rows of tubes. If the number of rows is 20 or higher, the value of this parameter is equal to 1.

Table 3.3 – Constants of equation (3.25) for the tube bank [13]

$Re_{D,max}$	C_1	m
$10-10^2$	0.90	0.40
10^2-10^3	1.00	0.40
$10^3-2 \times 10^5 \left(\frac{S_T}{S_L} < 2 \right)$	$0.35 \left(\frac{S_T}{S_L} \right)^{1/5}$	0.60
$10^3-2 \times 10^5 \left(\frac{S_T}{S_L} > 2 \right)$	0.40	0.60
$2 \times 10^5-10^6$	0.022	0.84

Table 3.4 – Constants of equation (3.25) depending on N_L for $N_L < 20$ [13]

N_L	1	2	3	4	5	7	10	13	16
C_2	0.64	0.76	0.84	0.89	0.92	0.95	0.97	0.98	0.99

The correlation proposed by Zukauskas is not continuous through the respective domain of Reynolds number, due to the using of the constants presented on Table 3.3, which implies that the values of the convective coefficient increase when the flow regime changes. Therefore, other correlation was found in order to compare the different values and to apply those that fit better within the real behaviour of the heat exchanger. Hausen correlated different test measurements, and the Nusselt number is defined for a staggered arrangement for a tube bank consisting of less than 16 rows as [30, 31]:

3. System Modelling

$$Nu_D = 0.35 \cdot F_a \cdot Re_{D,max}^{0.57} \cdot Pr^{0.31} \quad (3.27)$$

$$F_a = 1 + 0.1 \cdot a + \frac{0.34}{b} \quad (3.28)$$

where

F_a is the arrangement factor

a is the dimensionless longitudinal pitch ($a = S_L/D$) and

b is the dimensionless transversal pitch ($b = S_T/D$).

Taking into account the increase of surface area caused by using fins, inside which there is a temperature distribution, the air side convective resistance has to be corrected as follows

$$R_{conv,air} = \frac{1}{h_{air}A_{air}} = \frac{1}{h_{air} \cdot A_{tot} \cdot \eta_s} \quad (3.29)$$

where

A_{tot} is the total outside surface area and

η_s is the finned surface efficiency.

The convective coefficient is assumed the same as the calculated without taking into account the fins arrangement. The finned surface efficiency, η_s , is given as [9]

$$\eta_s = 1 - \frac{A_f}{A_{tot}}(1 - \eta_f) \quad (3.30)$$

where

A_f is the area of fins and

η_f is the fin efficiency.

This fin efficiency, η_f , may be described as the ratio between actual heat transfer and heat transfer when fins are at base temperature. In order to express the fin efficiency of continuous plate fins, the fin is divided in unity cells, which are determined by defining the adiabatic zones, considering that all tubes are at the same temperature. Figure 3.6 shows the representation of the unity cells for the staggered arrangement of tubes.

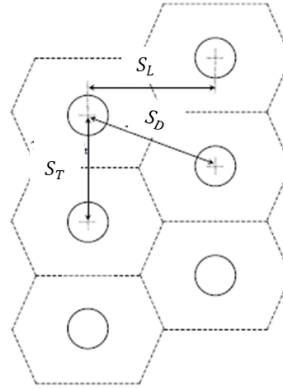


Figure 3.6 – Adiabatic zones [28].

When the fin unity cell geometry is hexagonal (staggered arrangement), the fin efficiency may be calculated using two different methods [28]:

- Equivalent circular radius: the fin efficiency is treated as for a circular fin, in which two approaches are possible. The first one consists in defining a circular fin, which has the same surface area as the hexagonal fin. The second one is known as Schmidt method and it is based on developed correlations to find an equivalent circular fin, which has the same fin efficiency as the hexagonal fin.
- Sector method: the plain fin surface is divided in several circular sectors, which fit the fin geometry profile and are generated from the fin center. The sector efficiency is analytically evaluated from the circular fin efficiency equations, using Bessel functions to determine the exact solution.

The most accurate method is the sector method. Nevertheless, the equivalent circular fin method is simpler and then commonly used. Considering tubes spacing in both directions similar, the equivalent circular radius method is used and the error caused by using this approximation is neglected. The equivalent circular radius, $r_{f,eq}$, is defined as [28]

$$r_{f,eq} = 1.27 \cdot \frac{S_T}{2} \sqrt{\frac{2 \cdot S_D}{S_T} - 0.3} \quad (3.31)$$

As mentioned before, the analytical solution for a circular fin, with adiabatic fin tip, is solved by using the modified Bessel functions of first and second kind. In order to simplify this circular efficiency formulation, i.e., to avoid the use of these functions, there is a formulation proposed in literature in which the error between the analytical solution and the approximation is lower than 2% over the typical range of conditions $r_{f,eq}/r \leq 6$ and $m \cdot (r_{f,eq} - r) < 2.5$ [28, 29]. The fin efficiency, η_f , is then obtained through the following equations.

$$\phi = \left(\frac{r_{f,eq}}{r} - 1\right) \left[1 + \left(0.3 + \left(\frac{m \cdot (r_{f,eq} - r)}{2.5}\right)^{1.5 - \frac{1}{12} \frac{r_{f,eq}}{r}} \left(0.26 \left(\frac{r_{f,eq}}{r}\right)^{0.3} - 0.3\right) \right) \ln\left(\frac{r_{f,eq}}{r}\right) \right] \quad (3.32)$$

$$m = \sqrt{\frac{2 \cdot h_{air}}{k_{fin} \cdot \delta_{fin}}} \quad (3.33)$$

$$\eta_f = \frac{\tanh(m \cdot r \cdot \phi)}{m \cdot r \cdot \phi} \cos(m \cdot r \cdot \phi) \quad (3.34)$$

where

r is the tube radius and

k_{fin} and δ_{fin} are the fin material thermal conductivity and thickness, respectively.

Considering outlet air temperatures lower than the inlet air dew point temperature, the water condensation occurs around tubes and fins inside the evaporator and this phenomenon is not evaluated.

Refrigerant side

The refrigerant side of the evaporator is now analysed in terms of its convective coefficient. It is assumed that no subcooled liquid enters in this component and the outlet state is saturated vapour. This last assumption represents an error because the compressor requires few superheated degrees at its entrance to guarantee dry compression. However, this amount of energy may be transferred from another source, e.g. outside air due to a lack of insulation, and it is defined as non-useful superheat. Considering tubes disposed horizontally, the boiling heat transfer coefficient, h_b , is the largest of these, h_{b1} , h_{b2} , h_{b3} and h_{b4} , given by the following equations [10]:

$$h_{b1} = 230Bo^{0.5} \cdot h_f \quad (3.35)$$

$$h_{b2} = 1.8 \cdot [Co(0.38 \cdot Fr_l^{-0.3})^n]^{-0.8} \cdot h_f \quad (3.36)$$

$$h_{b3} = F \cdot Bo^{0.5} \exp\{2.47 \cdot [Co(0.38 \cdot Fr_l^{-0.3})^n]^{-0.15}\} \cdot h_f \quad (3.37)$$

$$h_{b4} = F \cdot Bo^{0.5} \exp\{2.47 \cdot [Co(0.38 \cdot Fr_l^{-0.3})^n]^{-0.1}\} \cdot h_f \quad (3.38)$$

The remaining parameters, for the equations above, are obtained by the following equations:

$$h_f = 0.023Re_l^{0.8}Pr_l^{0.4} \left(\frac{k_l}{d}\right) \quad (3.39)$$

$$Re_l = \frac{G \cdot (1 - x) \cdot d}{\mu_l} \quad (3.40)$$

$$Bo = \frac{q''}{h_{lv} \cdot G} \quad (3.41)$$

$$Fr_l = \frac{G^2}{\rho_l^2 \cdot d \cdot g} \quad (3.42)$$

$$Co = \left(\frac{1 - x}{x}\right)^{0.8} \left(\frac{\rho_v}{\rho_l}\right)^{0.5} \quad (3.43)$$

$$F = \begin{cases} 14.70, & Bo < 0.0011 \\ 15.43, & Bo \geq 0.0011 \end{cases} \quad (3.44)$$

$$n = \begin{cases} 0, & Fr_l > 0.04 \\ 1, & Fr_l \leq 0.04 \end{cases} \quad (3.45)$$

where all parameters with 'l' and 'v' subscripts are obtained at saturated liquid and vapour, for a given saturation temperature [10]. Table 3.5 shows the correlation's verified range of tube diameter d , relative pressure p_r , Boiling number Bo , mass flux G , and the different fluids.

Table 3.5 – Verified range of boiling correlations [10]

D	1.1 to 27.1 mm
$p_r = p_{sat}/p_{crit}$	0.0053 to 0.78
$Bo \times 10^4$	0.22 to 74.2
G	10 to 11070 kg/(m ² s)
Fluids	Water, halocarbons, cryogenes, chemicals

ε -NTU analysis

As mentioned before, for convenience, the refrigerant is assumed to evaporate at a constant temperature inside the heat exchanger tubes. Therefore, the quotient between smaller and greater heat capacity rates between refrigerant and air, C_{min}/C_{max} , is equal to zero. Therefore, the heat transfer effectiveness is calculated as

$$\varepsilon = 1 - \exp(-NTU) \quad (3.46)$$

The number of transfer units, NTU , is calculated as

$$NTU = \frac{UA}{C_{air}} \quad (3.47)$$

where C_{air} is the air heat capacity rate.

After the calculation of the heat transfer coefficients, it is possible to obtain the outlet air conditions, for a given evaporation temperature, by the following equation

$$\varepsilon = \frac{q_{real}}{q_{max}} = \frac{\dot{m}_{air}(h_{air,in} - h_{air,out})}{\dot{m}_{air}(h_{air,in} - h_{air,out,@Tevap})} \quad (3.48)$$

where

$h_{air,in}$ and $h_{air,out}$ are the inlet and outlet air enthalpy and

$h_{air,out,@Tevap}$ is the hypothetical air enthalpy at evaporation temperature.

If the evaporation temperature is lower than inlet air dew point temperature, the relative humidity at this point is considered equal to one and the bypass effect is neglected. This bypass effect represents the non-uniformity of temperature within the airstream.

3.3.3 Condenser

After defining the heat transfer coefficient for both air and refrigerant sides of the evaporator, the condenser is now analysed. The air heat coefficient is obtained by using the same procedure as in the previous section, whereas a different approach is needed for the refrigerant side, due to the obvious difference in terms of flow pattern and evolution. Considering the internal flow in plain round tubes, the condensing heat transfer coefficient, h_c , is given by the following equations, depending on the flow regime [32, 33]:

$$h_c = \begin{cases} h_I, & \text{Regime I} \\ h_I + h_{Nu}, & \text{Regime II} \\ h_{Nu}, & \text{Regime III} \end{cases} \quad (3.49)$$

where h_I and h_{Nu} are defined as

$$h_I = h_{LT} \cdot \left(\frac{\mu_f}{14 \cdot \mu_g} \right)^n \cdot \left((1-x)^{0.8} + \frac{3.8 \cdot x^{0.76} \cdot (1-x)^{0.04}}{p_r^{0.38}} \right) \quad (3.50)$$

$$h_{Nu} = 1.32 \cdot Re_{LS}^{-\frac{1}{3}} \cdot \left(\frac{\rho_l \cdot (\rho_l - \rho_g) \cdot g \cdot k_f^3}{\mu_f^2} \right)^{\frac{1}{3}} \quad (3.51)$$

$$n = 0.0058 + 0.557 \cdot p_r \quad (3.52)$$

$$h_{LT} = 0.023 \cdot Re_{LT}^{0.8} \cdot Pr_f^{0.4} \quad (3.53)$$

$$Re_{LT} = \frac{G \cdot D \cdot Re_{LS}}{\mu_f} = \frac{G \cdot D \cdot (1-x)}{\mu_f} \quad (3.54)$$

$$Re_{GS} = \frac{G \cdot D \cdot x}{\mu_g} \quad (3.55)$$

As presented in equation (3.49), the heat transfer coefficient is defined as a function of the flow regime. Thus, for horizontal tubes, the different variants are now specified [32]:

Regime III if Re_{LS} and Re_{GS} both < 500 or if

$$J_g \leq 0.95 \cdot (1.254 + 2.27 \cdot Z^{1.249})^{-1} \quad (3.56)$$

Regime I if

$$J_g \geq 0.98 \cdot (Z + 0.263)^{-0.62} \quad (3.57)$$

Else Regime II

where J_g is the dimensionless vapour velocity and Z is the Shah parameter, which are defined as [32]

$$J_g = \frac{x \cdot G}{(g \cdot D \cdot \rho_g \cdot (\rho_l - \rho_g))^{0.5}} \quad (3.58)$$

$$Z = \left(\frac{1}{x} - 1\right)^{0.8} p_r^{0.4} \quad (3.59)$$

In Table 3.6 the verified range of internal diameter d , relative pressure p_r , mass flux G , vapour quality x , and fluids is presented.

Table 3.6 – Verified range of condensing correlations [10, 32]

D	2 to 49 mm
p_r	0.0008 to 0.905
G	4 to 820 kg/(m ² s)
x	0.01 to 0.99
Fluids	22 fluids, including water, hydrocarbons, halocarbons

ε -NTU analysis

Similarly to what has been presented for the evaporator analysis, the refrigerant is assumed to condensate at a constant temperature inside the heat exchanger. This approximation can generate errors, due to the high difference between saturation temperature and condenser inlet temperature, but considering that enthalpy difference is not as high such non-isothermal heat exchanger fraction is neglected. In addition, the subcooling degrees may cause differences on the heat coefficient value, but it is also neglected in a first analysis. Therefore, the quotient

between smaller and greater heat capacities is equal to zero. Thus, the heat transfer effectiveness is defined as

$$\varepsilon = 1 - \exp(-NTU) \quad (3.60)$$

and the number of transfer units, NTU , is also calculated as

$$NTU = \frac{UA}{C_{air}} \quad (3.61)$$

After the calculation of the heat transfer coefficients, it is possible to obtain the outlet air conditions, having the evaporation temperature, by the given equation

$$\varepsilon = \frac{q_{real}}{q_{max}} = \frac{\dot{m}_{air}(h_{air,in} - h_{air,out})}{\dot{m}_{air}(h_{air,in} - h_{air,out,@Tcond})} \quad (3.62)$$

where $h_{air,out,@Tcond}$ is the hypothetical air enthalpy at condensing temperature with the same absolute humidity of inlet air.

3.3.4 Compressor

Regarding the dimensioning process of the compressor, a simple thermal modelling of this component is performed, in which the thermodynamic properties at the outlet of the compressor are calculated by defining the enthalpy and entropy of the inlet refrigerant as well as its isentropic efficiency. Therefore, the desired outlet enthalpy, h_2 , is written as a function of the inlet enthalpy, entropy and the ideal outlet enthalpy, h_{2s} , corresponding to the hypothetical point, which could be obtained if the isentropic efficiency was equal to one.

$$h_2 = \frac{h_{2s} - h_1}{\eta_{is}} + h_1 \quad (3.63)$$

where h_1 is the inlet refrigerant enthalpy. The other input variable is the volume flow rate that is admitted by the compressor, \dot{V}_{ref} , which is considered constant, as an approximation, when the compressor is of the fixed speed type. Both independent variables, \dot{V}_{ref} and η_{is} , are obtained by consulting the catalogue of compressors in which all thermodynamic cycle is defined for several set points and then this values are equal to the mean value.

3.4 User Interface

In Figure 3.7 the user interface is presented in terms of input variables, whereas in Figure 3.8 the representation of the output variables in the user interface is shown. It is important to mention that this user interface was developed in Microsoft Excel.

<p>Note: It is recommended to analyze the nomenclature of the Report "AntonioBarbosa_MasterThesis" to identify the principal dimensions.</p>		Season Winter						
		Indoor Air		Outdoor air				
		V (m ³ /h)	T (°C)	Rel. Humidity	Rel. Humidity	Tmin	Tmax	
		1	80	20	0.5	0.8	-10	10
		2	150	20	0.5	0.8	-10	10
3	200	20	0.5	0.8	-10	10		
4	300	20	0.5	0.8	-10	10		

Membrane Based Heat exchanger	Use Case	Inputs					
		Counter flow	b	0.31	m		
		a	0.004	m	l	0.27	m
		N	95				
		Cross flow	b	2.09E-01	m		
		a	3.75E-03	m	l	1.45E-01	m
		N	65				
		Membrane	C	0.94	g/g		
		w_max	0.29	m/s	Dwm	8.00E-06	m
		esp	8.00E-04				

Condenser	Tubes arrangement	
	ST	25 mm
	SL	2165 mm
	Nlines	3
	Ntubes	18
	Type Staggered/Aligned	
	Fins	
	Thermal Conductivity	204 W/mK
	Width	0.12 mm
	Fin spacing	2.2 mm
Total length_spacing	415 mm	
Refrigerant		
D_tube	6.35 mm	
n_entrances	3	

Evaporator	Tubes arrangement	
	ST	25 mm
	SL	2165 mm
	Nlines	3
	Ntubes	18
	Type Staggered/Aligned	
	Fins	
	Thermal Conductivity	204 W/mK
	Width	0.12 mm
	Fin spacing	2.2 mm
Total length_spacing	415 mm	
Refrigerant		
D_tube	6.35 mm	
n_entrances	3	

Analysis of different flow rates					
		Indoor Air		Outdoor air	
Flow_min	Flow_max	T	Rel. Humidity	Rel. Humidity	T
50	300	20	0.5	0.8	7

Use Case					
		Indoor Air		Outdoor air	
Flow	T	Rel. Hum	Rel. humidity	T	0
180	20	0.5	0.8	0	0

Different use Cases	Counter flow	b	0.31	m				
		l	2.70E-01	m				
		N	95	m				
			h	0.3250	m			
			s	0.01	m			
			Cross flow	b	2.09E-01	m		
			a	3.75E-03	m	l	1.45E-01	m
			N	65				
			Membrane	C	0.94	g/g		
		w_max	0.29	m/s	Dwm	8.00E-06	m	
		esp	8.00E-04					

Variable Speed Compressor	
%	%
1	80
2	60
3	50
4	30

Compressor										
Design Point	Heating	Work	aporation	Temperal	Superheated	Degreecznzation	Temp cooled	Deg	Isentropic Efficiency	Volume Flow
Winter	1405	440	0	10	55	8.3	0.556	4.38E-04	0.556	4.38E-04
Rated Condition	1825	455	7.2	27.8	54.4	8.3	0.603	5.21E-04	0.603	5.21E-04
Summer	2270	488	15	10	55	8.3	0.607	5.29E-04	0.607	5.29E-04
Standard	1965	475	10	10	55	8.3	0.598	5.27E-04	0.598	5.27E-04
Average									0.590975	5.19E-04

Refrigerant Circuit Iteration

Figure 3.7 – User interface (input variables).

3. System Modelling

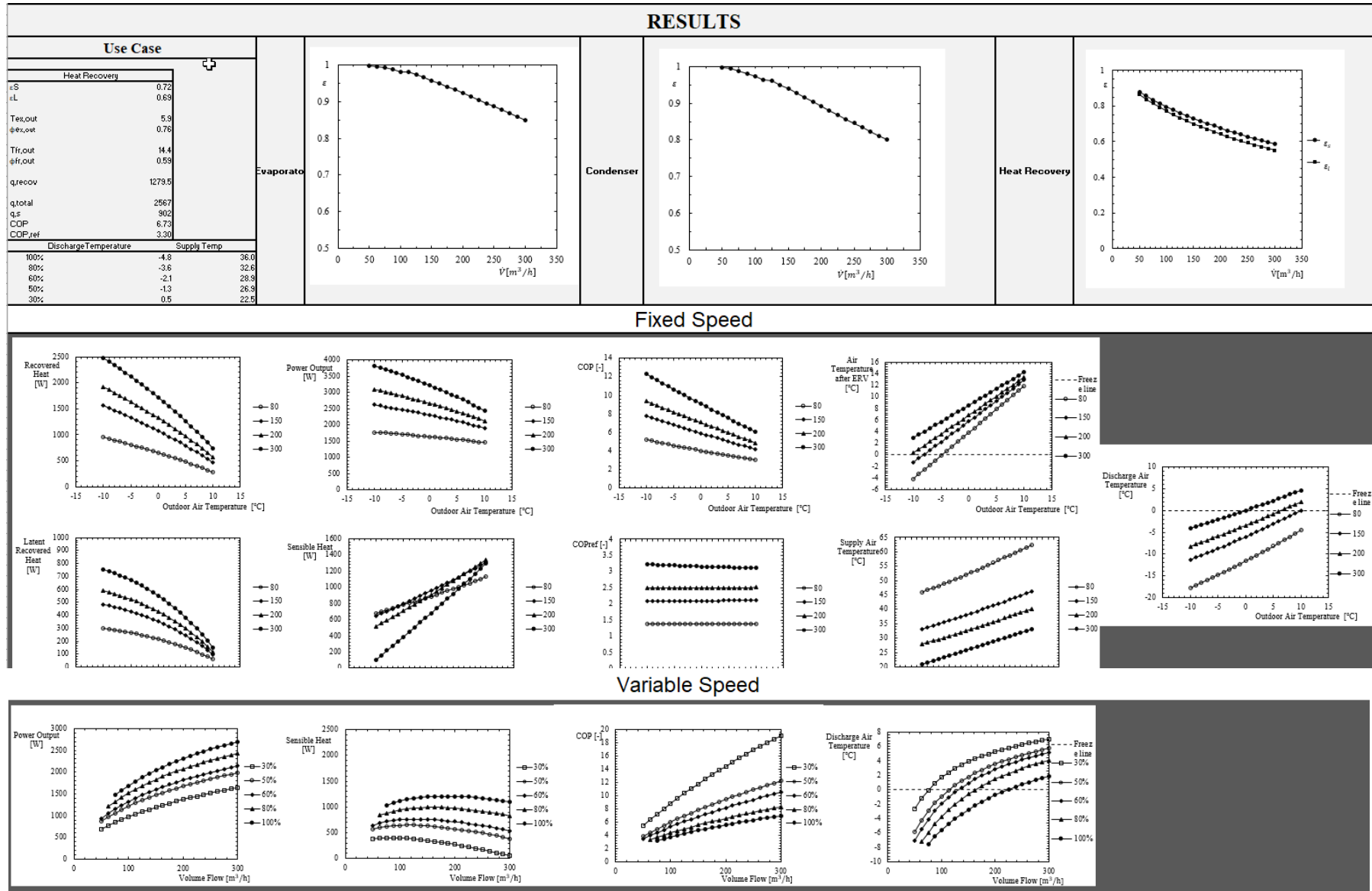


Figure 3.8 – User interface (output variables).

[Blank Page]

4 Simulation and Results

After defining all the heat and mass transfer concepts behind the dimensioning procedure to obtain the desired components, the input variables are defined and then an overall analysis of the energy balances is performed in order to compare the values calculated by this model with those obtained by testing the functional sample. Therefore, considering the limitation of resources, the evaporator, condenser and compressor are re-used from previous samples assembled within the development of new products. It is also important to mention that the phase change heat exchangers are geometrically equal.

The heat recovery exchanger that is tested does not have the capacity to transfer moisture and it will also be re-used from another application, which has duct connections and integration of fans, because of the high lead times to order and assemble a sample as a function of a specific dimensions and with duct connections. Consequently, a heat recovery ventilation unit is used instead of applying the enthalpy variant and the analysis of the transfer of moisture becomes only theoretical.

In the next subsections, the performance of the components is evaluated for the desired input variables and this analysis is divided in two parts: the first with the integration of the enthalpy exchanger and the second with the real solution, which will be validated by testing. Firstly, the components are separately evaluated and then the overall solution is considered.

4.1 Heat Recovery System

Considering the functional diagram presented in Section 3.1, both airstreams pass initially through the heat recovery system, so the analysis of the overall solution starts in this component. Therefore, the two different variants are analysed separately and the specific considerations are taken into account.

4.1.1 Heat Exchanger

The flat plate heat exchanger requires a simpler analysis when compared with enthalpy exchanger, because only heat transfer occurs, i.e., no moisture is transferred between the airstreams. Figure 4.1 shows a representation of the main dimensioning variables of the heat exchanger used in the modelling of its thermal performance.

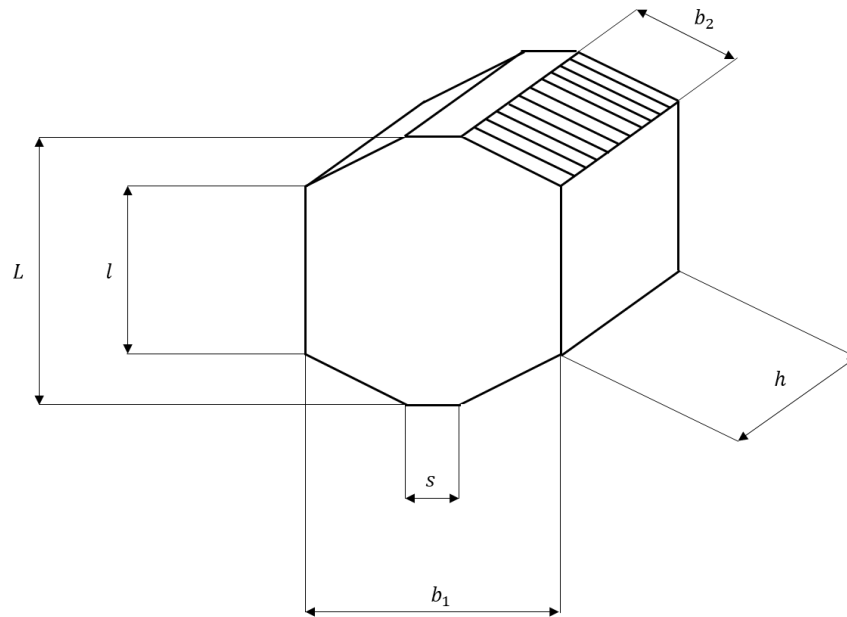


Figure 4.1 – Schematic representation of the main dimensions of the heat exchanger.

In Figure 4.2, the unity cell to define and evaluate the heat transfer process is presented as well as the remaining dimensions that are not shown in Figure 4.1, such as the plate spacing, a , and the plate thickness, t .

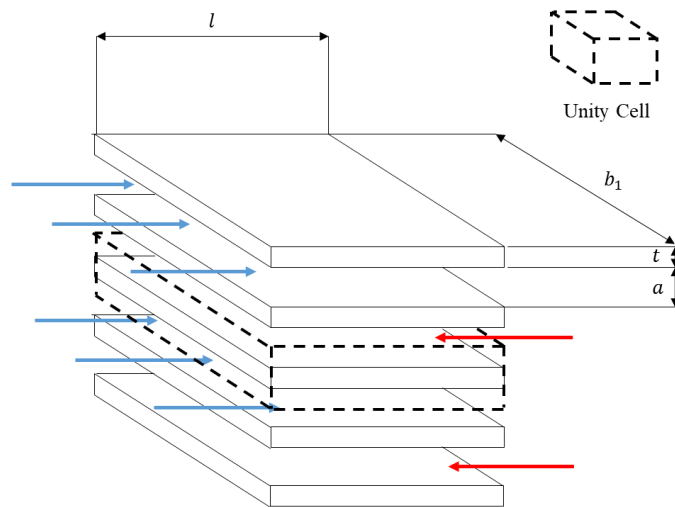


Figure 4.2 – Representation of a unity cell.

In Table 4.1 the input variables of the heat exchanger, which were defined in the previous figures, are presented as well as the number of plates N .

4. Simulation and Results

Table 4.1 – Input variables of the heat exchanger

l [mm]	270	t [mm]	0.25
L [mm]	540	$a_{counter}$ [mm]	2.1
s [mm]	10	a_{cross} [mm]	3.75
b_1 [mm]	310	$N_{counter}$	135
b_2 [mm]	210	N_{cross}	81
h [mm]	325		

Table 4.2 shows the wetted perimeter P , the cross section A , the hydraulic diameter D_h , and the total transfer area, $A_{transfer}$.

Table 4.2 – Output dimensions of the geometry of the heat exchanger

Cross Flow		Counter Flow	
P [mm]	425	P [mm]	624
A [mm ²]	0.78	A [mm ²]	0.66
D_h [mm]	7.37	D_h [mm]	4.25
$A_{transfer}$ [m ²]	11.3	$A_{transfer}$ [m ²]	0.91
b/a	56	b/a	145

In Figure 4.3, the sensible effectiveness, ε_s , is plotted as a function of the volume flow rate, \dot{V} , for the given geometry.

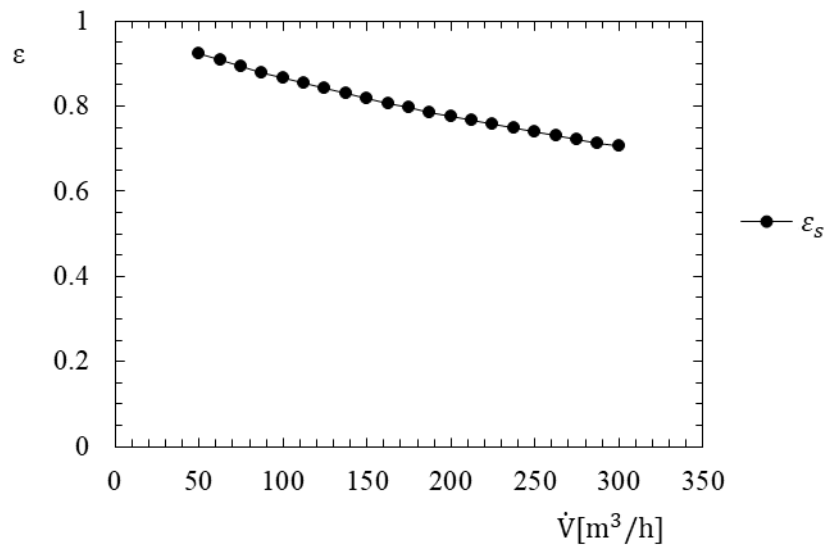


Figure 4.3 – Effectiveness as a function of volume flow rate in heat exchanger.

In Figure 4.4, the temperature of the exhaust airstream at the outlet of the heat recovery system is plotted as a function of outdoor air temperature and air volume flow rate. It is important to mention that the values of air volume flow rate presented in the legend are in cubic meters per hour.

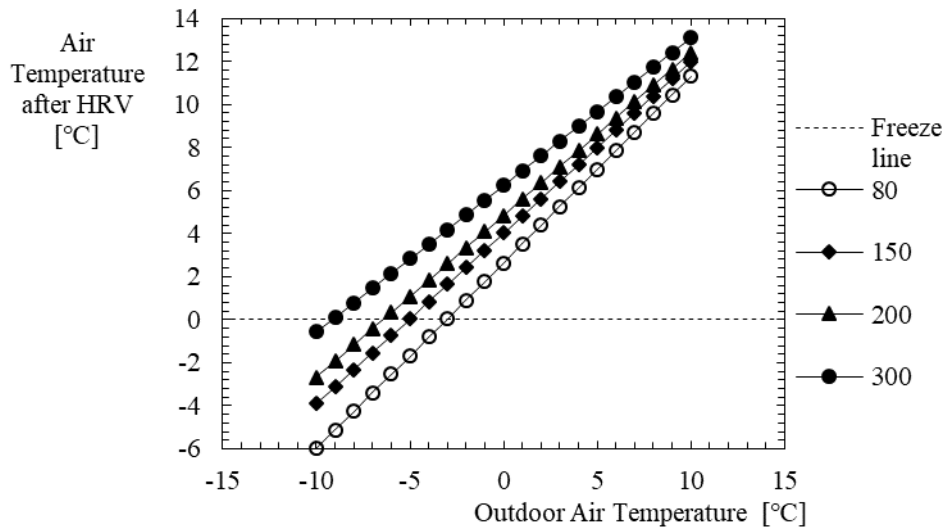


Figure 4.4 – Air Temperature at the outlet of heat recovery system as a function of outdoor air temperature and air volume flow rate [m³/h].

4.1.2 Enthalpy Exchanger

The dimensioning analysis of the membrane based enthalpy exchanger needs a previous discussion about the different types of this variant as well as the influence of membrane characterizing parameters on the thermal performance of the energy exchanger. Initially, in Figure 4.5, the dimensionless water content in the membrane is plotted as a function of the relative humidity of the supply air for different types of membranes. This variation of the membrane parameter, C_{sf} , is caused by using membranes composed by different materials, in which the linear type ($C_{sf}= 1$) is typically silica gel, the type with increasing slope ($C_{sf}= 2$) is a polymer and the other case ($C_{sf}= 0.7$) is a molecule sieve.

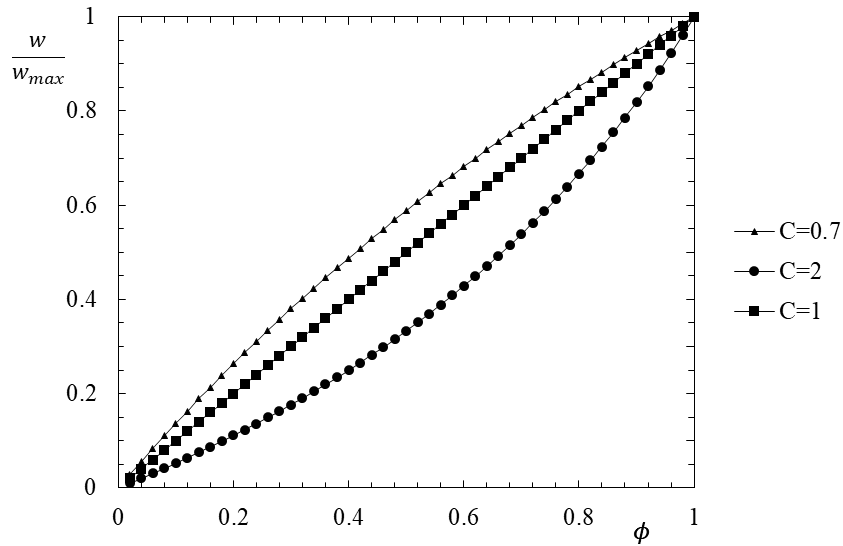


Figure 4.5 – Dimensionless water content as a function of relative humidity.

The influence of the operating conditions on the membrane mass diffusivity properties dimensionless parameter, ψ , equation 3.16, is also plotted for the different relative humidity as well as sorption curves in Figure 4.6.

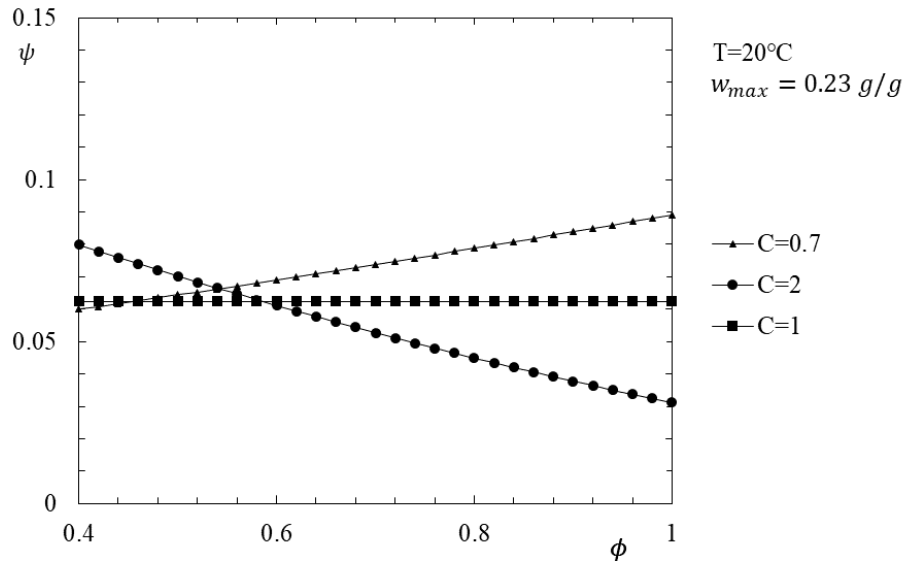


Figure 4.6 – Variation of the membrane permeability dimensionless parameter with relative humidity and material.

The plot presented in Figure 4.7 shows the variation of the same parameter, ψ , for different intake air temperatures for the molecule sieve variant ($C_{sf}=0.7$).

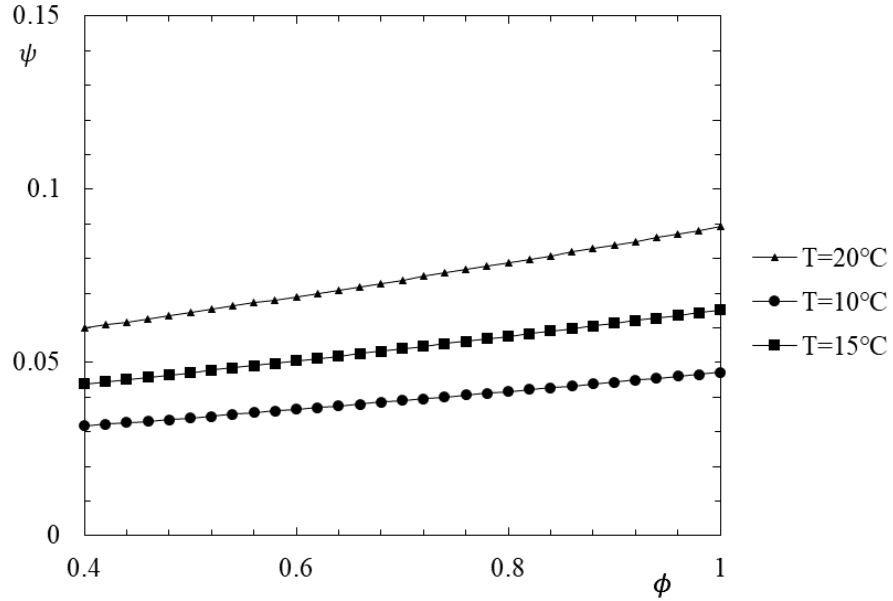


Figure 4.7 – Variation of the membrane permeability dimensionless parameter with relative humidity and intake air temperature.

In Table 4.3, the input variables of the heat exchanger, which were defined in the previous figures, are presented as well as the number of plates N , the sorption number C , the maximum moisture content w_{max} , and the water diffusivity in membrane D_{w-m} . These variables were obtained by combining the dimensioning data of the heat exchanger previously used with values of membranes presented in literature [26], in which the channel height as well as the membrane properties were maintained approximately constant.

Table 4.3 – Input variables of the enthalpy exchanger

l [mm]	270	$a_{counter}$ [mm]	2.3
L [mm]	540	a_{cross} [mm]	2.4
s [mm]	10	$N_{counter}$	105
b_1 [mm]	310	N_{cross}	54
b_2 [mm]	210	C	0.94
h [mm]	325	w_{max} [g/g]	0.29
t [mm]	0.8	D_{w-m} [m ² /s]	8E-6

Table 4.4 shows the wetted perimeter P , the cross section A , the hydraulic diameter D_h , the total transfer area $A_{transfer}$, and the mass conductive coefficient of membrane $h_{membrane}$, where the last one was obtained by calculating an average value of the

4. Simulation and Results

dimensionless parameter ψ for temperatures between 12 °C and 20 °C and relative humidity between 60% and 100%.

Table 4.4 – Output variables of the geometry of the enthalpy exchanger

Cross Flow		Counter Flow	
P [mm]	422	P [mm]	625
A [mm ²]	0.49	A [mm ²]	0.70
D_h [mm]	4.69	D_h [mm]	4.51
$A_{transfer}$ [m ²]	0.73	$A_{transfer}$ [m ²]	8.79
b/a	88	b/a	136
$h_{membrane}$ [m/s]		0.232	

In Figure 4.8, the sensible and latent effectiveness are plotted as a function of the volume flow rate. The sensible effectiveness presented in Figure 4.3 is also plotted here. It is possible to conclude that the sensible effectiveness is lower in ERV when compared with HRV system, as it was analysed previously.

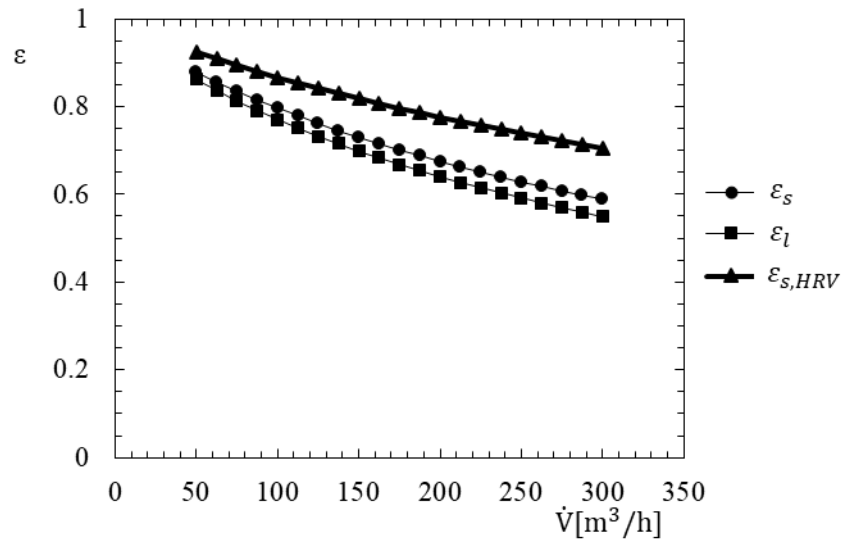


Figure 4.8 – Effectiveness as a function of volume flow rate in enthalpy exchanger.

In Figure 4.9, the temperature of the exhaust airstream at the outlet of the heat recovery system is plotted as a function of the same input variables. This behaviour may be compared with the equivalent by using HRV system presented in Figure 4.4, in which the frost formation tendency inside the heat exchanger is higher, due to the higher sensible effectiveness.

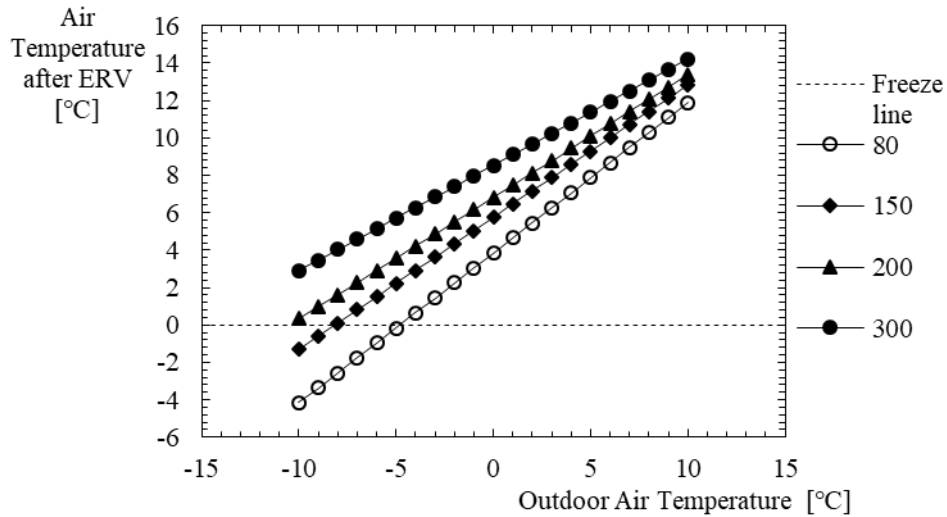


Figure 4.9 – Air temperature at the outlet of heat recovery system as a function of outdoor air temperature and air volume flow rate [m³/h].

4.2 Air-to-Refrigerant Heat Exchangers

The analysis of the condenser and evaporator requires a definition of the unity cell, which defines the heat transfer process by applying an adiabatic boundary condition. Thus, this unity cell is presented in Figure 4.10.

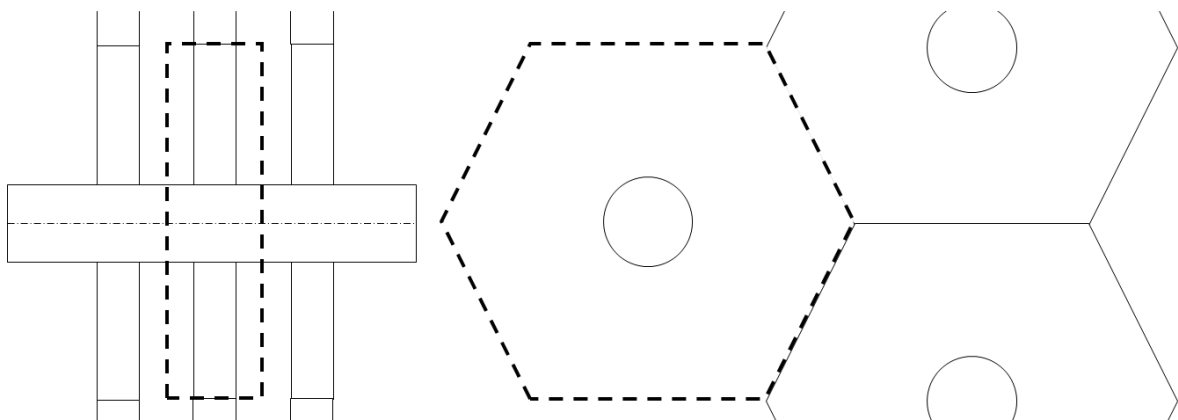


Figure 4.10 – Unity cell of the air-to-refrigerant heat exchangers.

4.2.1 Evaporator

The dimensioning of the evaporator is a function of the input variables previously defined as well as the fluids that participate in the heat transfer process. Considering both fluid sides, air and R134a, the main dimensions are defined in Table 4.5.

4. Simulation and Results

Table 4.5 – Dimensions of the evaporator

S_T [mm]	25	δ_{fin} [mm]	0.12
S_L [mm]	21.65	k_{fin} [W/(mK)]	204
N_L	3	Fin spacing [mm]	2.2
N_T	18	Length [mm]	415
D [mm]	6.35	$n_{entrances,ref}$	3

The evaporating temperature is assumed to be equal to 0 °C, the refrigerant mass flow rate is also assumed to be constant for the following evaluation and the convective heat coefficient is equal to the mean value of 15 different values of vapour quality, between its minimum and maximum value, $x_{in,ref}$ and $x_{out,ref}$, respectively. The main output variables for both sides are presented in Table 4.6.

Table 4.6 – Geometric output variables of the evaporator

X_D [mm]	12.5	$A_{conv,tubes}$ [m ²]	0.42
X_T [mm]	12.5	a [–]	3.41
$r_{f,eq}$ [mm]	13.3	b [–]	3.94
S_d [mm]	25.0	F_a [–]	1.43
A_f [m ²]	9.80	\dot{m}_{ref} [g/s]	8

Table 4.7 – Properties of the evaporator refrigerant side

$x_{in,ref}$	0.4
$x_{out,ref}$	1.0
$\overline{h_{ref}}$ [W/(m ² · K)]	1406

Both correlations regarding air-side, by Zukauskas and by Hausen [13, 30], are now analysed in Figure 4.11 in terms of the evolution of sensible effectiveness ε , with the volume flow rate \dot{V} , as well as the error between these different approaches, defined as

$$Error [\%] = 100 \cdot \frac{|\varepsilon_{Zukauskas} - \varepsilon_{Hausen}|}{\varepsilon_{Hausen}} \quad (4.1)$$

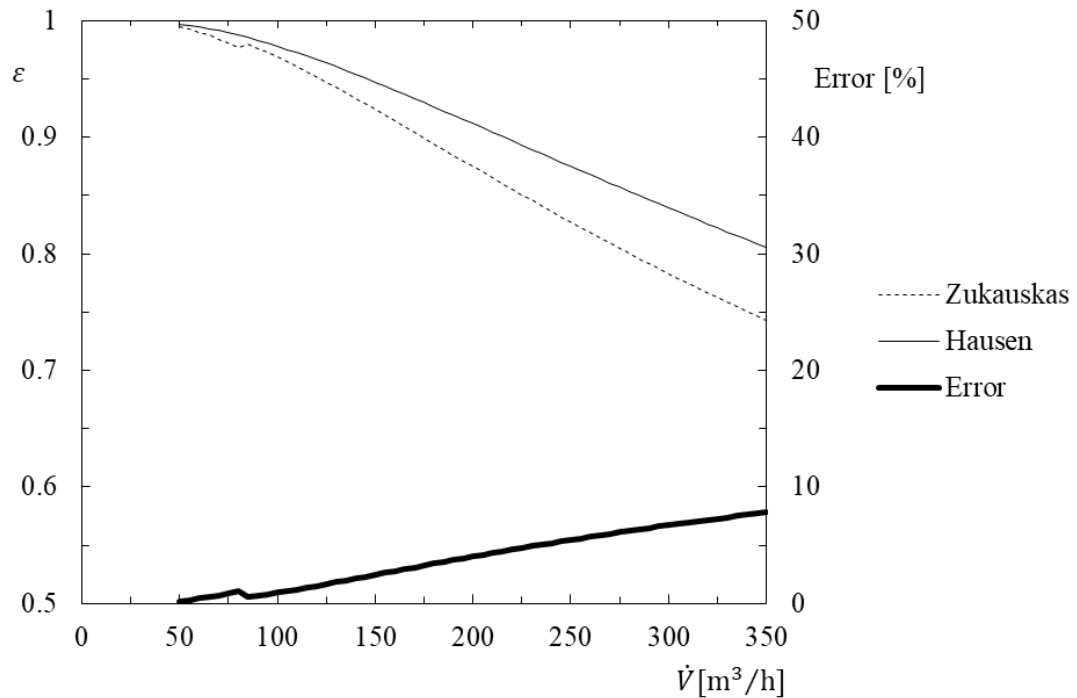


Figure 4.11 - Analysis of the results obtained by different correlations for the evaporator.

By looking to Figure 4.11, it is possible to conclude that the results obtained by both correlations have a difference lower than 10% for the considered range of volume flow rates. The error increases with the increasing of the volume flow rate and it is possible to verify that a change of flow regime occurs for values of volume flow rate approximately equal to 80 m³/h, which causes a small jump on the value predicted by using the correlation proposed by Zukauskas, but this discontinuity may be neglected due to low increase of effectiveness.

4.2.2 Condenser

Similarly with the evaporator, the dimensioning of the condenser is a function of the geometric input variables previously defined as well as the properties of the refrigerant within the operation range in which it works. Considering the same geometry, only the fluid properties change, especially the inlet and outlet vapour quality. Thus, this value is assumed to be equal to zero at the outlet and the refrigerant is at saturated liquid point at the condensing pressure or temperature. The correlations analysed in Section 3.3.2 are compared and the relative error is defined by equation (4.1). Table 4.8 shows the inlet and outlet amount of vapor in the condenser, as well as the mean refrigerant convective coefficient, considering a condensing temperature equal to 40 °C.

4. Simulation and Results

Table 4.8 – Properties of the condenser refrigerant side

$x_{in,ref}$	1.0
$x_{out,ref}$	0
$\overline{h_{ref}}[\text{W}/(\text{m}^2 \cdot \text{K})]$	902

In Figure 4.12, the sensible effectiveness is plotted as a function of the volume flow rate, for an airstream temperature equal to 30 °C.

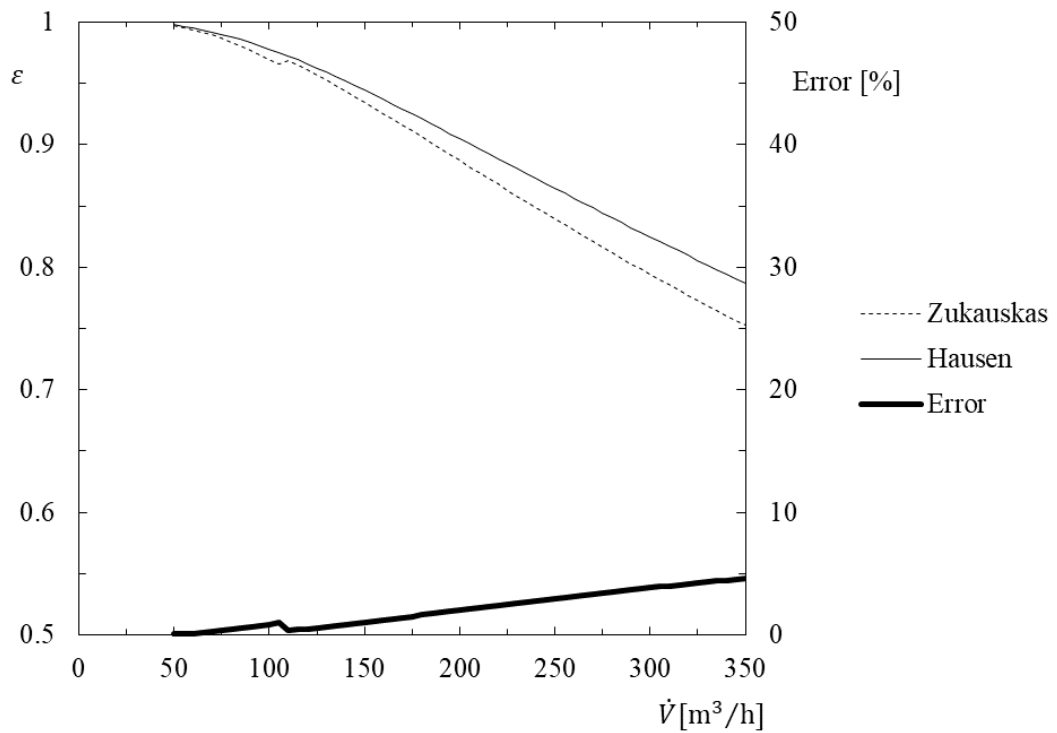


Figure 4.12 - Analysis of the results obtained by different correlations for the condenser.

4.3 Compressor

Considering the previously defined procedure, the analysis of the thermal performance of the compressor is performed by quantifying the volume flow rate and the isentropic efficiency, which are assumed equal to the mean values obtained by checking the data presented in the catalogues. Therefore, the values obtained for the selected compressor are presented in Table 4.9. The use of the EES software turns easier the definition of the refrigerant thermodynamic properties for each case and the nomenclature presented is the same as shown in the compressor catalogue.

Table 4.9 – Dimensioning data of the compressor

Point	Winter	Rated Condition	Summer	Standard	Average
Q_{heat} [W]	1405	1825	2270	1965	
W_{input} [W]	440	455	488	475	
T_e [°C]	0	7.2	15	10	
ΔT_{SH} [°C]	10	27.8	10	10	
T_c [°C]	55	54.4	55	55	
ΔT_{SC} [°C]	8.3	8.3	8.3	8.3	
η_{is}	0.556	0.603	0.607	0.598	0.591
\dot{V}_{ref} [m ³ /s]	4.98E-04	5.21E-04	5.29E-04	5.27E-04	5.19E-04

When the dynamic behaviour of the compressor is evaluated within a variation of its frequency, the value of refrigerant volume flow rate is multiplied by the respective frequency percentage, whereas the isentropic efficiency is assumed constant.

4.4 Overall Solution

The definition of the outlet points of the refrigerant circuit as well as the temperature of the refrigerant fluid during the phase change needs an iterative process to equalize the amount of energy transferred by both heat transfer and thermodynamics analysis. To perform this process, the following assumptions are defined:

- The superheated fluid at the entrance of the compressor is assumed to be with 5 K of super-heated degrees;
- The condensed fluid entries at the expansion valve at saturated liquid state, i.e., no degrees of sub-cooling are assumed;
- The pressure drop inside the refrigerant pipes and the heat exchangers are neglected;
- The ideal enthalpy at the outlet of the compressor, h_{2s} , is obtained by multiplying the enthalpy at 100% vapour quality at the corresponding condensation pressure by a factor as a function of k , which depends on the evaporation temperature. Figure 4.13 shows the value of this variable plotted as a function of the evaporating temperature for different condensing temperatures. As it is shown, this value does not have a large variance, so the values of an average temperature of 40°C is considered.

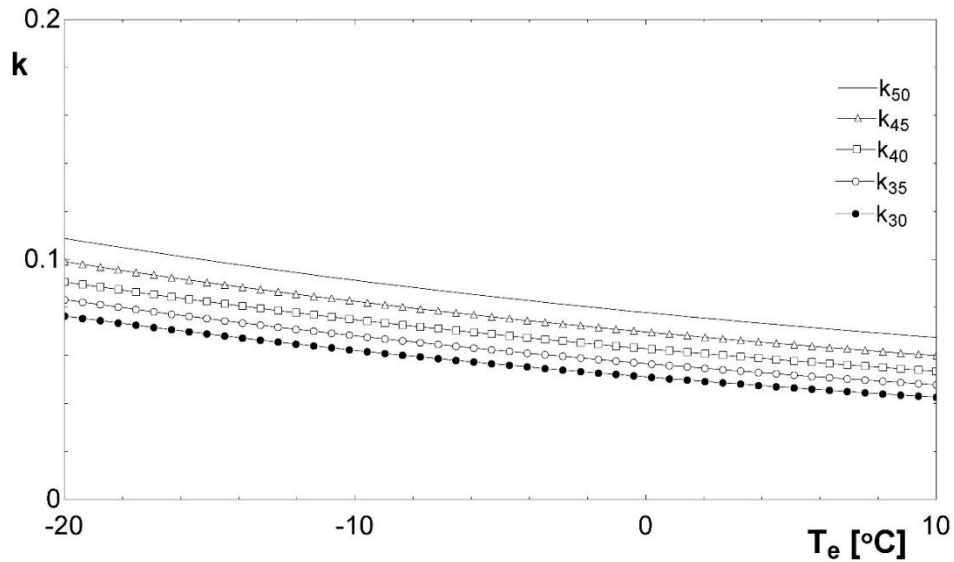


Figure 4.13 – Value of k as a function of evaporating temperature.

$$h_{2s} = (1 + k) \cdot h_{g,cond} \quad (4.2)$$

Firstly, the evaporator is evaluated and the energy received by the refrigerant, $\dot{q}_{evap,ref}$, and the energy transferred by heat transfer analysis, $\dot{q}_{evap,HT}$, are defined as

$$\dot{q}_{evap,ref} = \dot{m}_{ref} \cdot (h_{1,5k} - h_{f,cond}) \quad (4.3)$$

4. Simulation and Results

$$\dot{q}_{evap,HT} = \varepsilon_{evap} \cdot (h_{air,ent} - h_{air,Tevap}) \Rightarrow h_{air,Tevap} = -\frac{\dot{q}_{evap,HT}}{\varepsilon_{evap}} + h_{air,ent} \quad (4.4)$$

$$T_{evap} = f(h_{air,Tevap}) \quad (4.5)$$

where $h_{air,Tevap}$ is the equivalent enthalpy of the airstream at the evaporation temperature and this temperature is obtained when this value is known. Secondly, the procedure used for the evaporator is now defined for the evaluation of the condenser, in which the energy balance is

$$\dot{q}_{cond,ref} = \dot{m}_{ref} \cdot (h_2 - h_{f,cond}) \quad (4.6)$$

$$\dot{q}_{cond,HT} = \varepsilon_{cond} \cdot (h_{air,Tcond} - h_{air,ent}) \Rightarrow h_{air,Tcond} = \frac{\dot{q}_{cond,HT}}{\varepsilon_{cond}} + h_{air,ent} \quad (4.7)$$

$$T_{cond} = f(h_{air,Tcond}) \quad (4.8)$$

Figure 4.14 shows the iterative process used to obtain the desired convergence. This process is written in Visual Basic language in order to simplify the future using of the modelling in Excel.

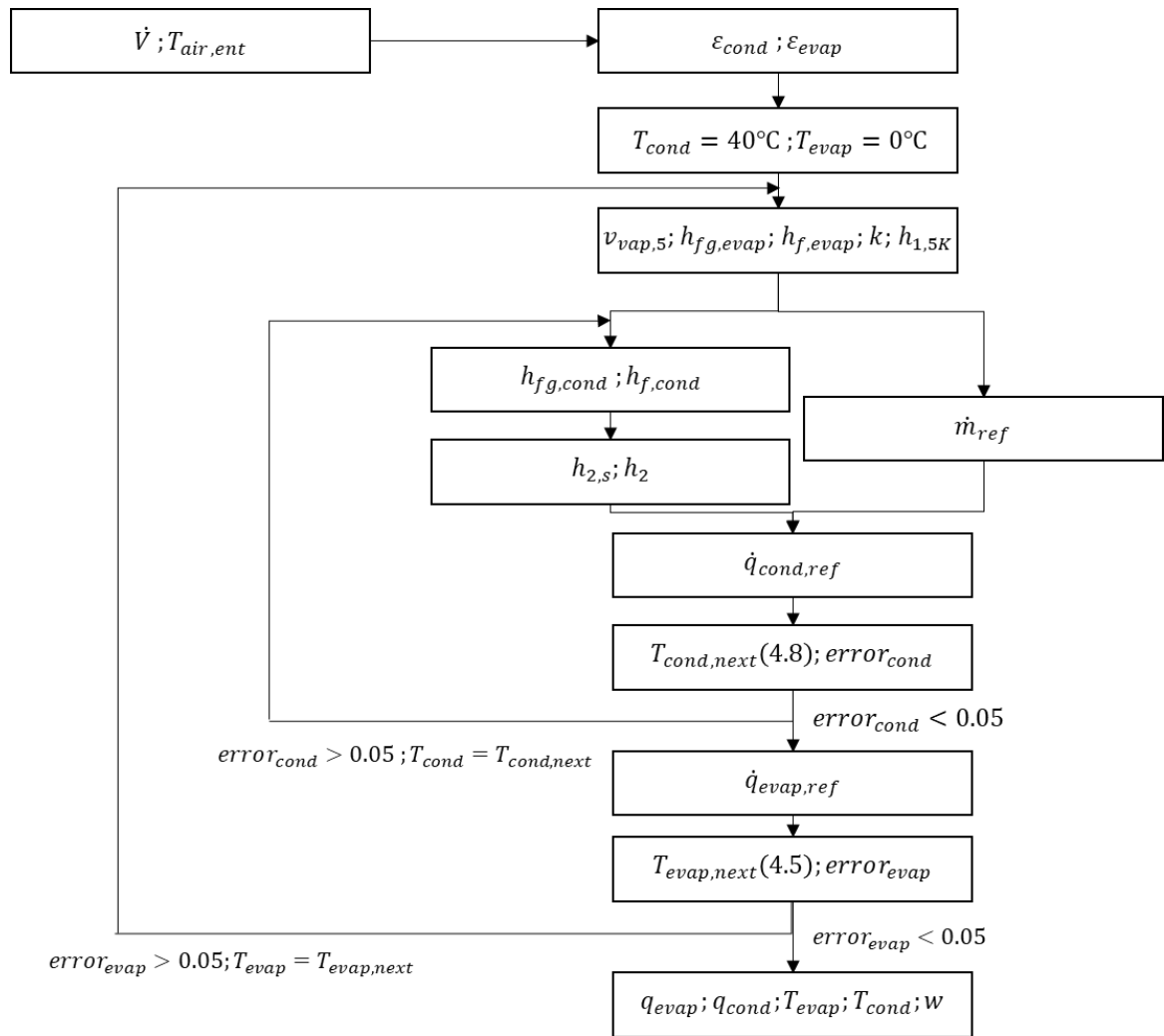


Figure 4.14 – Diagram of the iterative process.

In the next subsections, this iterative process is applied for the ranges of temperature and volume flow rates presented in Table 4.10 and both different types of heat recovery systems are analysed and compared.

Table 4.10 – Temperature and relative humidity ranges

Mode	Heating	Cooling
Outdoor air temperature	$-10 \leq T_{outdoor} [^{\circ}\text{C}] \leq 10$	$25 \leq T_{outdoor} [^{\circ}\text{C}] \leq 32$
Outdoor Air Relative Humidity	$\phi_{outdoor} = 80 \%$	$\phi_{outdoor} = 60 \%$
Indoor Air Temperature	$T_{indoor} = 20 \text{ }^{\circ}\text{C}$	$T_{indoor} = 25 \text{ }^{\circ}\text{C}$
Indoor Air Relative Humidity	$\phi_{indoor} = 50 \%$	$\phi_{indoor} = 50 \%$
Volume Flow Rate	$50 \leq \dot{V} [\text{m}^3/\text{h}] \leq 350, P = 1 \text{ bar}$	

In next sections, the system is evaluated in combined terms of heat transfer and thermodynamics, achieving convergence by using the iterative process presented in Figure 4.14. When the refrigerant temperature is outside of its compressor admissible range, i.e., $-20 \text{ }^{\circ}\text{C} < T_{ref} < 65 \text{ }^{\circ}\text{C}$, this component stops working and the simulation does not calculate any value.

4.4.1 Heat Recovery Ventilation

Heating Mode

Considering the using of the heat recovery system, the analysis of the overall solution is performed for heating and cooling mode. During heating mode, the compressor input frequency is modulated in order to evaluate the frost prevention procedure and the consequent decrease of power output. It is important to mention that the evaluation of the Coefficient of Performance, *COP*, does not take into account the fan power consumption.

In Figure 4.15 the heat recovered by using the heat recovery system is plotted as a function of outdoor air temperature and air volume flow rate. It is important to mention that the flow rates are in cubic meters per hour and the air volume flow rate removed from the home (exhaust air) is equal to the air volume flow rate that is added to the home (supply air), and that does not imply a steady state condition, because of changes on air density that cause a balance of air

4. Simulation and Results

mass flow different than zero. The error caused by this approximation was maintained because the quantity of air in the circuit in the experimental analysis will be evaluated in terms of air volume flow rate and this assumption will be taken into account with the respective error. The output variable achieves higher values for higher flow rates, and lower outdoor air temperatures.

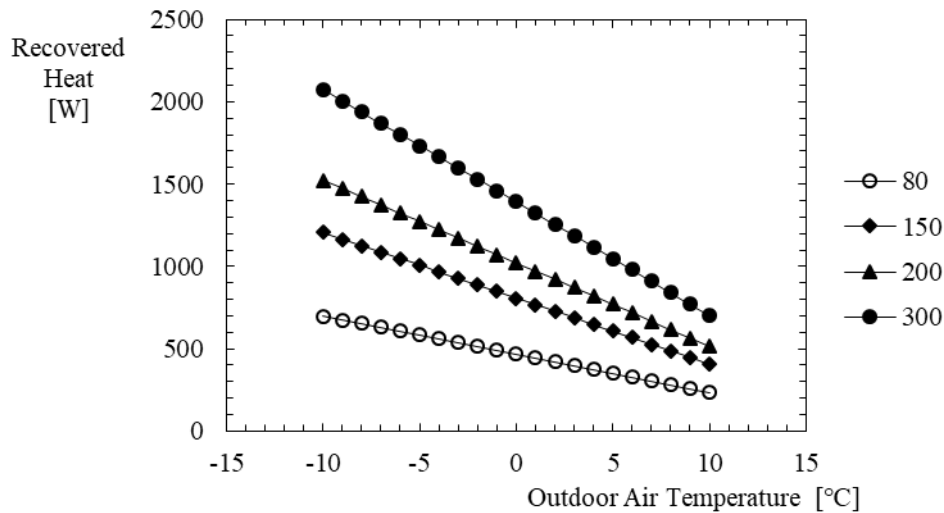


Figure 4.15 – Heat recovered as a function of the outdoor air temperature and air volume flow rate [m^3/h].

Fixed Speed

In Figure 4.16, the power output, i.e., the energy transferred to the fresh air, is plotted as a function of the outdoor temperature and the different volume flow rates. The evolution of power output shows an increase with the increase of air volume flow rate and a decrease with higher outdoor air temperature, because less heat is recovered in the heat recovery system as it is presented in Figure 4.15.

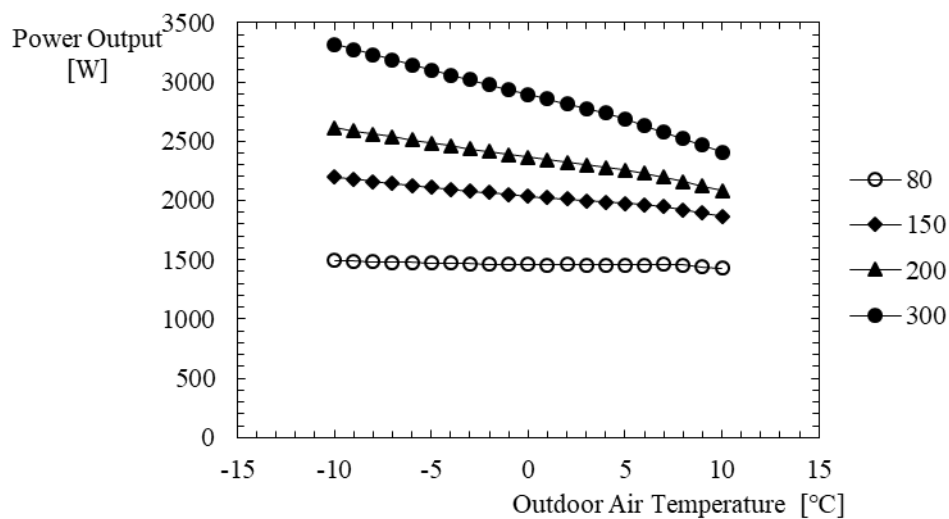


Figure 4.16 – Power output as a function of the outdoor air temperature and air volume flow rate [m^3/h].

In Figure 4.17, the exchanged sensible heat is presented as a function of the same input variables.

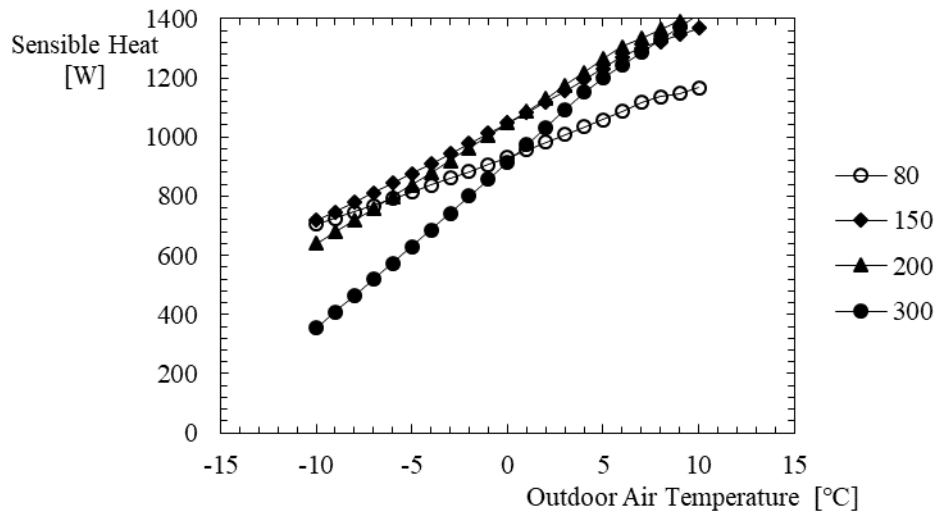


Figure 4.17 – Sensible heat as a function of the outdoor air temperature and air volume flow rate [m³/h].

In Figure 4.18 and in Figure 4.19, the overall *COP* as well as the refrigerant cycle *COP* are plotted as a function of the same input variables. The overall *COP* evolution does not consider the fan power consumption and this variable shows a decrease with higher outdoor air temperatures, because less heat is recovered in the heat recovery system, whereas the refrigerant cycle *COP* shows an opposite evolution, due to the increase of evaporating temperature with higher outdoor air temperatures, which increases the efficiency of the refrigerant cycle.

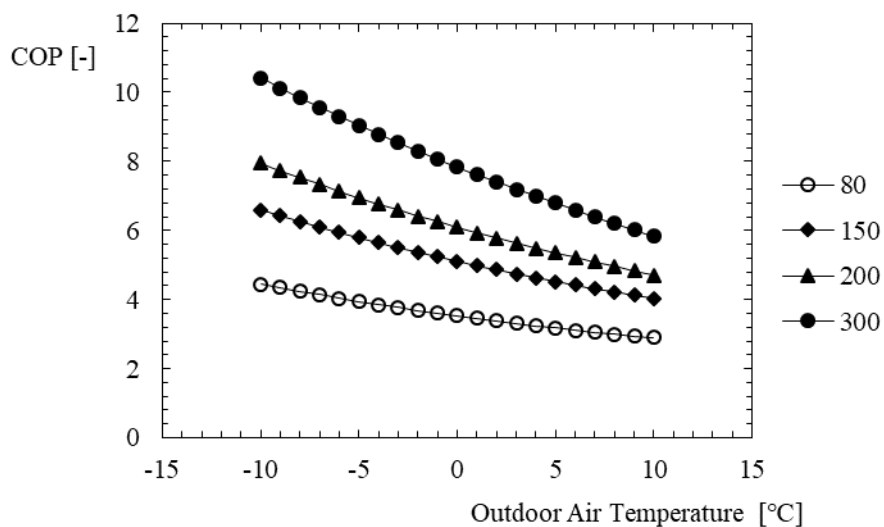


Figure 4.18 – *COP* as a function of outdoor air temperature and air volume flow rate [m³/h].

4. Simulation and Results

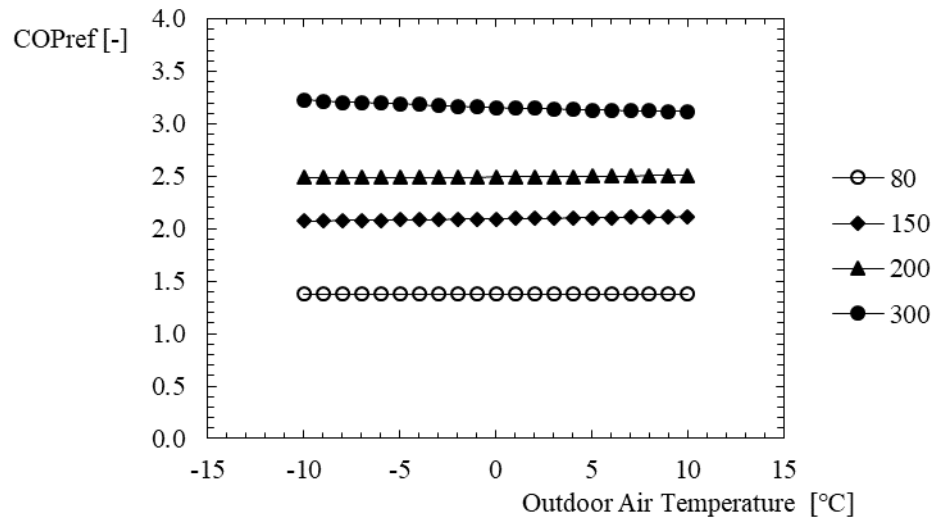


Figure 4.19 – *COP* of refrigerant cycle as a function of outdoor air temperature and air volume flow rate [m^3/h].

Finally, Figure 4.20 and Figure 4.21 show the variation of discharge air and supply air temperatures as a function of the same input variables. In the first plot, a zero Celsius degrees line were added in order to evaluate the conditions of frost formation, which shall be avoided, in order to maintain the heat convective coefficients as high as possible. Both plots show that with lower flow rates, the output temperatures achieve extreme values, due to the lower heat capacity of the airstream.

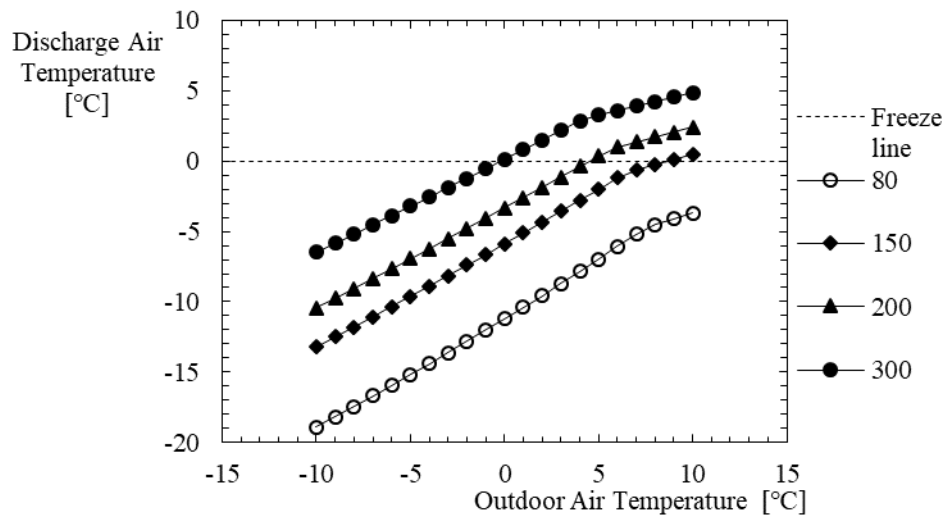


Figure 4.20 – Discharge air temperature as a function of outdoor air temperature and air volume flow rate [m^3/h].

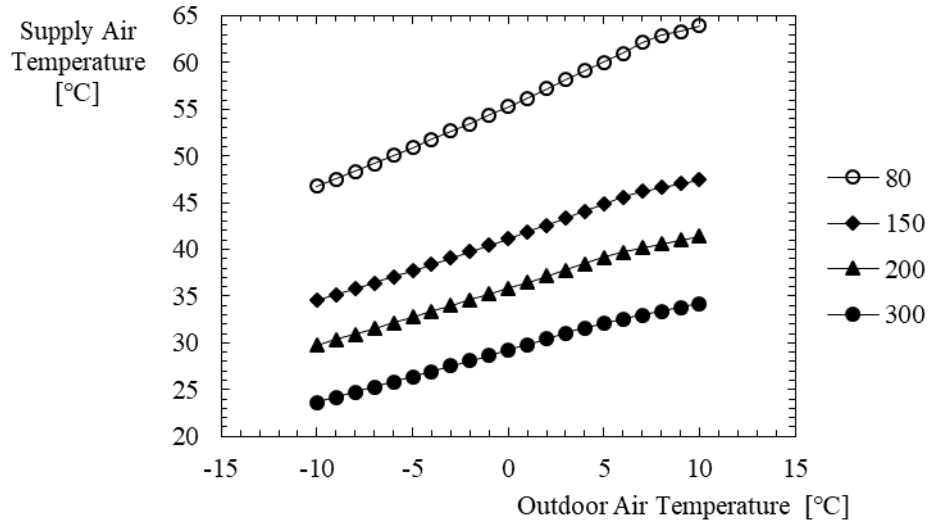


Figure 4.21 – Supply air temperature as a function of outdoor air temperature and air volume flow rate [m³/h].

Variable Speed

Considering the possibility of changing the frequency of the compressor, the main output variables are plotted as a function of the volume flow rate for the defined range of frequencies. Table 4.11 shows the outdoor air conditions for this analysis of compressor frequency variation.

Table 4.11 – Outdoor air conditions for variable speed analysis during heating mode (HRV)

Outdoor Air Temperature

$$T_{outdoor} = 7\text{ }^{\circ}\text{C}$$

Outdoor Air Relative Humidity

$$\phi_{outdoor} = 80\%$$

Figure 4.22 and Figure 4.23 show the power output and sensible heat as a function of the air volume flow rate and compressor input frequency, in which higher values are achieved for higher frequencies, due to higher refrigerant flow rate.

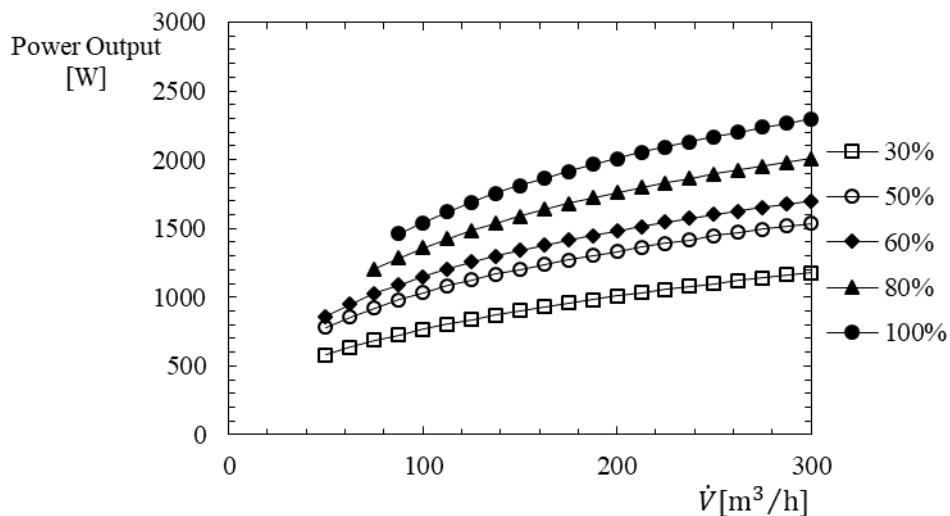


Figure 4.22 – Power output as a function of the air volume flow rate and frequency.

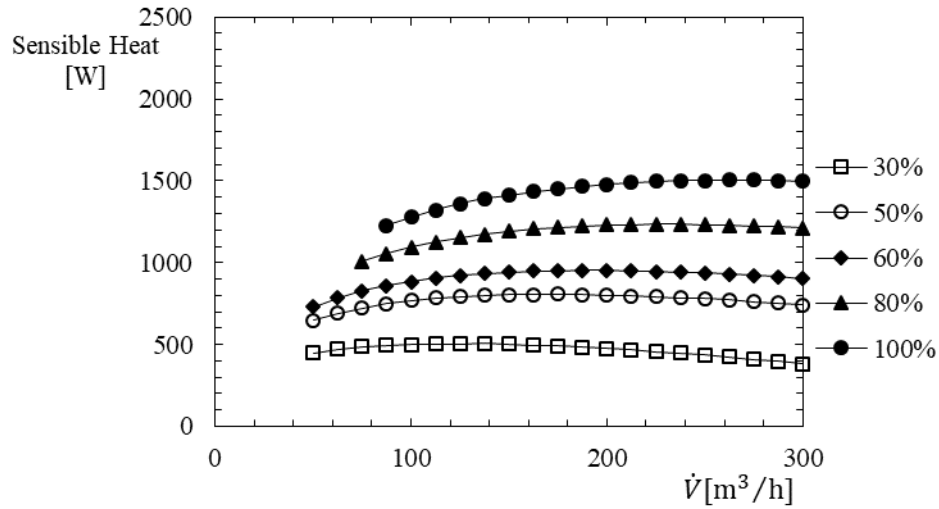


Figure 4.23 – Sensible heat as a function of the air volume flow rate and frequency.

In Figure 4.24, the *COP* is plotted as a function of the same input variables and this parameter assumes higher values when the frequency is lower, due to lower work input, whereas Figure 4.25 shows the variation of discharge air temperature, in which is possible to verify conditions of volume flow rate and frequency input at a given temperature to start frost formation.

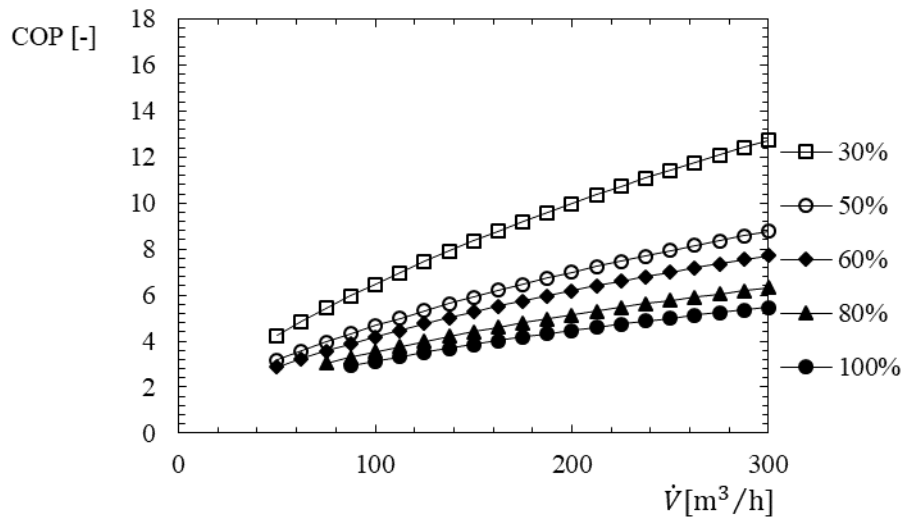


Figure 4.24 – Coefficient of performance (*COP*) as a function of the air volume flow rate and frequency.

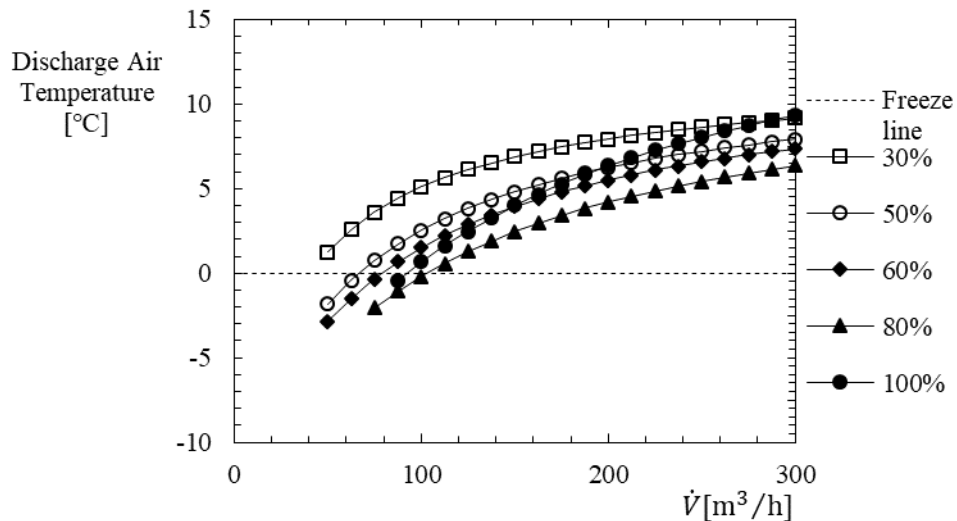


Figure 4.25 – Discharge air temperature as a function of the air volume flow rate and frequency.

Cooling Mode

Regarding the cooling mode, Table 4.10 shows the humidity and temperature ranges that are used to evaluate the solution. The recovered heat within the HRV is presented in Figure 4.26, in which the higher slope verified with higher volume flow rates are caused by the increase of the airstream energy capacity.

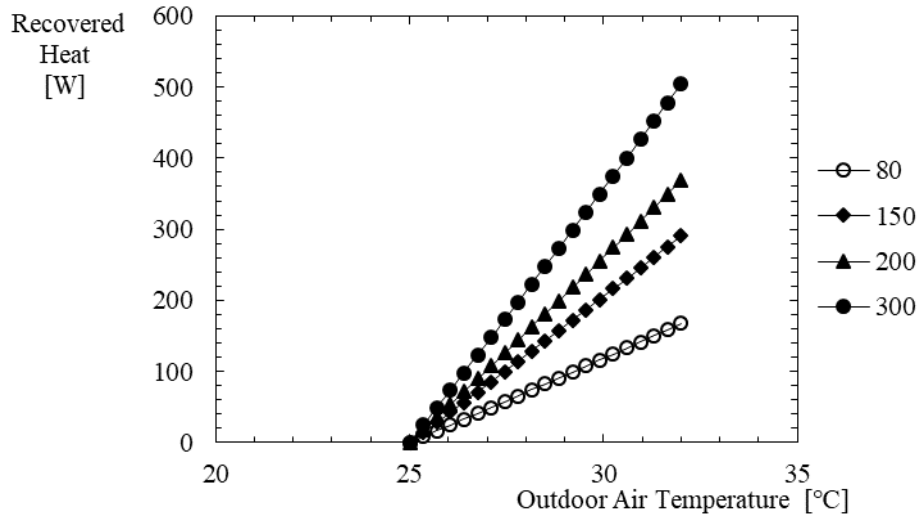


Figure 4.26 – Recovered heat as a function of outdoor air temperature and air volume flow rate [m³/h] for cooling mode.

The analysis of the cooling mode is only performed in terms of power output, sensible heat and energy efficiency ratio, for fixed and variable speed operation modes, because the other variables may be obtained as a function of these and frost formation does not occur within the operation during this season.

Fixed Speed

In Figure 4.27, the cooling capacity is plotted as a function of outdoor air temperature and air volume flow rate, whereas in Figure 4.28 the sensible heat removed from the home is defined. For a flow rate equal to $80 \text{ m}^3/\text{h}$ and several operating points at $150 \text{ m}^3/\text{h}$ ($T > 28^\circ\text{C}$), the values do not appear due to the high discharge air temperatures needed, which leads to high condensing temperatures and such results are out of the compressor's envelope. Therefore, when these conditions occur, the reduction of the frequency has to be considered, to decrease the work input by the compressor and then the condensing temperature.

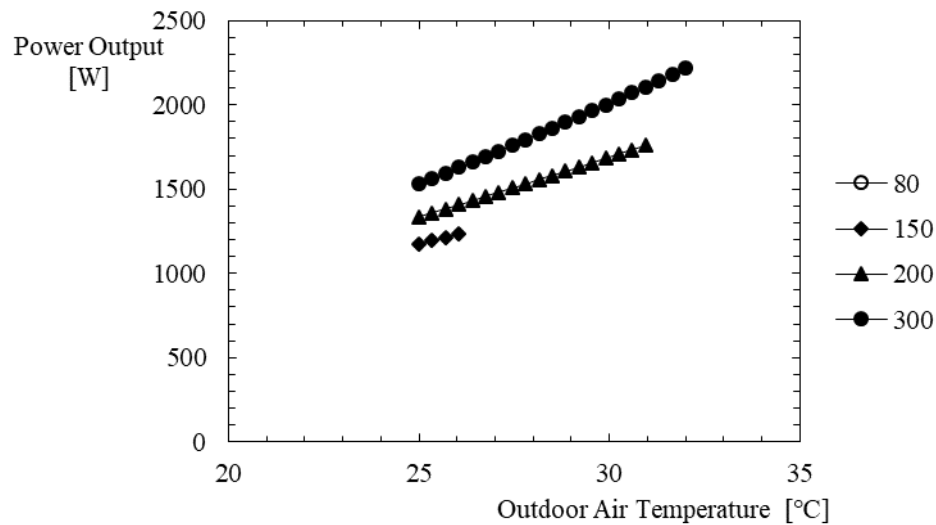


Figure 4.27 – Cooling power output as a function of the outdoor air temperature and air volume flow rate [m^3/h].

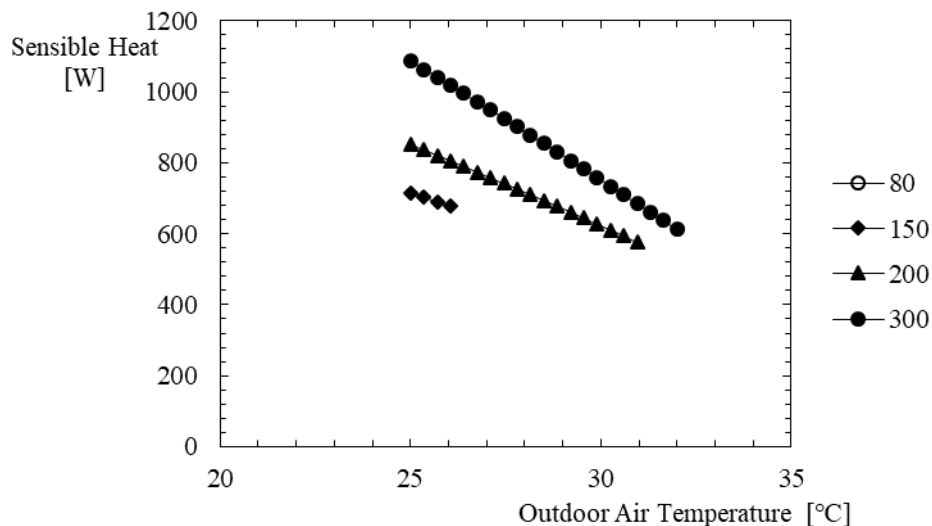


Figure 4.28 – Sensible heat as a function of the outdoor air temperature and air volume flow rate [m^3/h].

In Figure 4.29 the *EER* of the overall solution is represented as a function of the same variables, whereas in Figure 4.30 the discharge air temperature is plotted and it is possible to verify the

limitation of the compressor envelope, where condensing temperatures higher than 65 °C are not taken into account.

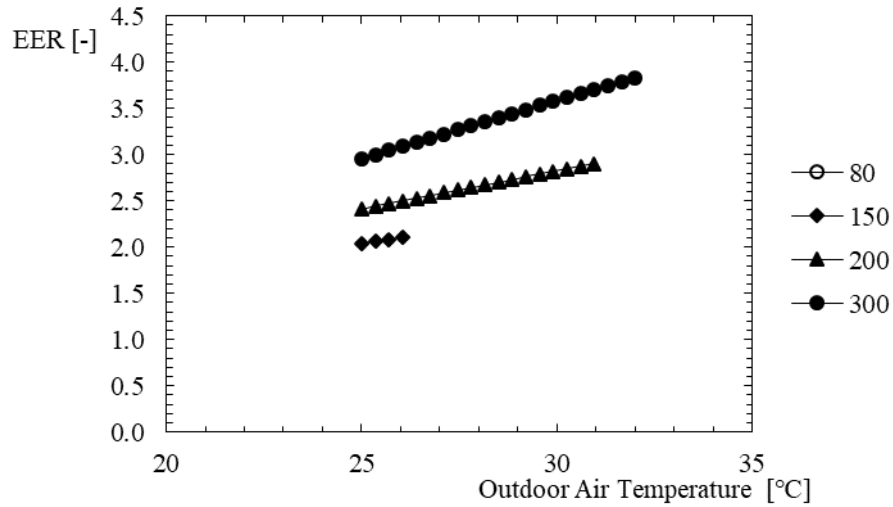


Figure 4.29 – *EER* as a function of the outdoor air temperature and air volume flow rate [m³/h].

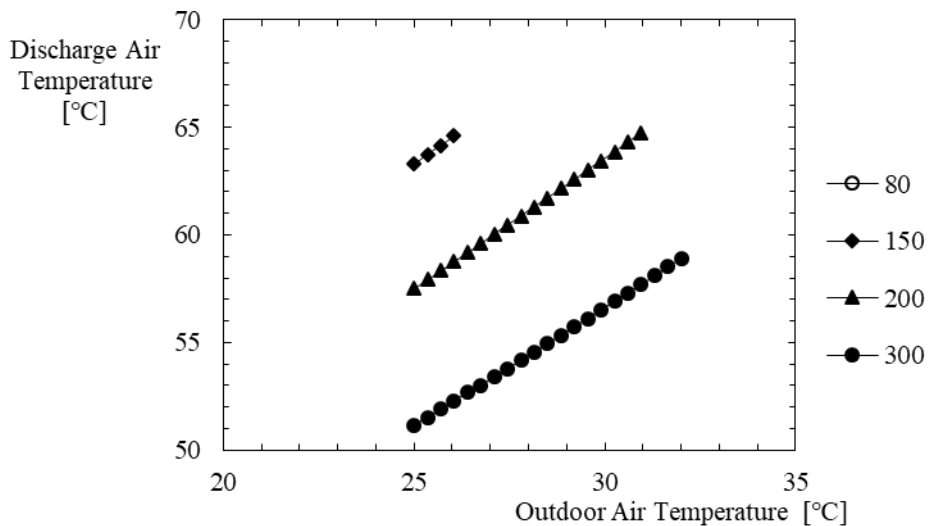


Figure 4.30 – Discharge air temperature as a function of the outdoor air temperature and air volume flow rate [m³/h].

Variable Speed

Regarding the analysis of the variation of the input frequency of the compressor, the outdoor air conditions are defined in Table 4.12.

Table 4.12 – Outdoor air conditions for variable speed analysis during cooling mode (HRV)

Outdoor Air Temperature

$$T_{outdoor} = 30 \text{ }^{\circ}\text{C}$$

Outdoor Air Relative Humidity

$$\phi_{outdoor} = 60 \text{ } \%$$

Consequently, in Figure 4.31, in Figure 4.32 and in Figure 4.33 the cooling capacity (power output), sensible heat removed from the house and energy efficiency ratio are represented as a

4. Simulation and Results

function of the air volume flow rate and compressor input frequency for the given outdoor air conditions.

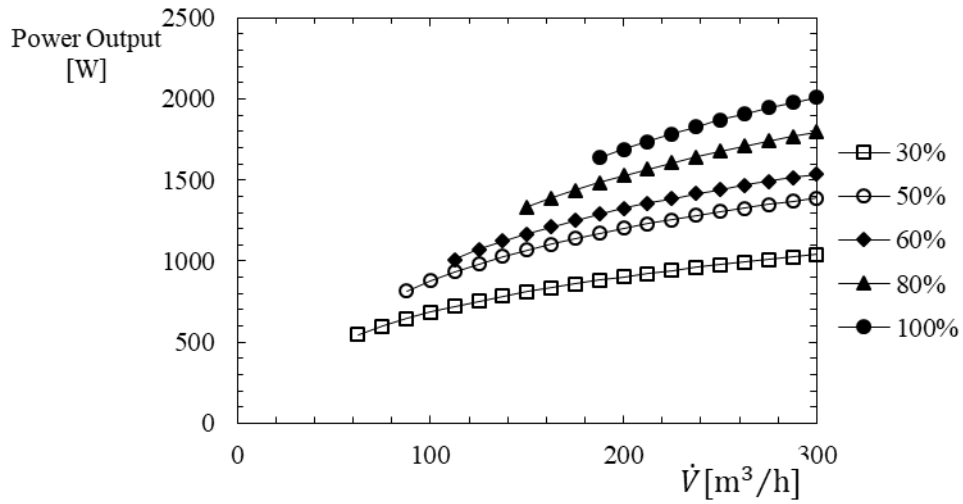


Figure 4.31 – Cooling power output as a function of the air volume flow rate and frequency.

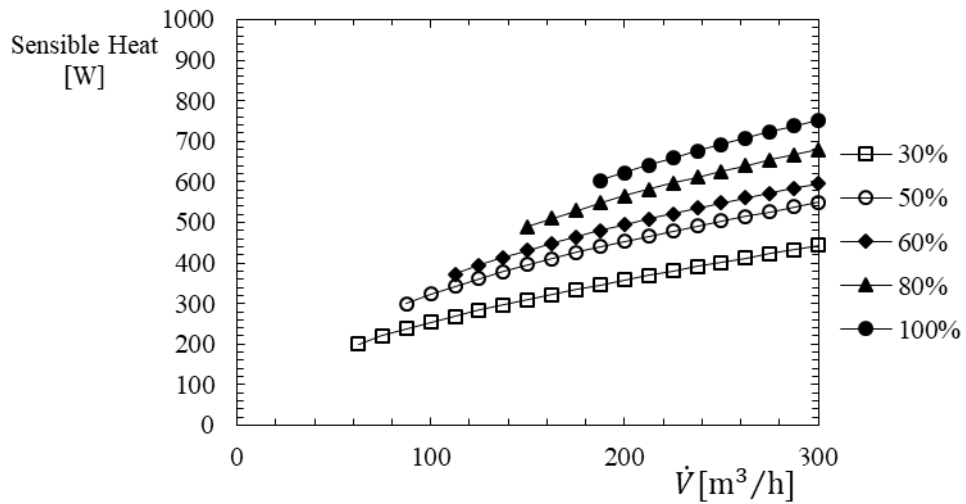


Figure 4.32 – Sensible heat as a function of the air volume flow rate and frequency.

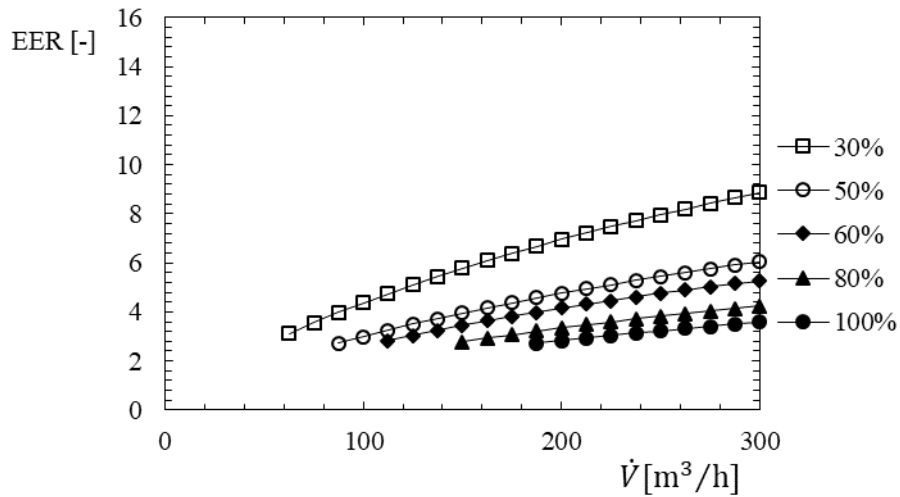


Figure 4.33 – *EER* as a function of the air volume flow rate and frequency.

4.4.2 Energy Recovery Ventilation

Regarding the analysis of the enthalpy recovery ventilation system, this variant is now evaluated by applying the same approach as it was done with only the sensible heat recovery system. Therefore, the heating mode is firstly defined.

Heating Mode

Similarly, total recovered heat is plotted in Figure 4.34 as a function of outdoor air temperature and volume flow rate, in which the values of this output variable are higher than those presented in Figure 4.15, because this value is influenced by the additional capacity of energy recovery, which can be checked in Figure 4.35, where the latent recovered heat is presented.

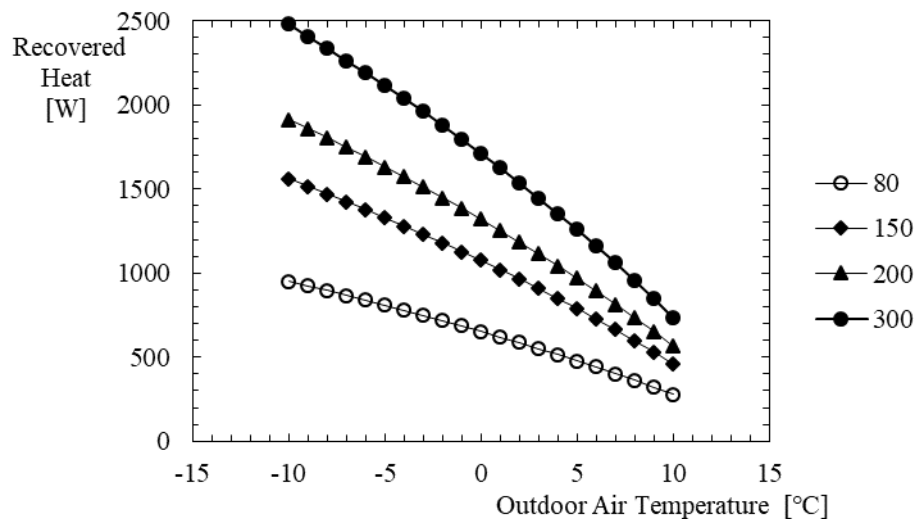


Figure 4.34 – Recovered heat as a function of the outdoor air temperature and air volume flow rate [m^3/h].

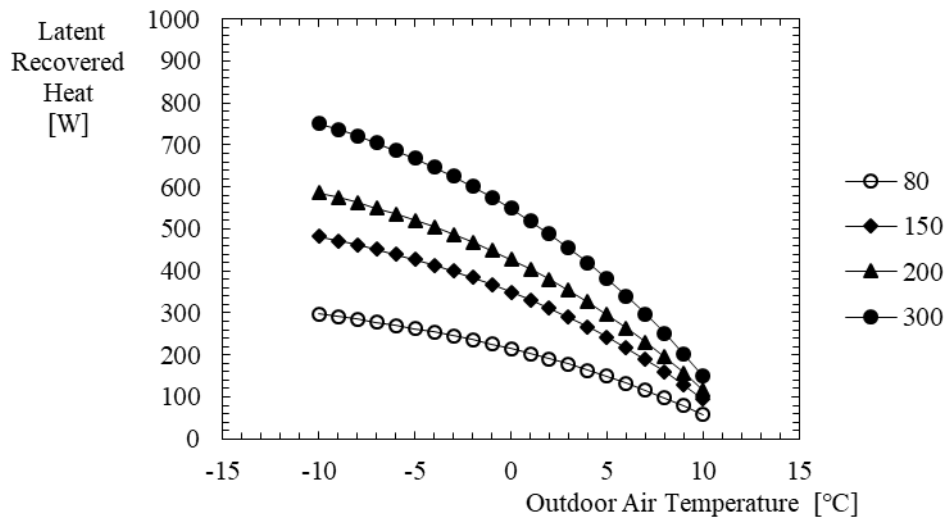


Figure 4.35 – Latent recovered heat as a function of the outdoor air temperature and air volume flow rate [m^3/h].

Fixed Speed

The power output is plotted as a function of the same input variables in Figure 4.36, while Figure 4.37 shows the sensible heat transferred to the house. The first variable has higher values than the equivalent ones presented in Figure 4.22, due to the higher energy recovered, whereas the sensible heat remains approximately constant. For volume flow rates equal to $80 \text{ m}^3/\text{h}$, all outdoor air temperatures are admissible within the compressor's envelope, which does not occur with HRV. This is explained by the fact that the airstream temperature at the entrance of the condenser is lower with ERV (lower sensible effectiveness of ERV), which implies lower condensing temperatures.

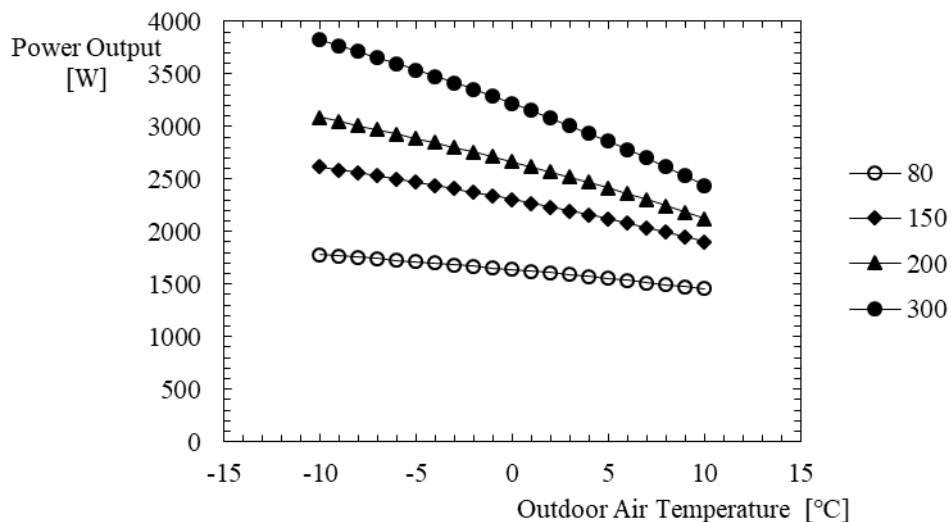


Figure 4.36 – Power output as a function of the outdoor air temperature and air volume flow rate [m^3/h].

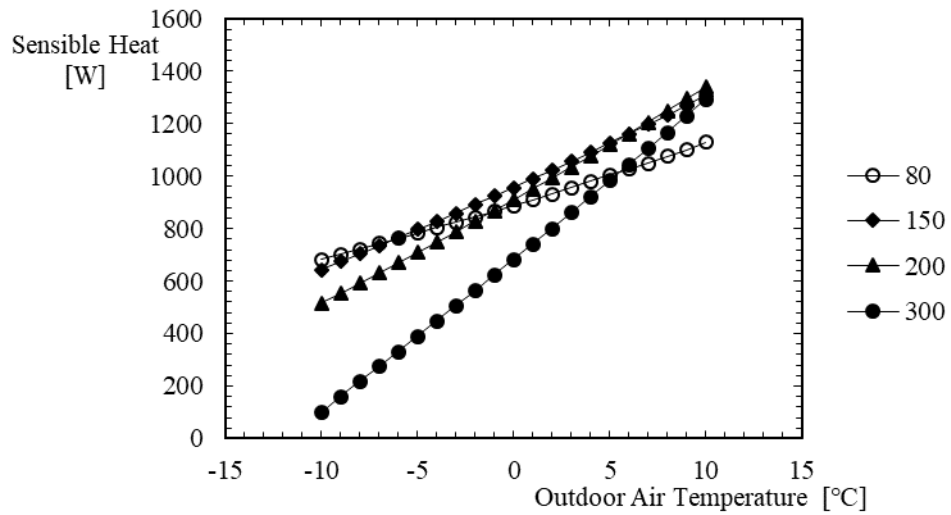


Figure 4.37 – Sensible heat as a function of the outdoor air temperature and air volume flow rate [m³/h].

The coefficients of performance of the overall solution and of the refrigerant cycle are presented in Figure 4.38 and in Figure 4.39 as a function of the same variables.

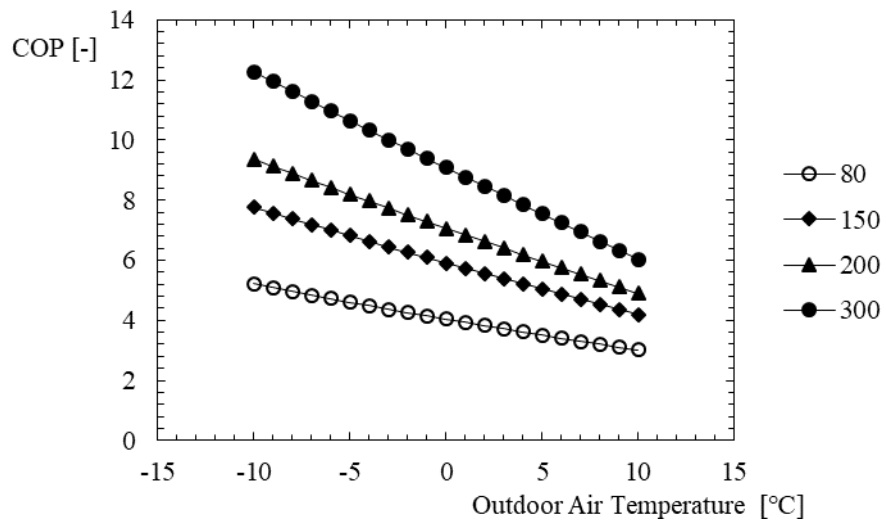


Figure 4.38 – COP as a function of the outdoor air temperature and air volume flow rate [m³/h].

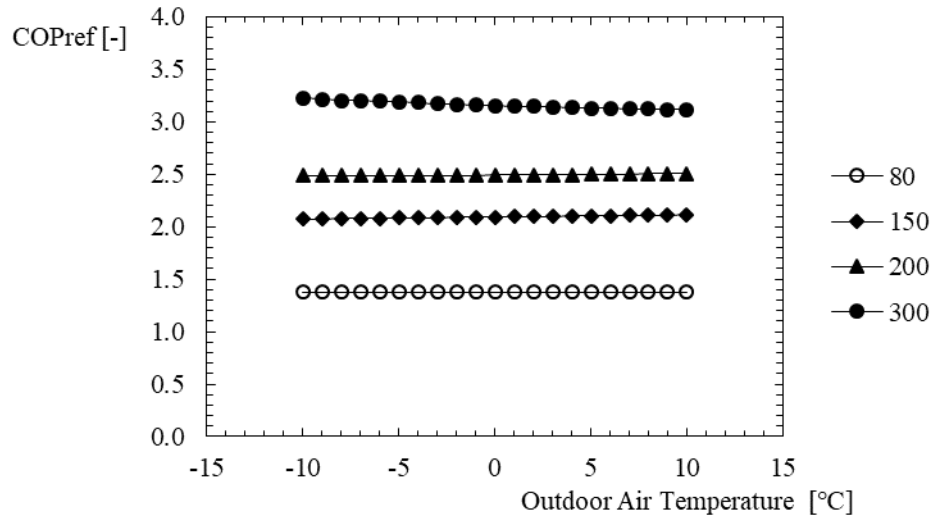


Figure 4.39 – COP of the refrigerant cycle as a function of the outdoor air temperature and air volume flow rate [m³/h].

In Figure 4.40, discharge air temperature values are presented for the same studied cases, and it is possible to conclude that frost formation tendency is higher when ERV is used instead of the variant with HRV system. Similarly, Figure 4.41 shows the supply air temperature for the different working points.

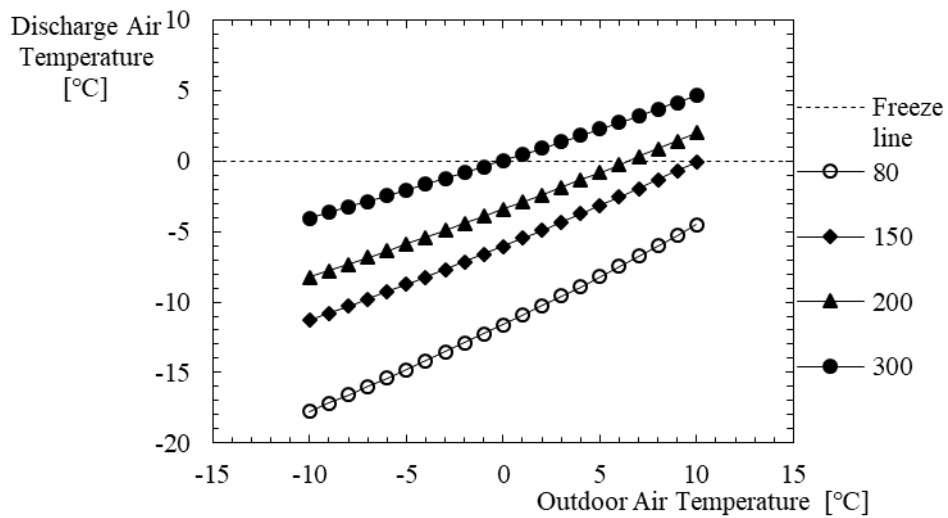


Figure 4.40 – Discharge air temperature as a function of the outdoor air temperature and air volume flow rate [m³/h].

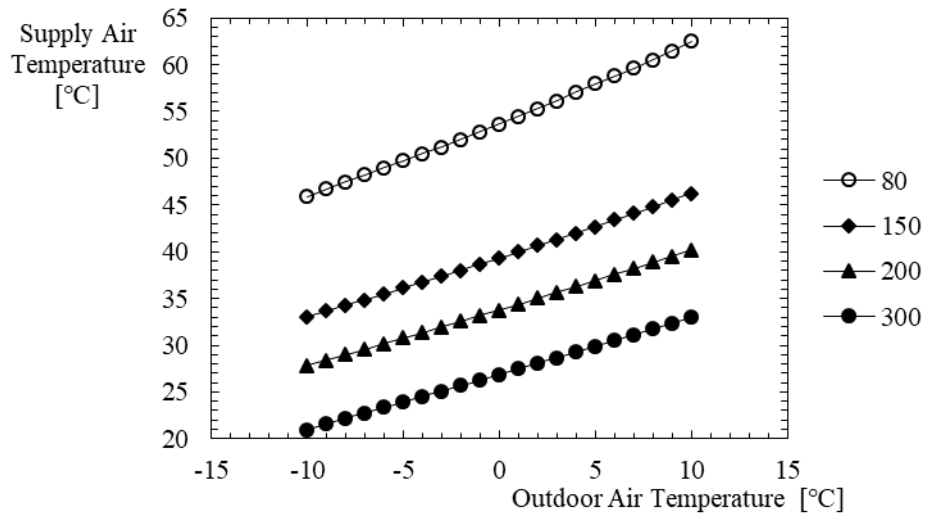


Figure 4.41 – Supply air temperature as a function of the outdoor air temperature and air volume flow rate [m³/h].

Variable Speed

The variation of frequency is also performed within the use of ERV and the air conditions are the same of the HRV case (presented in Table 4.11). Consequently, in Figure 4.42 the power output is plotted as a function of the air flow rate and compressor input frequency, whereas in Figure 4.43 the exchanged sensible heat is represented.

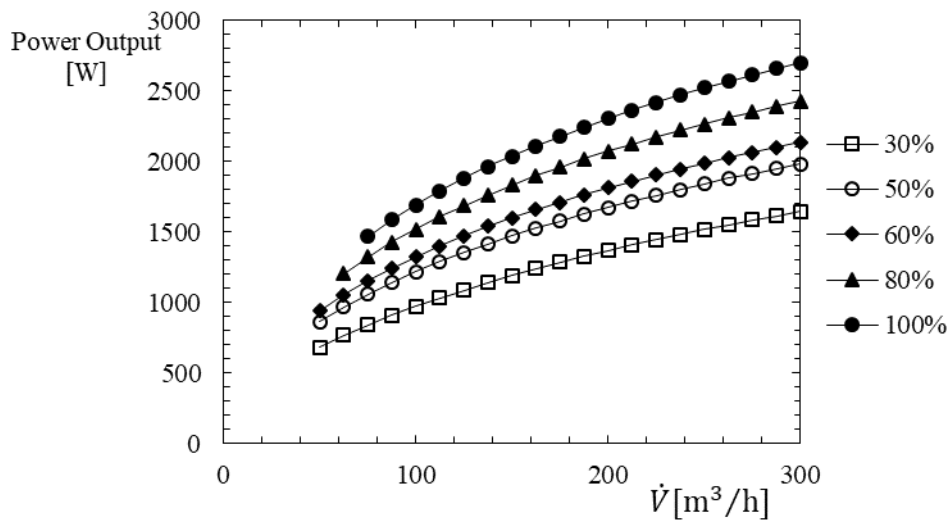


Figure 4.42 – Power output as a function of the air volume flow rate and frequency.

4. Simulation and Results

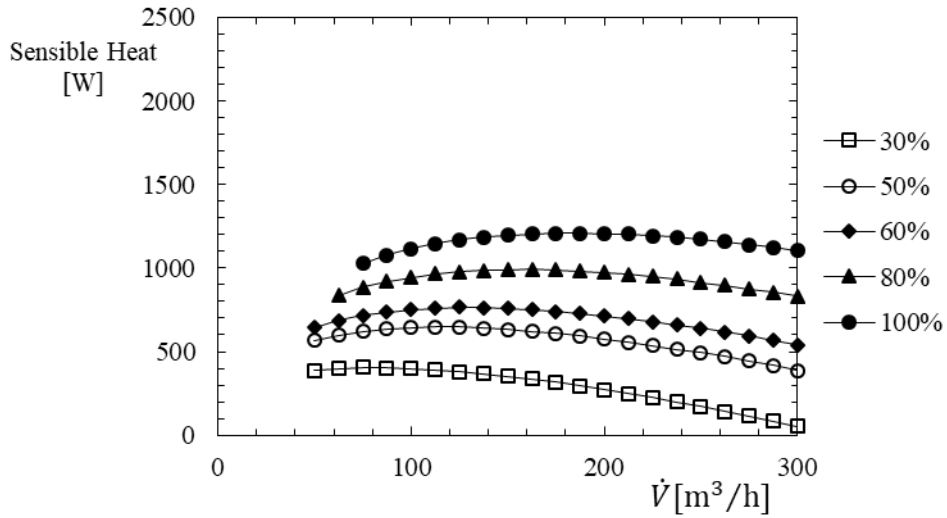


Figure 4.43 – Sensible heat as a function of the air volume flow rate and frequency.

In Figure 4.44, the values of coefficient of performance are presented for the same input variables and Figure 4.45 shows the corresponding discharge air temperature.

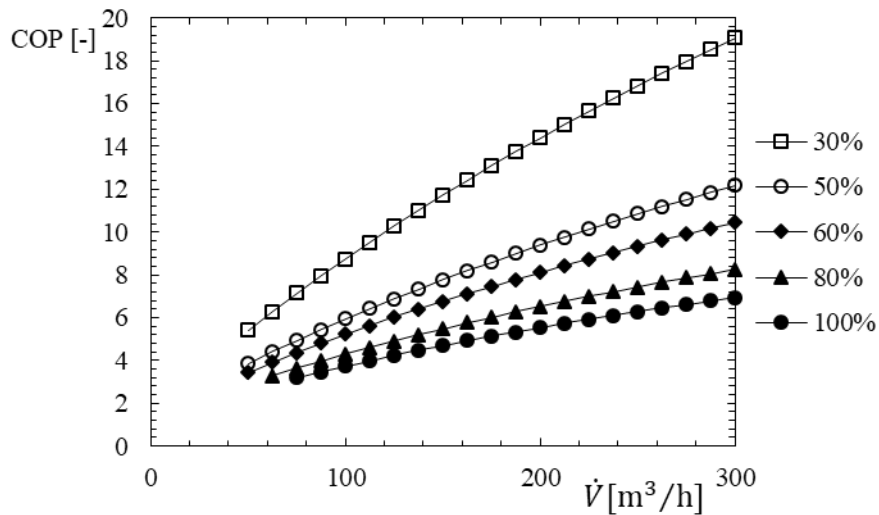


Figure 4.44 – *COP* as a function of the air volume flow rate and frequency.

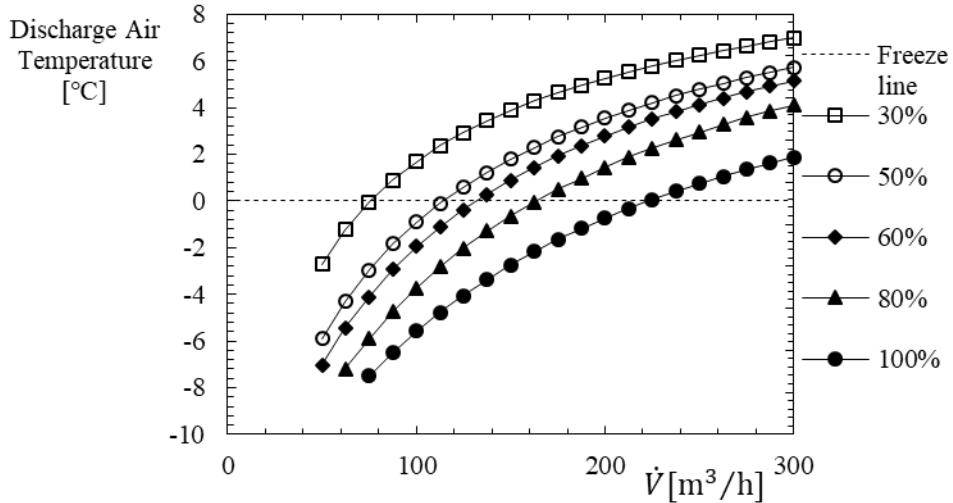


Figure 4.45 – Discharge air temperature as a function of the air volume flow rate and frequency.

Cooling Mode

Similarly with the approach of Section 4.4.1, the cooling mode is defined by the power output (cooling capacity), sensible heat and energy efficiency ratio for the different working modes in terms of compressor’s capacity: fixed and variable speed. Firstly, the total and latent recovered heat are presented in Figure 4.46 and Figure 4.47, respectively.

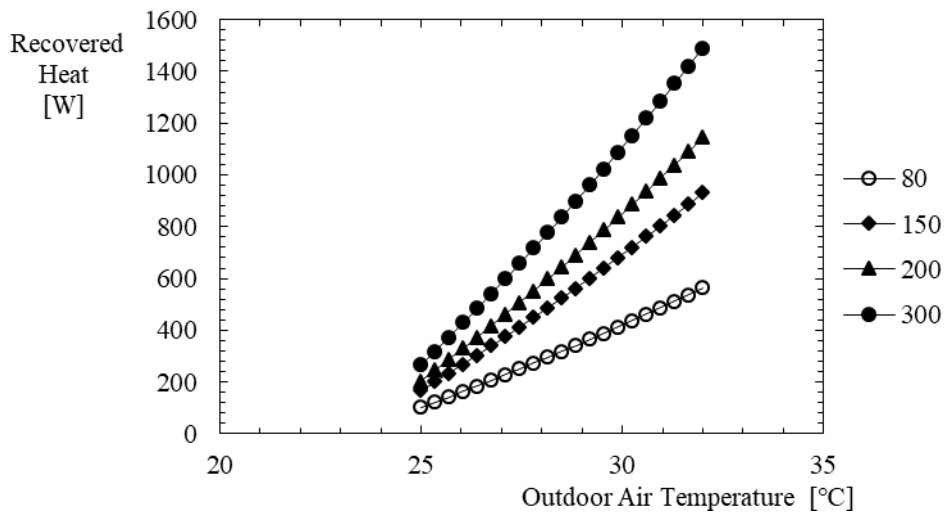


Figure 4.46 – Recovered heat as a function of the outdoor air temperature and air volume flow rate [m³/h].

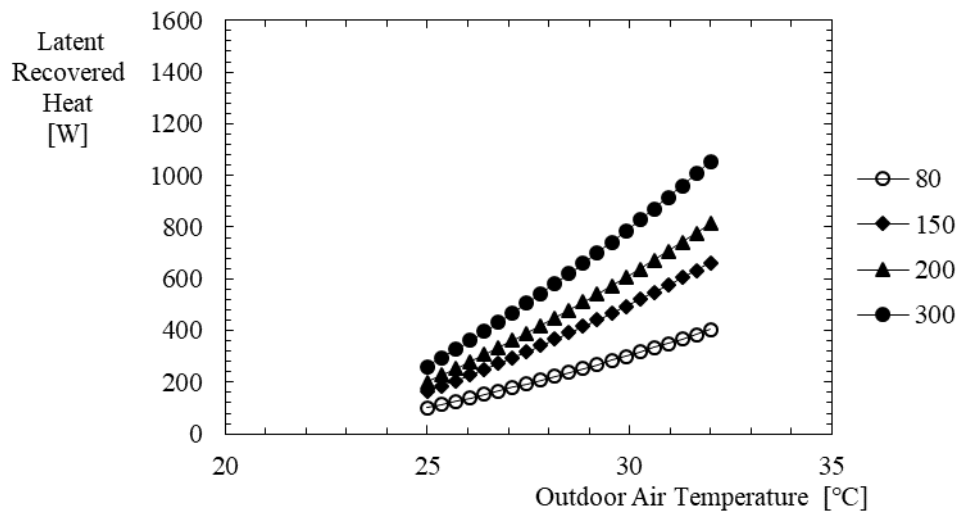


Figure 4.47 – Latent recovered heat as a function of the outdoor air temperature and air volume flow rate [m³/h].

Fixed Speed

Figure 4.48 shows the variation of power output with outdoor air temperature and air flow rates, whereas in Figure 4.49 and in Figure 4.50 the sensible (cooling) heat and energy efficiency ratio are presented, respectively.

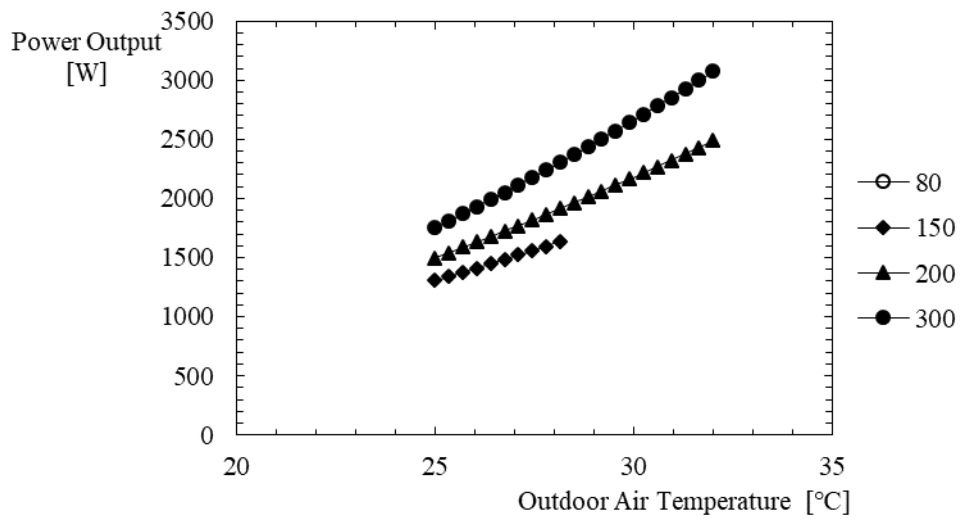


Figure 4.48 – Cooling power output as a function of the outdoor air temperature and air volume flow rate [m³/h].

4. Simulation and Results

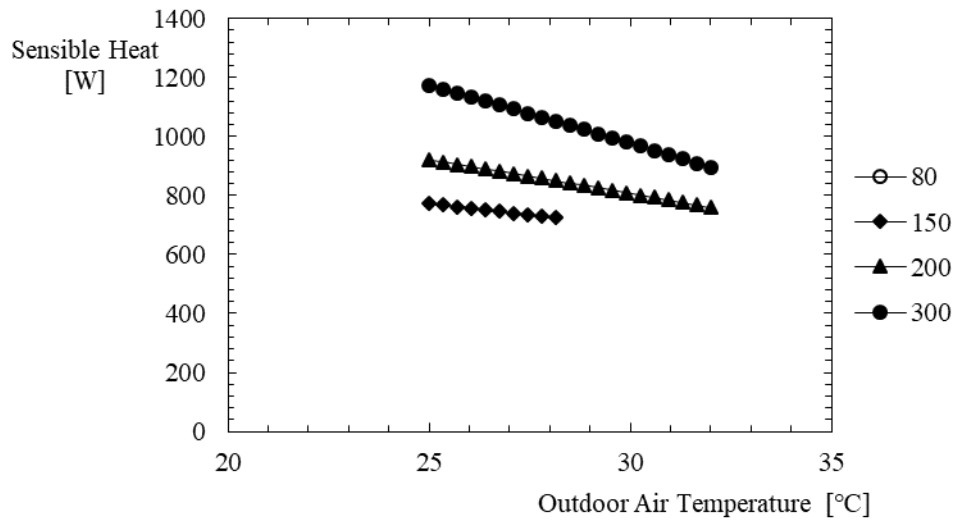


Figure 4.49 – Sensible heat as a function of the outdoor air temperature and air volume flow rate [m³/h].

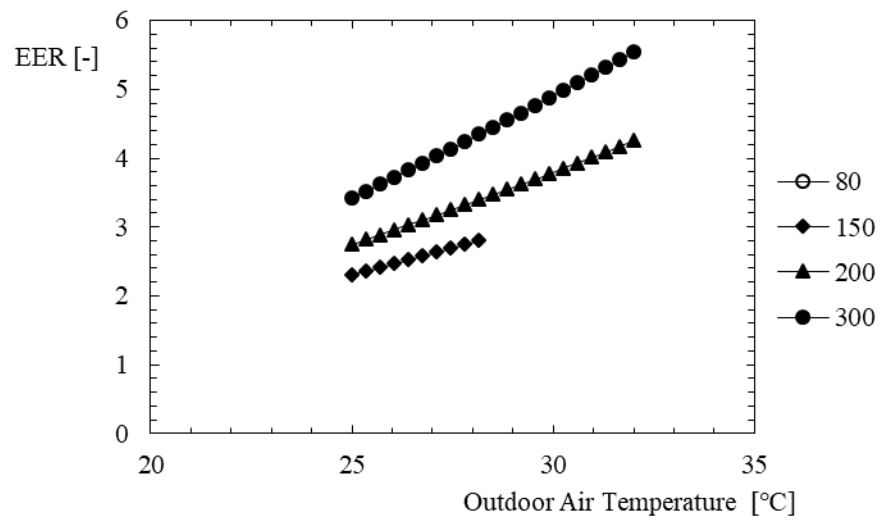


Figure 4.50 – *EER* as a function of the outdoor air temperature and air volume flow rate [m³/h].

In Figure 4.51 the discharge air temperature is plotted as a function of the same input variables.

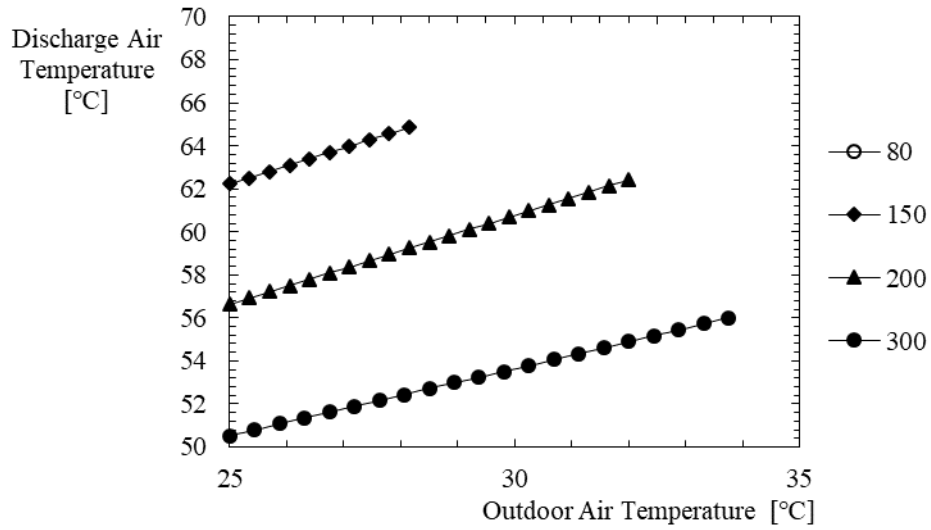


Figure 4.51 – Discharge air temperature as a function of the outdoor air temperature and air volume flow rate [m³/h].

Variable Speed

Regarding the analysis of variation the compressor input frequency, outdoor air conditions are the same as defined in Table 4.12 and power output, sensible heat and energy efficiency ratio are plotted as a function of air volume flow rate and frequency from Figure 4.52 to Figure 4.54, respectively.

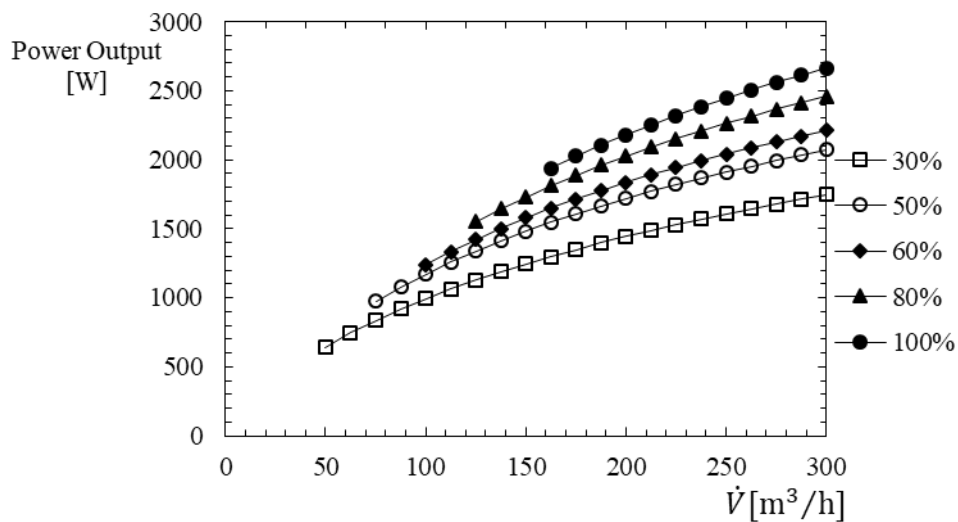


Figure 4.52 – Cooling power output as a function of the air volume flow rate and frequency.

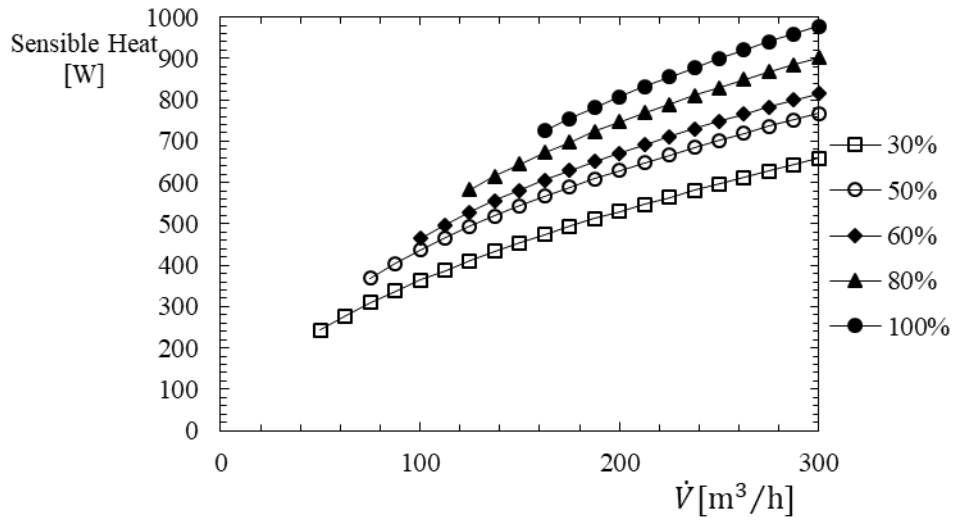


Figure 4.53 – Sensible heat as a function of the air volume flow rate and frequency.

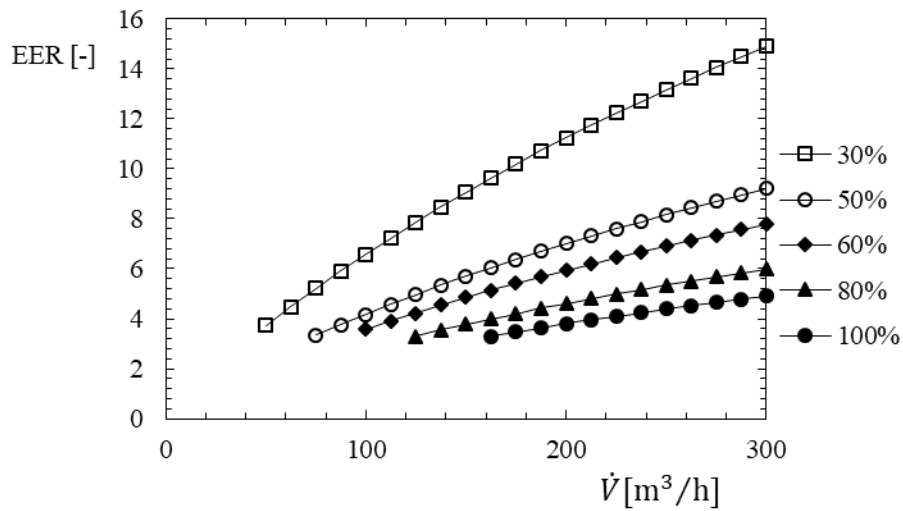


Figure 4.54 – *EER* as a function of the air volume flow rate and frequency.

4.4.3 Comparison between the HRV and ERV

In order to compare the solutions presented in the previous sub-sections, the main parameters are disposed in Table 4.13 for heating mode, where the best solution is selected as well as a brief commentary is stated to justify the difference of the values.

4. Simulation and Results

Table 4.13 – Comparison during heating mode

Parameter	Best solution	Comment
Sensible effectiveness	HRV	Lower plate thickness increases the number of channels, which cause an increase of transfer surface area.
Latent effectiveness	ERV	Membrane based heat exchanger turns possible the transfer of moisture.
Air Temperature after HE	ERV	Lower ε_S leads to higher temperature after HE; Frost formation inside the HE is avoided with ERV.
Recovered Heat	ERV	ERV has lower ε_S , but the gain of ε_L causes an increase of the overall ε .
Power Output	ERV	ERV has higher overall ε and that causes an increase of power output for a similar heating effect of the refrigerant cycle.
Sensible Heat	HRV	HRV has slightly higher values, due to the higher ε_S of the HRV.
COP	ERV	Higher power output leads to higher COP, considering an equivalent value of power consumption.
COP_{ref}	-	The values of both solutions are similar.
Discharge Air Temperature	HRV	Higher potential of energy of the airstream at the entrance of evaporator causes an increase of discharge air temperature. However, by changing the input frequency of the compressor, the heat transferred from the airstream in the evaporator decreases and then the frost formation may be avoided.

Considering the comparison between both solutions during cooling mode, the conclusions regarding power output, sensible heat and energy efficiency ratio (equivalent to *COP*) are the same as during heating mode because of the same reasons. The using of the solution with ERV also implies the advantage of having lower discharge air temperatures (after the condenser), which causes that the condensing temperature is higher than the maximum of the compressor envelope for higher values of outdoor air temperature. This fact turns possible to work with lower values of air flow rate or higher outdoor air temperatures during cooling mode.

[Blank Page]

5 Experimental Analysis

Regarding the experimental analysis, a functional sample is assembled to test and evaluate the performance of the incorporation of a heat recovery system within the heat pump refrigerant cycle. Firstly, the location of the components is defined by representing them in a Piping/Ducting and Instrumentation Diagram (P/D & ID), which also presents the relevant sensors. Secondly, the climate chamber used to guarantee different outdoor air temperatures is described in terms of its working temperature and relative humidity ranges. After, testing procedure is planned, leading to the definition of the used test points. Finally, the results are graphically presented

5.1 Piping/Ducting and Instrumentation Diagram

The definition of the testing procedure becomes transparent by representing all the components and measurement instruments in the Piping/Ducting and Instrumentation Diagram as it is presented in Figure 5.1, in which the green and yellow circuits are related to R134a refrigerant and ventilation circuits, respectively.

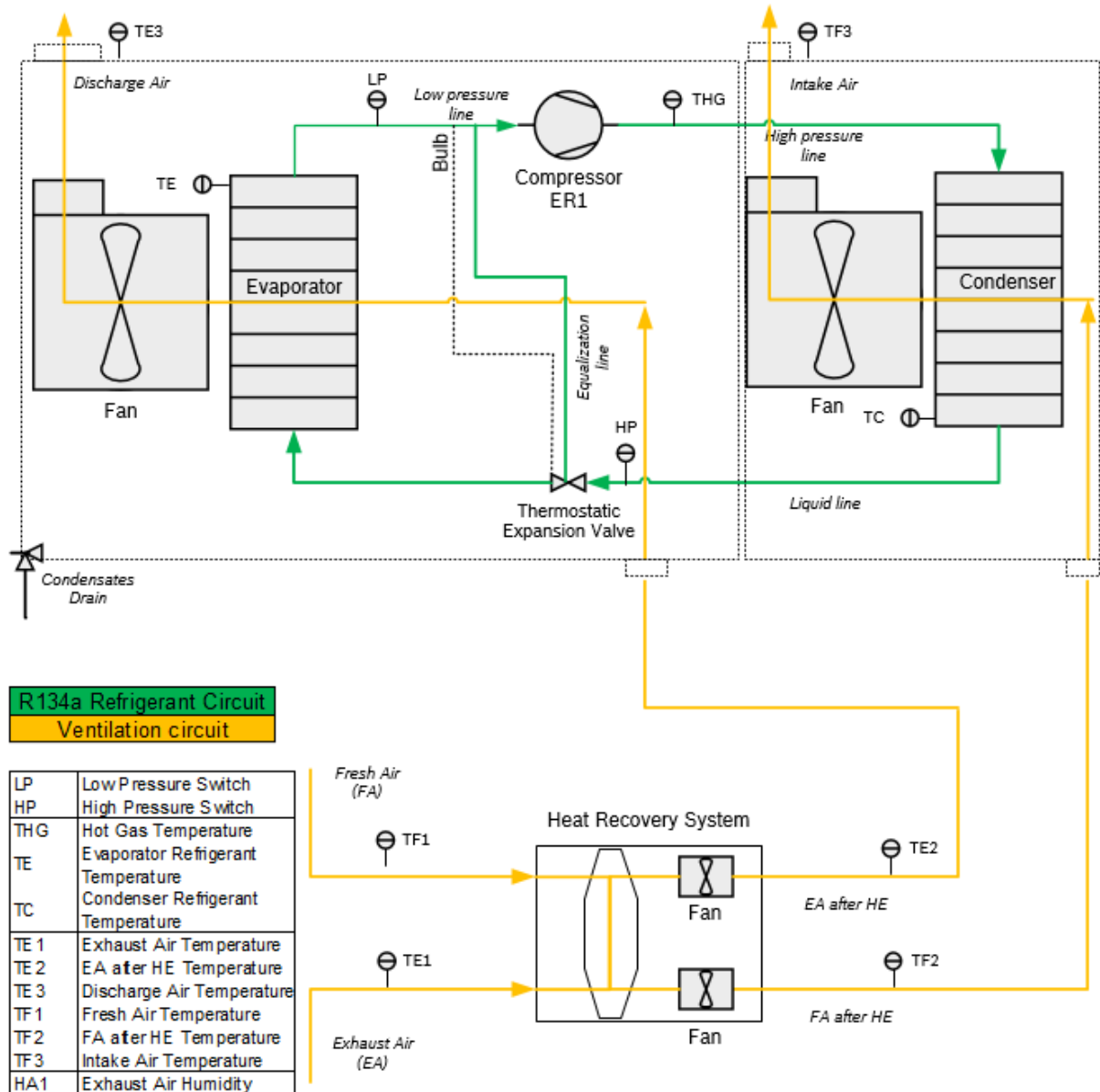


Figure 5.1 – Piping/Ducting and Instrumentation Diagram.

As presented in Figure 5.1, the external electrical heater is not applied to this sample and a heat recovery system solution is used. It is also important to mention that the air volume flow rate will be evaluated in “TE3” and in “TF3” points for exhaust and fresh airstreams, respectively.

5.2 Climate Chamber

The using of a climate chamber, which controls both temperature and relative humidity of the air, ensures the control of the outdoor air conditions and turns possible to define the desired values. Therefore, Table 5.1 shows the range of these variables of air inside the climate chamber.

Table 5.1 – Temperature and Relative Humidity ranges of the climate chamber

Temperature Range	$-20\text{ °C} \leq T \leq 60\text{ °C}$
Relative Humidity Range	$10\% \leq \phi \leq 100\%$

Figure 5.2 shows the user interface of the climate chamber, in which is possible to control the values of temperature and relative humidity of the internal air. The pressure is maintained at atmospheric pressure.



Figure 5.2 – User interface of the climate chamber.

5.3 Measurement Devices

5.3.1 Temperature

Regarding the instrumentation used to measure the different temperature values, the variant used is the thermistor. Its name derives from the term “thermally sensitive resistors” and is available in two types, NTC and PTC, negative and positive temperature coefficient, respectively. The NTC thermistor is the commonly used to measure temperature and it has a highly nonlinear change decrease of resistance with increases in temperature. The higher resistance change per degree of temperature (high resolution), the high level of repeatability and stability and the fast response to temperature changes, due to the small size, are the main advantages when it is compared with RTD or thermocouple variants [34, 35].

The NTC thermistors are typically defined by its constant, β , measured in Kelvin and it is obtained by the given formulation [36]:

$$\beta = \frac{\ln\left(\frac{R_T}{R_{T_0}}\right)}{\frac{1}{T} - \frac{1}{T_0}} \quad (5.1)$$

5. Experimental Analysis

where

T and T_0 are respectively the desired and reference temperatures in Kelvin, and

R_T and R_{T_0} are the electric resistance at T and T_0 , respectively.

The used sensors are defined as R0, R40 and R80, and its reference number is related with the temperatures values that are expected to be measured, i.e., R0 is more suitable for measuring low temperature values, whereas the higher values are measured by R80.

Table 5.2 – Sensors specific values [37]

Sensor	T_0 [°C]	T [°C]	R_{T_0} [kΩ]	R_T [kΩ]	β [K]	Tolerance
R0	-20	50	46.32	1.686	3872	1%
R40	0	80	32.82	1.259	3932	1%
R80	20	100	25.03	1.344	3999	1%

Figure 5.3 shows the variation of the values electrical resistance of the different sensors as a function of the temperature.

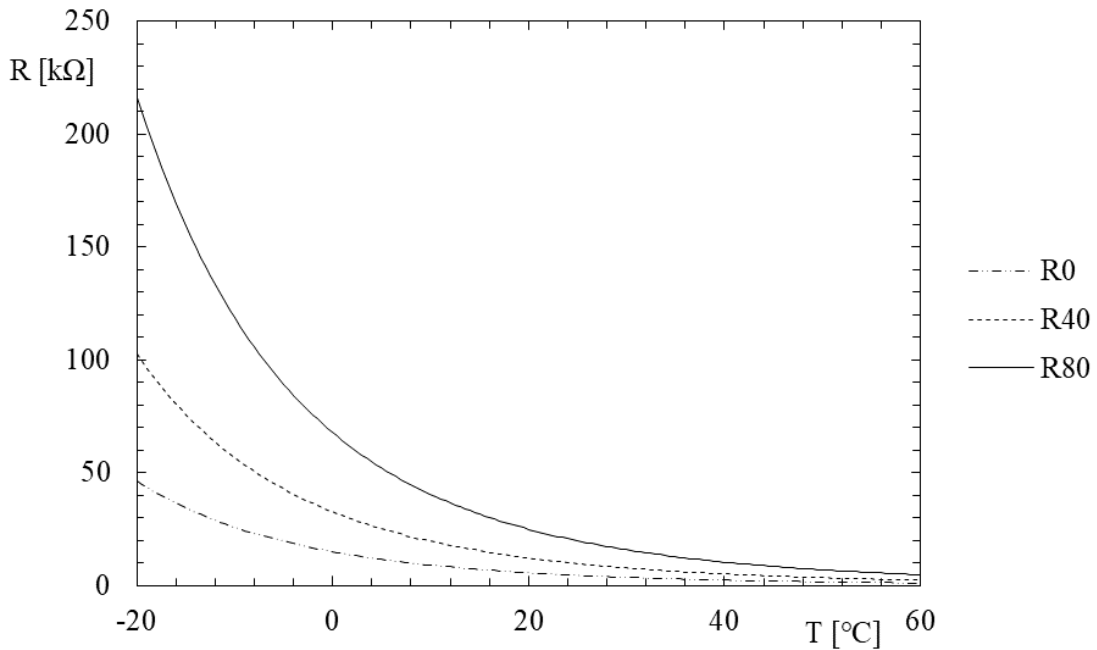


Figure 5.3 – Electrical resistance of the different sensors.

Considering the high variation of electrical resistance needed to verify a variation of temperature values, due to the non-linearity of the characteristic curve of the thermistors and the high values of electrical resistance, the error caused by the electrical resistance of the cables is neglected. However, the value of this parameter is calculated by the following expression to validate this assumption:

$$R_e = \frac{\rho_e \cdot l}{A} \quad (5.2)$$

where ρ_e is the electrical resistivity. Assuming a maximum length of 10 m, a cross section area of 0.5 mm² and that the cables are made of copper ($\rho_e=1.724 \times 10^{-8} \Omega\text{m}$ at 20 °C), the electrical resistance caused by the cables is equal to 0.335 Ω , which is a very low value when compared with those presented in Figure 5.3. In Table 5.3 the variant of each sensor is presented.

Table 5.3 – Correspondence between sensors name and variant

Sensor name	Sensor variant	Sensor name	Sensor variant
TE	R0	TF1	R40
TE3	R0	TF2	R40
THG	R80	TF3	R40
TE1	R40	TC	R40
TE2	R40		

5.3.2 Air Volume Flow Rate

Regarding the measurement of the air volume flow rate, a measuring tube is used in which a difference of pressure caused by a reduction of diameter is measured and the desired variable is obtained. In Figure 5.4 the flow rate calibration curve is plotted as a function of the pressure drop as well as the 6th order polynomial adjustment which fits those values obtained from the specifications of this measurement device.

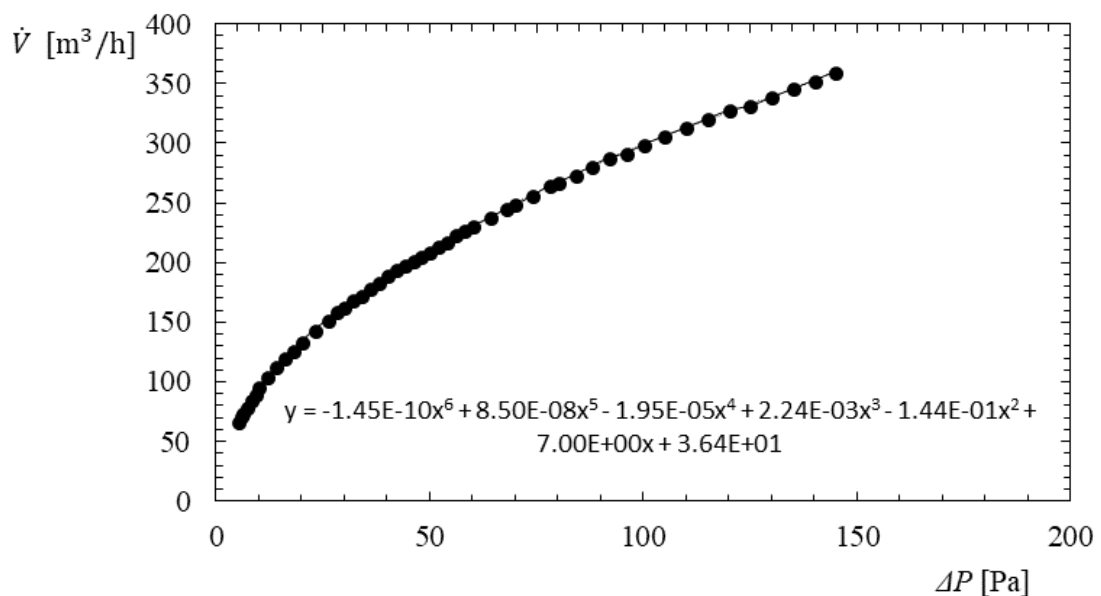


Figure 5.4 – Calibration curve of the air volume flow rate measurement.

5. Experimental Analysis

It is important to mention that this calibration curve was obtained for 20 °C and 1013.25 mbar of airstream temperature and pressure, respectively. Both airstream volume flow rates are evaluated at different conditions than 20 °C and the values of temperature change during the different operation points. This approximation causes an error due to the variation of air properties (density and viscosity, for example), which change the behaviour of the air flow passing through this obstacle, but this error is maintained because of a lack of air flow measurement devices. Figure 5.5 shows the measurement device to evaluate the air volume flow rate (obstruction type) whereas in Figure 5.6 the pressure differential transducer is presented.



Figure 5.5 – Volume flow rate measurement device.

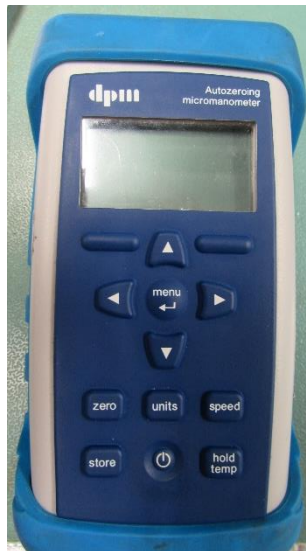


Figure 5.6 – Pressure differential transducer.

In Appendix B, the procedure to quantify the uncertainties of the measurements is defined for each relevant influence variable as well as its influence on the global uncertainty of the output variables.

5.4 Functional Sample

In this section, the main components of the functional sample and the corresponding piping connections are presented. In Figure 5.7, the evaporator, compressor and expansion valve are presented, whereas in Figure 5.8 the fixed speed rotary compressor is shown.

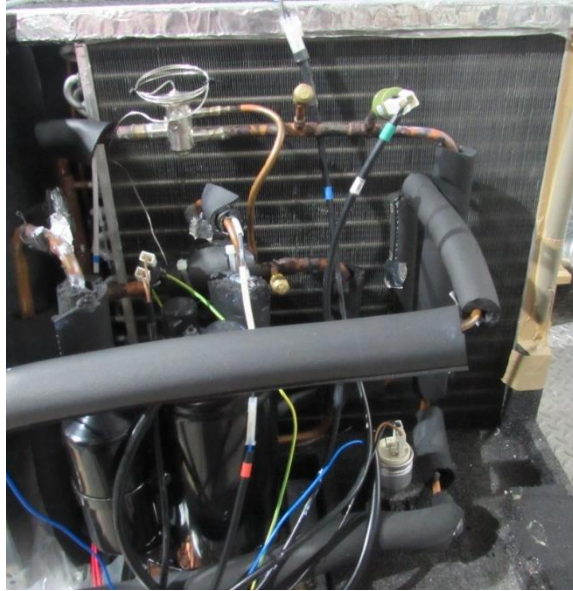


Figure 5.7 – Evaporator, compressor and expansion valve.



Figure 5.8 – Fixed speed rotary compressor.

A top view of the connection between the refrigerant boxes is shown in Figure 5.9 in which it is possible to verify the considerable probability of air leakage and this error is not taken into account in the volume flow rate measurements.

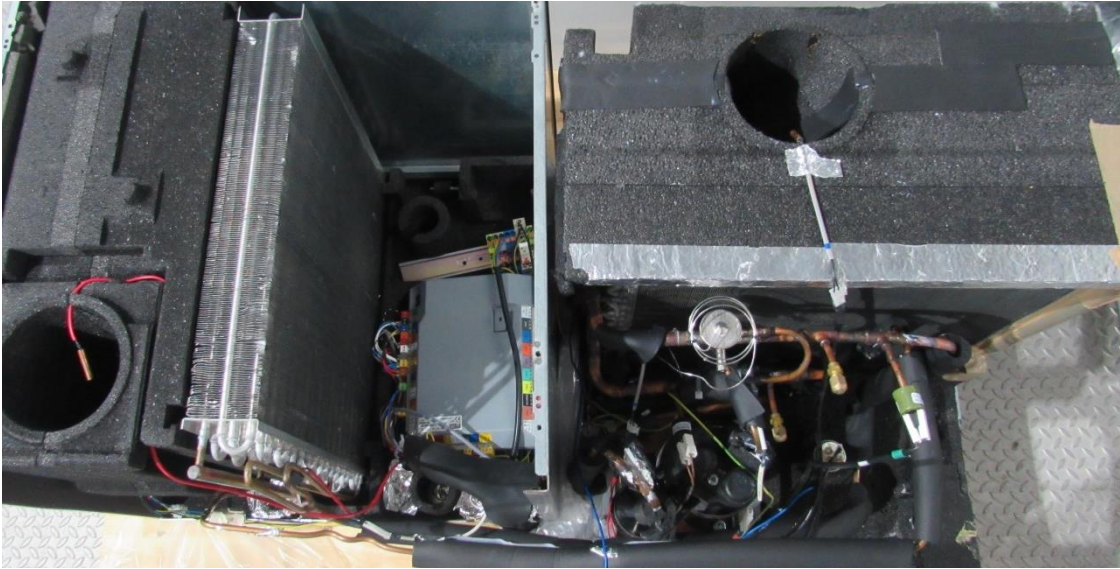


Figure 5.9 – Connection between condenser and the other components.

Figure 5.10 shows the HRV system, whereas Figure 5.11 presents the connection between the components and the duct connection between the HRV system as well as the climate chamber at low temperature. It is important to mention that both circuits are inside the climate chamber at ambient temperature (20 °C).



Figure 5.10 – Heat Recovery Ventilation system.

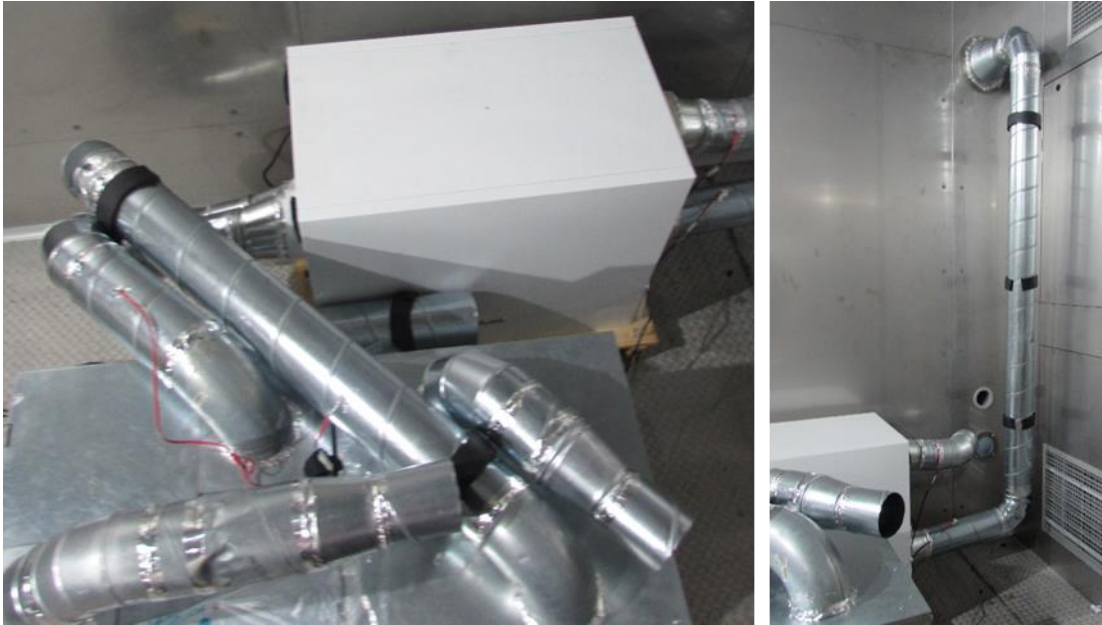


Figure 5.11 – Duct connection between refrigerant boxes, HRV and climate chamber.

Finally, the electrical connection to electrically feed the system and to read the output variable values of temperature and power consumption is presented in Figure 5.12.

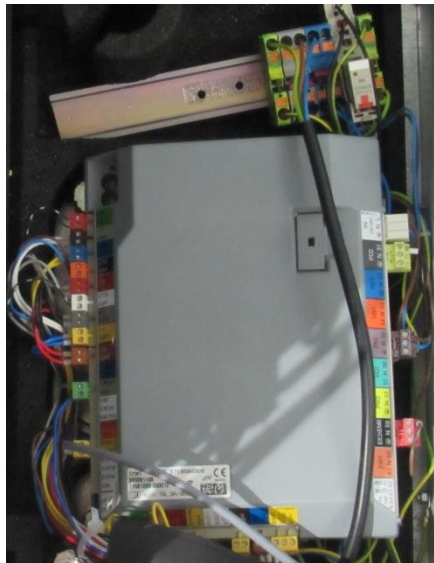


Figure 5.12 – Electrical connections.

5.5 Refrigerant Charge

The refrigerant charge process becomes an important step to achieve an optimum operation point, in which a minimal consumption of refrigerant, due to resources scarcity and environmental questions, and an optimal efficiency of the vapour compression cycle have to be satisfied. Therefore, the minimum charge is defined as that ensuring stable operation at conditions in which the upstream liquid column to the expansion device is sufficient to avoid bubbles formation inside this component. As mentioned before, a minimum value superheated degrees at the entrance of the compressor have to be guaranteed in order to avoid the entrance of liquid inside the compressor [38, 39, 40].

During operation, the distribution of refrigerant depends on the density of the fluid at specific thermodynamic conditions and on its internal volume. Considering a typical operation of a refrigeration circuit, the refrigerant is in vapour form between the outlet of the evaporator and the entrance of the condenser, and the refrigerant charge contained in these parts is neglected. The condenser contains a high amount of refrigerant in the two-phase and sub-cooling regions and most of the refrigerant charge is in the region where the liquid phase of the fluid occurs, i. e. in a considerable part of the condenser and liquid line (between condenser and expansion valve), and this amount will rise with the existence of subcooled degrees. The evaporator is the remaining component in which a relevant refrigerant charge is required due to the two-phase fluid flow through it [38]. In Table 5.4 the refrigerant charge is obtained as a function of the main dimensions of the relevant parts mentioned previously, as well as the assumed temperature for a typical operation point, the density of the refrigerant at liquid phase and an estimation of the volumetric fraction of liquid when two-phase fluid is expected. The density values were obtained from EES software.

Table 5.4 – Refrigerant charge distribution

Component	Temperature [°C]	ρ_l [kg/m ³]	% of liquid	D [mm]	L [m]	m_{ref} [kg]
Evaporator	5	1278	20	6.5	22.41	0.190
Condenser	35	1147	30	6.5	22.41	0.256
Liquid line	35	1147	100	10	1.46	0.132
Total						0.577

The values presented in Table 5.4 represent a first approximation of the refrigerant charge, in order to fill the refrigerant circuit with a minimum amount of fluid. Then, the amount of refrigerant is adjusted to obtain the desired subcooled and superheated degrees at the entrance of the expansion valve and compressor, respectively. When the refrigerant charge is higher than the required value, the subcooled and superheated degrees decrease and the risk of damaging the compressor, due to having liquid phase at its inlet, or to have bubbles formation becomes real, and the performance of the refrigerant cycle drops. Therefore, the critical operation point has to be defined to ensure that the refrigerant charge is sufficient to avoid these phenomena. In general, most of the extra charge remains at liquid phase inside the condenser outlet, causing a reduction of the area available for refrigerant condensation and consequently a decrease of the performance of the cycle [38].

The use of a liquid receiver could be a solution to compensate fluctuations of refrigerant mass flow rate and then ensuring a optimum value of subcooled and superheated degrees. That would imply a higher efficiency of the process. However, this component requires an increase of refrigerant charge, because the fluid is at liquid phase inside the liquid receiver and the desired reduction of refrigerant charge would not be achieved [38].

Considering the previous assumptions and the information presented in Table 5.4, the refrigerant circuit is filled with 0.550 kg of fluid as a first approximation and the next step of adjusting this value to achieve the desired conditions is now described. This amount of refrigerant is higher than the quantity used in the equivalent refrigerant circuits of the air-to-water heat pump, because the condenser is a refrigerant-to-air type, instead of refrigerant-to-water, and this leads to higher dimension of refrigerant circuit inside this component. It is important to mention that a vacuum test had to be performed to ensure that no refrigerant leakage occurs.

All relevant points are defined in terms of their temperature, by using the temperature sensors defined in Section 5.3.1. As mentioned in Section 5.4, the using of isolation around refrigerant tubes in liquid line (between condenser and expansion valve) or hot gas line (between compressor and condenser) is analysed in terms of temperature difference between the referred points in Section 5.7.1.

5.6 Test Points

Considering the limitation of resources and time, the test points to evaluate the performance of the functional sample are the same as the used to evaluate air-to-water appliances and only the heating mode is analysed. The values are presented in DIN EN 14511:2013 norm, and this is the standard to evaluate “Air conditioners, liquid chilling packages and heat pumps with electrically driven compressors for space heating and cooling”, in which the second part shows the required test conditions.

Table 5.5 – Air-to-air test conditions [41]

Outdoor air conditions		Indoor air conditions	
Dry bulb temperature [°C]	Wet bulb temperature [°C]	Dry bulb temperature [°C]	Wet bulb temperature [°C]
12	11	20	15 max
7	6	20	15 max
2	1	20	15 max
-7	-8	20	15 max

Regarding the values of air volume flow rate, this parameter is chosen to avoid the frost formation inside the evaporator, because neither external electrical heater nor compressor input frequency changing are used to compensate this phenomenon. Therefore, the range of air volume flow rate is defined by using the results of the modelling and applying the air conditions presented in Table 5.5.

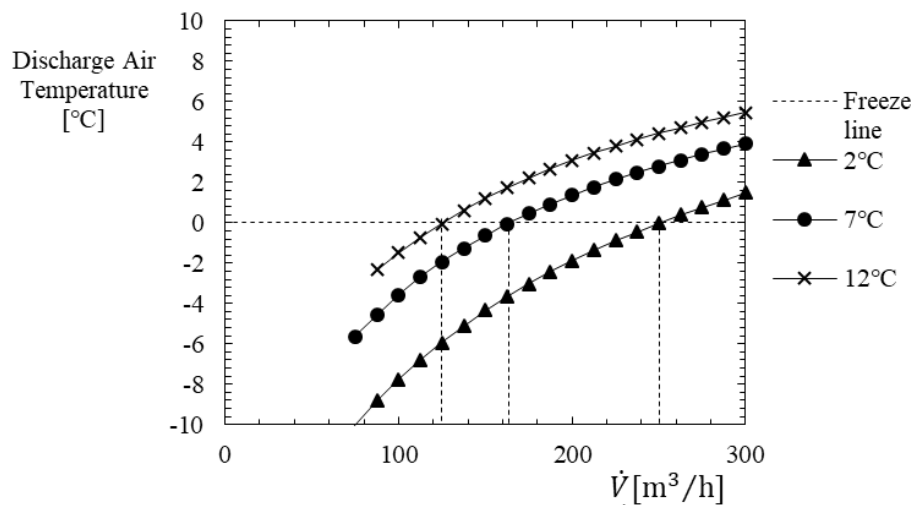


Figure 5.13 – Discharge air temperature as a function of air volume flow rate and outdoor air temperature.

5. Experimental Analysis

The minimum values of volume flow rate are then defined by looking at Figure 5.13 and these approximated values are presented in Table 5.6.

Table 5.6 – Minimum values of volume flow rate

T [°C]	\dot{V} [m ³ /h]
2	250
7	160
12	120

Therefore, the desired values of volume flow rate are defined as well as the corresponding pressure differential by the adjustment to the 6th order polynomial presented in Figure 5.4. This information is shown in Table 5.7.

Table 5.7 – Values of volume flow rate and difference of pressure to be measured by the manometer

$T = 2$ °C		$T = 7$ °C		$T = 12$ °C	
\dot{V} [m ³ /h]	ΔP [Pa]	\dot{V} [m ³ /h]	ΔP [Pa]	\dot{V} [m ³ /h]	ΔP [Pa]
250	70.3	160	28.8	120	15.9
270	81.7	190	41.0	150	25.1
285	91.0	220	54.8	180	36.7
300	101.0	250	70.3	210	50.1
		280	87.8	240	64.9
		300	101.0	270	81.7
				300	101.0

5.7 Test Results

Regarding the results of the tests, several parameters are initially evaluated to quantify the thermal loss in refrigerant pipes caused by the high length of liquid and gas lines and the influence of insulating these tubes, as well as the analysis of subcooled and superheated degrees to verify the refrigerant charge. After, the Heat Recovery Ventilation system is evaluated by the same variables as in Section 0, as well as the refrigerant phase change heat exchangers and the overall solution. It is important to mention that all the results are obtained after establishing of steady-state regime of the output variables.

5.7.1 Refrigerant Charge and Insulation Analysis

The using of insulation is now studied in order to minimize the heat losses through the refrigerant circuit. Firstly, considering that the higher temperature drop of the refrigerant occurs in gas zone, which does not necessarily mean that this is the region characterized by the higher energy loss, this part is evaluated. The refrigerant pipe between the evaporator and the compressor is not insulated because this hypothetical rise of temperature is not avoided in order to guarantee the vapour phase at the entrance of the compressor. The superheated and subcooled degrees as well as the temperature drop through gas and liquid lines are evaluated for two different values of air volume flow rate, in order to take into account the variation of phase-change temperatures. In Table 5.8 the location of the 10 mm thick layer of neoprene pipe insulation is presented for each test.

Table 5.8 – Location of insulation

Test number	Insulation in the refrigerant circuit
1	No
2	Gas line (Between refrigerant boxes)
3	Gas line (all)
4	Gas and liquid lines

The values of superheated degrees ΔT_{sh} , subcooled degrees ΔT_{sc} , temperature drop in liquid line ΔT_{liq} , and temperature drop in gas line ΔT_{gas} , are presented for each test point in Figure 5.14 and in Figure 5.15, for low and high air volume flow rates, respectively. The inlet temperature of air is maintained approximately constant and equal to 20 °C.

5. Experimental Analysis

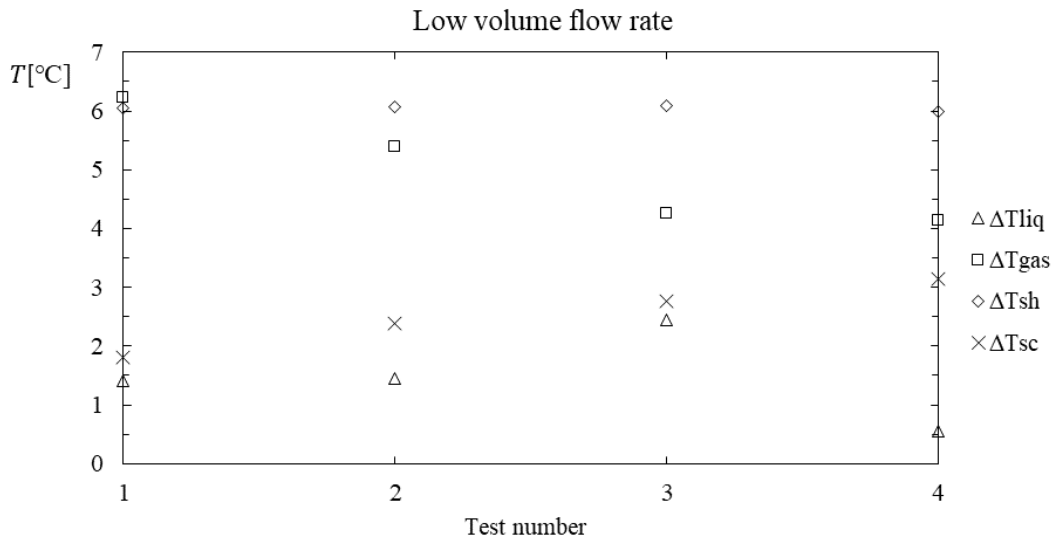


Figure 5.14 – Insulation analysis for low volume flow rate.

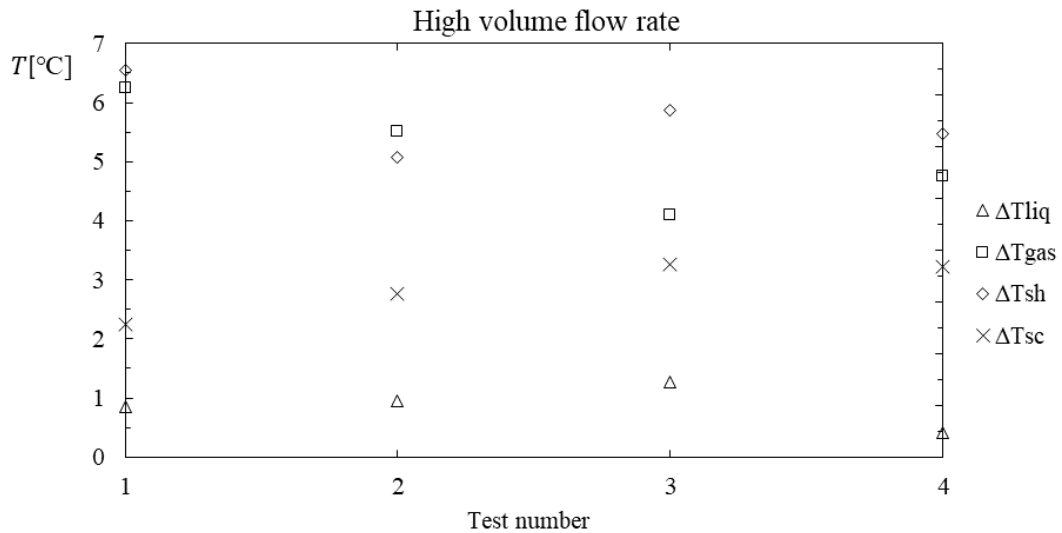


Figure 5.15 – Insulation analysis for high volume flow rate.

From the analysis of the values presented in both figures it is possible to verify that with lower volume flow rates (and consequently higher condensing and lower evaporating temperatures), the temperature drop through gas and liquid lines is higher because of the higher temperature difference between refrigerant and air. The superheated degrees are approximately constant for both cases and equal to 6 °C, a value inside the recommended range. The values of subcooled degrees and the refrigerant charge are assumed to be correct. With the application of insulation, the temperature drop decreases significantly, and the conditions of the test number 4 are maintained for the evaluation of the overall solution.

5.7.2 Results Analysis

After the application of the insulation around the refrigerant tubes, the testing procedure starts. Therefore, the test results are presented in Appendix C for each test point defined in Section 5.6. By looking at the tables presented in this appendix, it is possible to conclude that the values of work input of the compressor are lower than the values predicted by the modelling and it may be explained by the probable increase of isentropic efficiency of the compressor when the difference of phase change temperatures is lower or by the variation of volumetric efficiency as a function of the pressure ratio.

It is also possible to verify that the values of condensing temperature T_C , are always higher than the values of fresh air passing after the condenser T_{F3} , which means that the heat transfer analysis of the compressor has to be adjusted in order to quantify the higher hot gas temperatures at the outlet of the compressor. This analysis could not be performed because of the limited number of sensors available for the high pressure refrigerant circuit.

Now, the sensible effectiveness of the Heat Recovery Ventilation system is analysed and its results are presented in Figure 5.16 for each test point. The experimental values are defined in terms of its global uncertainty by following the procedure explained in Appendix B.

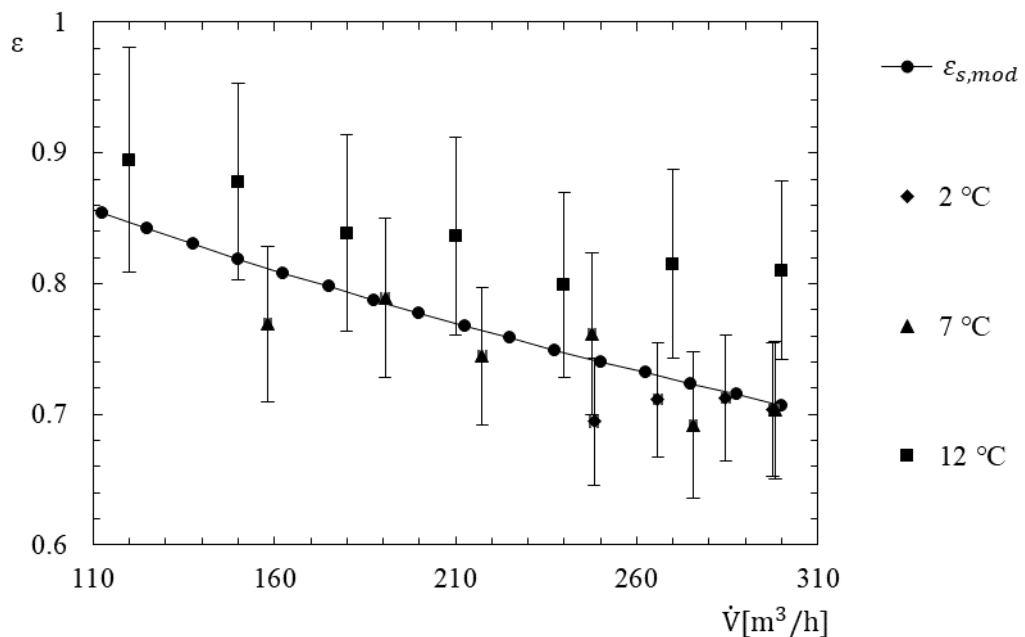


Figure 5.16 – Sensible effectiveness of the HRV.

The results presented in Figure 5.16 show that the values obtained by the modelling in Section 4.1.1 fit in the experimental values and the higher difference occurs in the results of the tests at 12 °C of outdoor air temperature, which are the values with higher uncertainty due to the lower value of the denominator, because of the low temperature difference between outdoor and indoor airstreams.

5. Experimental Analysis

The evaporator is also analysed in terms of its sensible effectiveness and the values are presented in Figure 5.17, as well as the error bars taking into account the global uncertainty of the values.

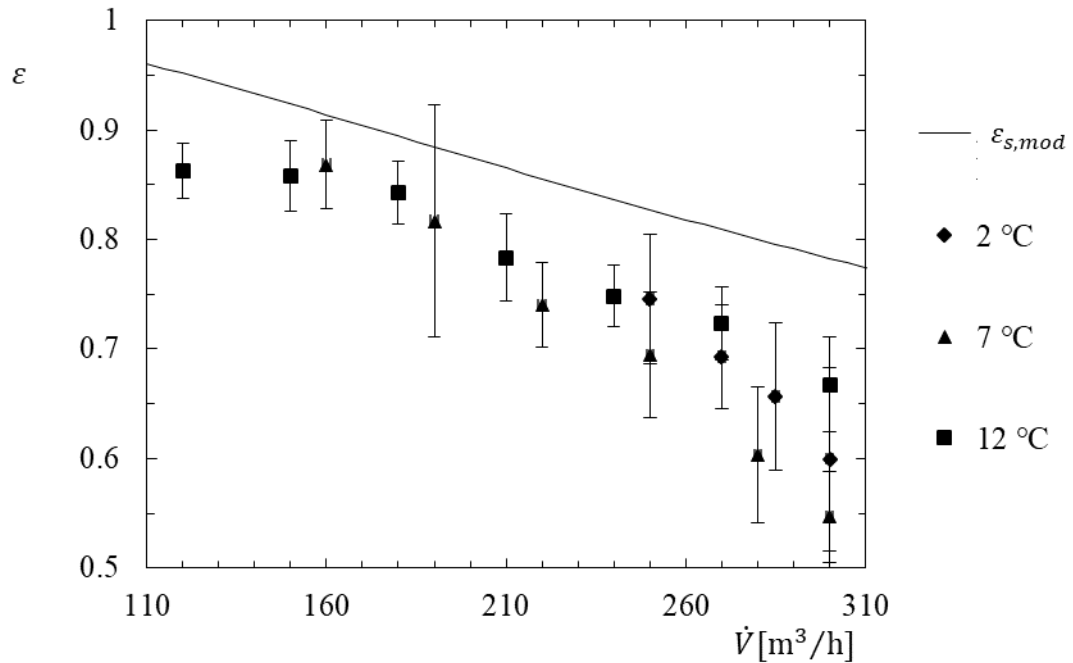


Figure 5.17 – Sensible effectiveness of the evaporator.

The measured values of sensible effectiveness of the evaporator are lower than those obtained by the modelling which may be caused by differences in refrigerant flow rate in the three different paths inside this component, and the decreasing of effectiveness in lower side fluid flow rate may not compensate the increasing of effectiveness in the other. However, this difference is not higher than 25 % and it is acceptable because of the using of correlations, that by themselves have also high uncertainty values.

The experimental values of the power output are also plotted as a function of the air volume flow rate and outdoor air temperature, in Figure 5.18, with the corresponding error bars and modelling results.

5. Experimental Analysis

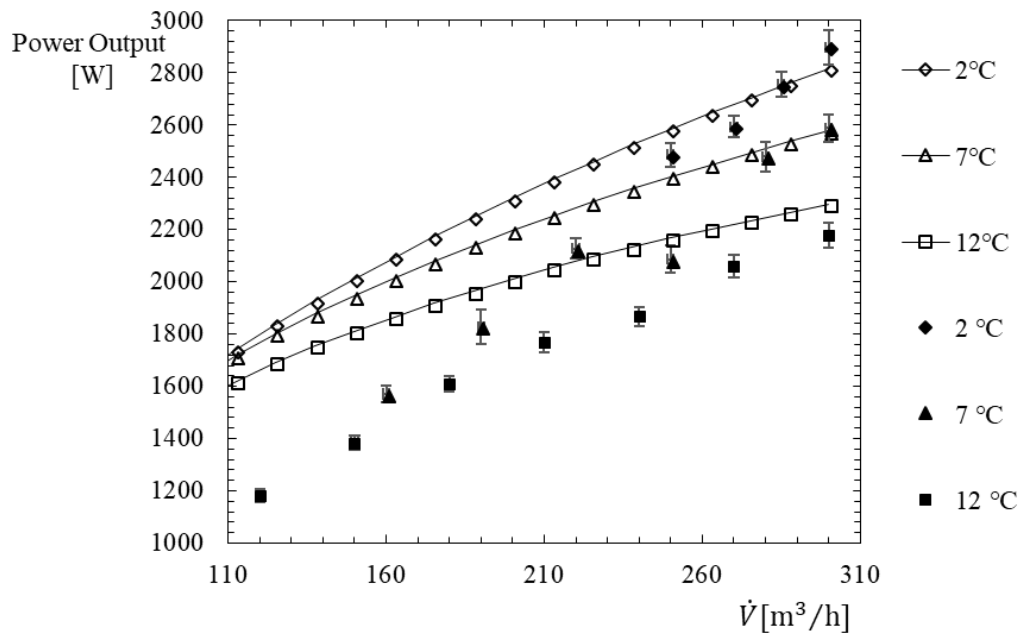


Figure 5.18 – Power output of the overall solution from experimental analysis (separated points) and modelling (connected by a line).

Through the analysis of the data presented in Figure 5.18, it can be concluded that the experimental values are lower than the modelling values, but such difference decreases with the increase of air volume flow rate. For lower values of volume flow rate, the difference between the values has a maximum of approximately 25%.

Figure 5.19 shows the value of the coefficient of performance for the same input variables as well as the error bars referring to the global uncertainty.

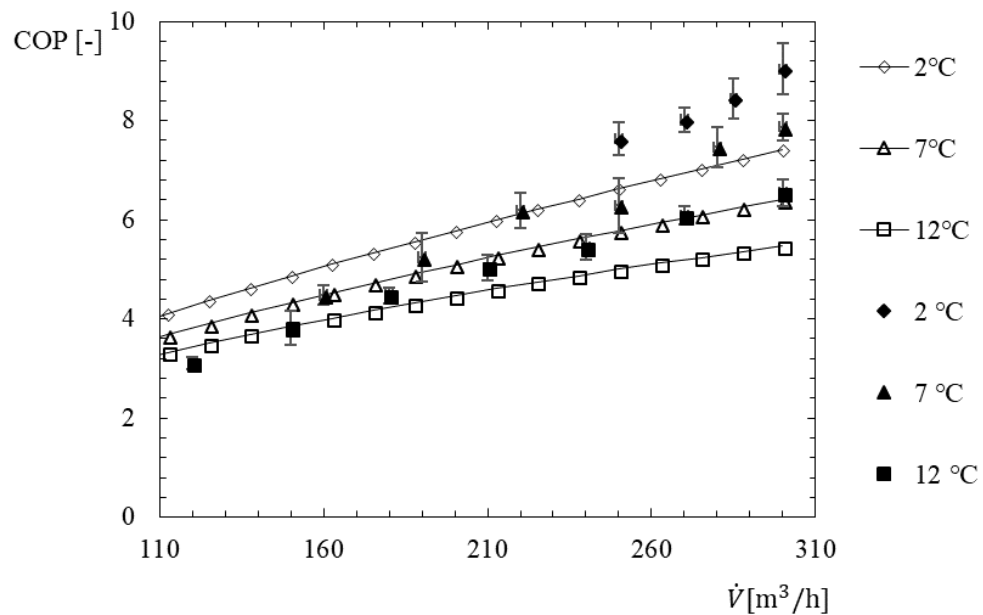


Figure 5.19 – COP of the overall solution from experimental analysis (separated points) and modelling (connected by a line).

5. Experimental Analysis

The experimental values of the coefficient of performance presented in Figure 5.19 are higher than those predicted by the modelling and this is explained because of the lower work input verified in the experimental case. As it was mentioned in Section 3, the value of the coefficient of performance does not take into account the power consumption of the fans and that fact leads to a decrease of this output variable.

In Figure 5.20 the discharge air temperature is plotted as a function of the air volume flow rate for the different outdoor air temperatures.

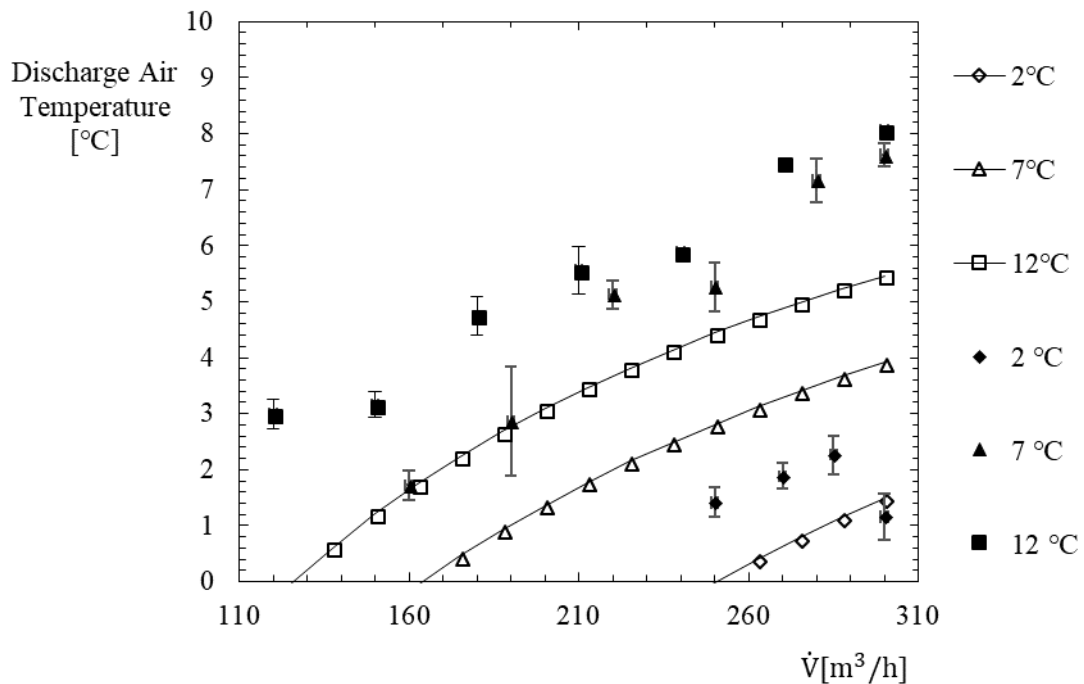


Figure 5.20 – Discharge air temperature from experimental analysis (separated points) and modelling (connected by a line)..

The experimental values of discharge air temperature are higher than the ones obtained by the modelling and it may be explained by the lower sensible effectiveness of the evaporator as well as the fluctuations on the test conditions. The values of power output, COP and discharge air temperature are a function of indoor and outdoor air temperatures and these input variables are not fixed during the experiments, causing test conditions slightly different from the modelling conditions, leading to different results.

6 Conclusions and Future Work

6.1 Conclusions

The subject of discussion of this dissertation was the development of a solution that integrates a heat recovery system within an air-to-air heat pump circuit. The requirements of low energy consumption and indoor air quality were considered the main objectives of the project, and it was ensured by extracting most of the energy potential of exhaust airstream to transfer it to the clean and fresh intake airstream. The influence of having moisture content between acceptable levels was also discussed in order to prevent human health and material wear problems.

Different solutions of heat recovering were discussed and the main difference of these is the ability of transferring moisture between the airstreams. While a typical heat recovery system only turns possible the transfer of sensible heat, an energy recovery system allows the transfer of latent heat, due to its permeable separation layer. This membrane based enthalpy exchangers are the most used variant of this technology in the residential sector, due to its antimicrobial capacity as well as the possibility to wash with water, which decrease the maintenance costs. The moisture recovery is also important to avoid the energy waste as condensate form, which occur in the heat recovery systems. However, the low number of suppliers turns its price higher and then the purchasing process becomes prolonged.

The compact circuit was defined by its functional diagram, in which the main components and its position are selected. The technical requirements of air volume flow rate respects the norms related to hygiene, health and environment and the system was dimensioned for the residential using. The different components are analysed in terms of heat and mass transfer concepts, whereas the refrigerant circuit is modelled by combining the previous analysis with thermodynamics in order to establish the energy balance. To perform this analysis, an iterative process is realized, which defines the evaporating and condensing temperatures as well as the airstream temperatures after passing through the phase change heat exchangers. In parallel, a user interface was designed in order to turn possible the variation of the different dimensioning variables and check its influence on the output variables.

All the dimensioning data was defined, the refrigeration circuit iterative process was performed and the overall solutions with different types of heat recovering were compared. The overall effectiveness of the ERV is higher than with HRV, due to its capacity of recovering latent heat, although the lower sensible effectiveness. Due to its lower sensible effectiveness, the frost formation inside the heat exchanger is avoided with ERV. The power output and coefficient of

performance are higher with ERV because of the higher heat recovered by this solution, whereas the higher sensible effectiveness of the HRV increases the sensible heat of this solution when compared with ERV. The discharge air temperature, which is the variable that quantifies the frost formation tendency in the evaporator, is lower with ERV because of the lower energy potential of the exhaust airstream at the entrance of the evaporator, causing a higher temperature drop to achieve the same cooling effect. However, the analysis of variation of the compressor input frequency was important to quantify the influence of the variation of the refrigerant flow rate, which might reduce the energy removed in the evaporator during undesired outdoor air temperatures and the discharge air temperature increases avoiding frost formation.

Regarding the experimental analysis, in the Piping/Ducting and Instrumentation Diagram the main components were defined as well as the positioning of the sensors and the outdoor and indoor air temperatures were emulated by two different climate chambers. The temperature sensors were defined as well as the volume flow rate measurement tube, calibrated at 20 °C, but the measurement of this variable for both airstreams is evaluated for values of temperature different than this value. By doing this approximation, an error was assumed but it was not quantified, because of the lack of material and experimental time. The functional sample was assembled by using the components of two different refrigerant boxes of exhaust-air heat pumps and the air leakage to or from each box was not quantified. Considering that the sample is not as compact as it should be, due to the high number of connections between the components and that the quantification of the air leakage overall solution is not easy, this might cause an error on the results. The refrigerant charge was quantified in terms of the relevant paths of this fluid density, but the circuit was filled with a lower quantity in order to maintain a security level to avoid liquid at the entrance of the compressor and bubbles formation in the expansion valve. The test points were defined by checking the volume flow rates in which frost formation occurred and then the values of this variable were defined. The insulation of the high pressure path of the refrigerant circuit resulted in lower temperature drops in the gas and liquid lines. It was maintained like that for the tests, as well as the refrigerant charge that was checked by the measurements of the subcooled and superheated degrees.

Considering the test results, the values of sensible effectiveness of the evaporator and the HRV do not represent a considerable difference when compared with those obtained by the modelling. The values of the outlet airstream of the condenser were higher than the condensing temperature, which may be explained by the relevant temperatures of the hot gas refrigerant point and the values of the modelling were not comparable. The power output of the experimental procedure is lower than the values obtained by the modelling, especially for low

air volume flow rates, which can be caused by any error on the flow rate measurement and the existence of air leakage. The values of the coefficient of performance are higher within the experimental analysis due to the lower work input, and this may be caused by the probable higher isentropic efficiency of the compressor. The values of discharge air temperature obtained by the measurements are lower than those predicted by the modelling and this is caused by the lower sensible effectiveness of the evaporator as well as the fluctuations of climate chamber temperatures and air leakage problems.

6.2 Future Work

The development of a real solution is a process that requires continuous improvements and a dynamic behaviour to respect the different requirements and expectations. Thus, some considerations about the future works are taken into account.

Firstly, it is recommended to assemble a compact solution that concentrates all the components (ERV, instead of HRV, and refrigerant circuit) in a box and this would reduce the air leakage between the components and then reduce the errors in the measurements. During the analysis of this solution, the quantification of the pressure drop through the components would be helpful to verify the power consumptions of the fans.

The analysis of the heat transfer process in the condenser has also to be improved in order to quantify the transfer of energy of the refrigerant during the hot gas state and then evaluate its sensible effectiveness. The evaluation of all points at high pressure during operation would also be relevant to evaluate the compressor behaviour during the test points.

The analysis of the simultaneous heating capacity of the airstream and of the domestic hot water system feed up flow, by changing the refrigerant circuit. This change of the refrigerant and the hydraulic circuits may be performed by the replacement of the refrigerant-to-air condenser by a refrigerant-to-water variant to heating up the water flow and the airstream heating process is performed by using a water-to-air heat exchanger. This solution would be interesting especially during the periods in which the outdoor air temperatures are not extreme, i.e., there is not a very high heating demand, and the energy potential of the air at the entrance of the evaporator would be higher.

Regarding the measurement procedure, the calibration of the volume flow rate as a function of the airstream temperature, the using of humidity sensors to quantify the air enthalpy and the measurement of the atmospheric pressure, are three suggestions that would reduce the errors caused by the experimental procedure and improve the quality of the results. The using of high-resolution volume flow rate sensors would be helpful to quantify the air leakage and then define improvements in the design. A better control of the indoor air inside the climate chamber, by applying a discretization of the heating and cooling sources and then guarantee the desired values of temperature and relative humidity at a constant level, would be an important step to improve the internal conditions of the air inside it.

A strategy to control the exchanged air volume flow rate as a function of the levels of CO₂ of the exhaust airstream would be recommended. This control strategy would also define an

optimum operation point by combining the changing of compressor input frequency and external electrical heater in order to avoid frost formation and minimize the energy consumptions during these operation points.

7 References

- [1] "Bosch Website," [Online].
- [2] Bosch, "Bosch Today 2017," 2017.
- [3] IEA, Energy Technology Perspectives 2017.
- [4] Eurostat. [Online].
- [5] BPIE, Indoor air quality, thermal confort and daylight., 2015.
- [6] ASHRAE, ASHRAE HVAC Systems and Equipment Handbook, 2016.
- [7] Steinemann, Anne; Wargocki, Pawel; Rismanchi, Behzad, "Ten questions concerning green buildings and indoor air quality," *Building and Environment*, pp. 351-358, 2017.
- [8] REHVA, Indoor and Outdoor Environmental Quality.
- [9] Wang, Shan K., Handbook of Air Conditioning and Refrigeration, New York: McGraw-Hill, 2000.
- [10] ASHRAE, Handbook—HVAC Systems and Equipment, 2012 .
- [11] Stoecker, W. F.; Jones, J. W., Refrigeration and Air Conditioning, New York: MacGraw-Hill, 1982.
- [12] Gosney, W., Principles of Refrigeration, London: Cambridge University Press, 1982.
- [13] Incropera, Frank P.; Dewitt, David P.; Bergman, Theodore L.; Lavine, Adrienne S., Fundamentals of Heat and Mass Transfer, 7th edition, Chicago: John Wiley & Sons, 2011.
- [14] Nasr, Mohammad Rafati; Fauchoux, Melanie; Besant, Robert W.; Simonson, Carey, "A review of frosting in air-to-air energy exchangers," *Renewable and Sustainable Energy Reviews*, pp. 538-554, 2014.
- [15] Afonso, Clito F., Refrigeração, Oporto: AEFEUP, 2013.
- [16] Nyers, Jozsef; Stuparic, Daniel; Nyers, Arpad, "COP of refrigerants in heat pumps," 2015.

- [17] Jactard, Aurélie; Li, Zelin, "Investigation of field methods for evaluation of air-to-air heat pump performance," Gotenburg, 2011.
- [18] "Refrigerants," Industrial Heat Pumps, How it works. [Online]. [Accessed March 2018].
- [19] "Engineering Equation Solver".
- [20] Nilan Catalogue. [Online]. [Accessed March 2018].
- [21] Alonso; Liu, Peng; Mathisen; Ge, Gaoming; Simonson, Carey, "Review of heat/energy recovery exchangers for use in ZEBs in cold climate countries," *Builing and Envirnment*, pp. 228-237, 2015.
- [22] Mardiana-Idayu, A.; Riffat, S.B., "Review on heat recovery technologies for building applications," *Renewable and Sustainable Energy Reviews*, pp. 1241-1255, 2012.
- [23] Zehnder, "UK-Taiwan Lo Carbon Sustainable Cities Forum," 2012.
- [24] O'Connor, D.; Calautit, J.K.; Hughes, B.R., "A Review of Heat Recovery Technology for Passive Ventilation Applications," *Renewable and Sustainable Energy Reviews*, pp. 1481-1493, 2016.
- [25] Liu, Peng; Mathisen, Hans Martin; Alonso, Maria Justo; Simonson, Carey, "A frosting limit model of air-to-air quasi-counter-flow membrane energy exchanger for use in cold climates," *Applied Thermal Engineering*, pp. 776-789, 2017.
- [26] Zhang, Li-Zhi, Total Heat Recovery: Heat and Moisture Recovery from Ventilation Air, Nova Science Publishers, 2008.
- [27] Aarnes, Sofie Maria; Mathisen, Hans Martin; Alonso, Maria Justo, Membrane Based Heat Exchanger, 2012.
- [28] Perrotin, Thomas; Clodic, Denis, Fin efficiency calculation in enhanced fin-and-tube heat exchangers in dry conditions, 2003.
- [29] Naphon, Paisarn; Wongwises, Somchai, Heat transfer coefficients under dry- and wet-surface conditions for a spirally coiled finned tube heat exchanger, 2004.

- [30] Hausen, H., Heat Transfer in Conter Flow, Parallel Flow and Cross Flow, New York: McGraw-Hill, 1983.
- [31] Khan, W.A.; Culham, J.R.; Yovanovich, M.M., "Convection heat transfer from tube banks in crossflow: Analytical approach," *International Journal of Heat and Mass Transfer*, pp. 4831-4838, 2006.
- [32] Shah, M. M., "An improved general correlation for condensation for heat transfer during film condensation in plain tubes," *HVAC & R Research*, pp. 889-913, 2009.
- [33] Lee, Hyungsoon; Mudawar, Issam; Hasan, Mohammad M., "Flow condensation in horizontal tubes," *International Journal of Heat and Mass Transfer*, pp. 31-45, 2013.
- [34] Omega Temperature handbook, Technical Reference Section.
- [35] Benedict, Fundamentals of Temperature, Pressure and Flow Measurements, John Wiley & Sons, 1972.
- [36] "NTC Thermistor Beta," Ametherm. [Online]. [Accessed May 2018].
- [37] Thermistor Type Catalogue, Shibaura Electronics.
- [38] "Refrigerant Charge Reduction in Refrigerating Systems," Internation Institute of Refrigeration, Paris, 2014.
- [39] Yoo, Jin Woo; Kim, Dong Ho; Kim, Mo Se; Kim, Min Soo, "Control Method of Circulating Refrigerant Amount For Heat Pump System," in *Intrantional Refrigeration and Air Conditioning Conference*, 2014.
- [40] Jin, Shengham, "Refrigerant and Lubricant Charge in AC Heat Exchangers: Experimentally Validated Model," in *International Refrigeration and Air Condition Conference*, 2014.
- [41] DIN, "DIN EN 14511," 2013.
- [42] Kanury, A. Murty, Introduction to Combustion Phenomena, London: Gordon and Breach, 1975.

7. References

- [43] Tsilingiris, P. T., "Thermophysical and transport properties of humid air at temperature range between 0 and 100C," *Energy Conversion and Management*, pp. 1098-1110, 2008.
- [44] Çengel, Y.; Boles M. A., *Thermodynamics: an engineering approach*, New York: McGraw-Hill, 1998.
- [45] Howell, J.; Buckius, R., *Fundamentals of Engineering Thermodynamics*, New York: McGraw-Hill, 1987.
- [46] Coleman, Hugh W.; Steele, W. Glenn, *Experimentation and Uncertainty Analysis for Engineers*, New Jersey: John Wiley & Sons, Inc., 1998.
- [47] Wang, Qing; Zissler, Nick; Holden, Roger, "Evaluate error sources and uncertainty in large scale measurement systems," *Robotics and Computer - Integrated Manufacturing*, vol. 29, no. 1, pp. 1-11, 2013.

Appendix A

Properties of the fluids

Regarding the properties of the fluids, these values have to be calculated for each point that is inside the range of temperatures mentioned on Section 0. Therefore, the database of the Engineering Equation Solver, EES, and this software is used and the values are adjusted within a 6th order polynomial as a function of the desired variable. In the next equation, the basic adjustment equation for a random dependent variable, r , is defined as a function of the independent variable, x , and the seven coefficients, which will be determined for each case.

$$r = a_0 + a_1 \cdot x + a_2 \cdot x^2 + a_3 \cdot x^3 + a_4 \cdot x^4 + a_5 \cdot x^5 + a_6 \cdot x^6 \quad (\text{A. 1})$$

Firstly, the thermophysical and transport properties of the air are defined, in which it is assumed the following air temperature range: $-20 \text{ }^\circ\text{C} < T_{air} < 65 \text{ }^\circ\text{C}$. It is important to mention that these properties are defined as a function of the airstream temperatures in Celsius degrees.

Table A.1 –Parameters of air thermophysical and transport properties

	μ [Pa · s]	k [W/(m · k)]	c_p [J/(kg · K)]
a_0	1.72E-05	2.44E-02	1.01E+03
a_1	4.99E-08	7.66E-05	-5.92E-03
a_2	-1.49E-11	-3.27E-08	1.14E-03
a_3	1.81E-13	-9.06E-11	2.68E-05
a_4	-4.64E-14	-2.31E-11	-1.82E-06
a_5	1.15E-15	7.07E-13	3.42E-08
a_6	-8.41E-18	-5.64E-15	-2.22E-10

After the definition of the previous properties, there are other parameters which may be calculated: thermal diffusivity α , kinematic viscosity ν , and Prandtl number Pr . The air density, ρ , is defined when the humid air is analysed.

$$\alpha = \frac{k}{\rho \cdot c_p} \quad (\text{A. 2})$$

$$\nu = \frac{\mu}{\rho} \quad (\text{A. 3})$$

$$Pr = \frac{v \cdot c_p}{k} \quad (A.4)$$

Regarding the diffusivity of water in air, this value was obtained by consulting literature [42], from which the following correlation was used

$$D_{w-a} = D_0 \left(\frac{T}{T_0}\right)^m \left(\frac{P}{P_0}\right), \text{ where } \begin{cases} T_0 = 298 \text{ K} \\ P_0 = 1 \text{ atm} \\ m \approx 2, \text{ condensable gas} \\ D_0 = 0.23 \frac{\text{cm}^2}{\text{s}} \end{cases} \quad (A.5)$$

Considering the properties defined for the mean temperature value for each airstream, the influence of the relative humidity for a fixed temperature on these values is neglected, because the variation of the thermophysical and transport properties of humid air is low at temperature values below 25 °C [43]. Therefore, the only variable in which the relative humidity was taken into account, due to its higher influence, is the air density.

The analysis of humid airstreams has to take into account the amount of water for determined conditions of temperature and relative humidity. When these variables are known, the moisture content w , the specific enthalpy h , and the density, ρ , are defined respectively as [12, 44, 45]

$$\frac{\phi}{w} = \frac{e^{\frac{5294}{T+273.15}}}{10^6} - 1.61 \cdot \phi \quad (A.6)$$

$$h = c_p \cdot T + w \cdot (2501 + 1.86 \cdot T) \text{ [kJ/kg]} \quad (A.7)$$

$$\rho = \frac{p}{R_{da} \cdot T \cdot (1 + 1.6078 \cdot w)} \text{ [kg/m}^3\text{]} \quad (A.8)$$

where

T is the air temperature,

c_p is the air specific heat at constant pressure,

p is the atmospheric pressure, and

R_{da} is the perfect gas constant for dry air.

It is important to refer that the second term of the right side of the enthalpy equation may be neglected with an error lower than 5%.

Finally, the thermophysical properties of the refrigerant fluid are defined as a function of the evaporating and condensing temperature. In Table A.2, the desired parameters for the R134a refrigerant cycle are defined as a function of the evaporation temperature, which are defined within the following range of the independent variable: $-20 \text{ °C} \leq T_{evap} \leq 25 \text{ °C}$.

Table A.2 – Parameters of evaporating temperature properties

	$v_{evap,5K}$ [m ³ /kg]	$h_{fg,evap}$ [kJ/kg]	$h_{f,evap}$ [kJ/kg]	$h_{1,5K}$ [kJ/kg]	k [–]
a_0	7.10E-02	1.99E+02	5.19E+01	6.28E-02	2.55E+02
a_1	-2.47E-03	-7.60E-01	1.34E+00	-1.06E-03	6.05E-01
a_2	5.20E-05	-2.25E-03	1.37E-03	1.38E-05	-9.52E-04
a_3	-8.64E-07	-9.48E-06	4.08E-06	-1.32E-07	-4.78E-06
a_4	1.25E-08	-1.79E-06	5.19E-08	3.44E-10	-1.89E-07
a_5	-1.68E-10	-2.03E-08	3.77E-09	-6.01E-12	-6.90E-09
a_6	1.55E-12	2.70E-09	-7.85E-11	1.04E-13	2.69E-10

Regarding the properties dependent of the condensing temperature, Table A.3 shows the desired parameters to obtain the properties of the refrigerant for this phase change phenomena. These properties are defined for the following range of the condensing temperature: $-20\text{ °C} \leq T_{cond} \leq 65\text{ °C}$.

Table A.3 – Parameters of condensing temperature properties

	$h_{fg,cond}$ [kJ/kg]	$h_{f,cond}$ [kJ/kg]
a_0	2.01E+02	5.14E+01
a_1	-1.09E+00	1.40E+00
a_2	1.69E-02	-2.19E-04
a_3	-6.31E-04	-1.49E-05
a_4	1.10E-05	1.92E-06
a_5	-1.06E-07	-3.34E-08
a_6	4.08E-10	1.98E-10

Appendix B

Uncertainty analysis

Regarding the uncertainty analysis, Coleman and Steele recommend to start this procedure by identifying the main error sources, which are divided in systematic and random errors [46, 47]. In a measurement series, the systematic error is not observable and it is the lower error obtained after calibration, whereas the random error is more difficult to evaluate because there is no consistency and this type of error is linked to a procedure or human error. However, if enough measurements are taken, the results should form a normal distribution curve and this uncertainty is quantified.

An estimation of the fixed or random error, B_{X_i} and P_{X_i} respectively, for each measured variable X_i , is needed to apply the general expression of uncertainty analysis or fundamental equation of error propagation as [46]

$$\delta_r = \sqrt{\left(\frac{\partial r}{\partial X_1} \cdot \delta_{X_1}\right)^2 + \left(\frac{\partial r}{\partial X_2} \cdot \delta_{X_2}\right)^2 + \dots + \left(\frac{\partial r}{\partial X_N} \cdot \delta_{X_N}\right)^2} \quad (\text{B. 1})$$

where

$r = r(X_1, X_2, \dots, X_N)$ is the measured value,

δ_r is the uncertainty of the result,

δ_{X_i} is the uncertainty of the variable X_i .

It is important to mention that δ_r and δ_{X_i} should be analysed as B_r and B_{X_i} , or as P_r and P_{X_i} according to the case in analysis. After defining the different uncertainties, the global uncertainty in the result is expressed as a combined of both variants as [46]

$$U_r = \sqrt{B_r^2 + P_r^2} \quad (\text{B. 2})$$

Therefore, the measured variable r is defined as [46]

$$r = \bar{r} \pm U_r \quad (\text{B. 3})$$

The systematic uncertainty is calculated by the fundamental equation of error propagation previously presented, and the main variables which influence the final result have to be defined. On the other hand, random uncertainty is defined as a function of the standard deviation of the sample S_{X_i} , as well as the student's t distribution parameter for a 95% confidence interval as [46]

$$P_{X_i} = \pm t \cdot S_{X_i} = \pm t \frac{1}{N-1} \left\{ \sum_{k=1}^N [(X_i)_k - \bar{X}_i]^2 \right\}^{\frac{1}{2}} \quad (\text{B. 4})$$

where

N is the number of readings,

$(X_i)_k$ is one reading value of the variable X_i and

\bar{X}_i is the mean value of the sample.

After the introduction of the theory of the errors, in the next subsections the uncertainty linked to the measurements is analysed for temperature and air flow rate values and the influence in power output of this errors is defined at the end.

Uncertainty in the measurements of temperature

Regarding the analysis of uncertainties of temperature, the influence variables are firstly defined. As mentioned in Section 5.3.1, the temperature sensors are of the NTC resistor type, which implies that an electrical circuit is assembled, being followed by an analog-to-digital signal converter in order to discretize the values. The electrical circuit is represented in Figure B.1 and it is possible to verify that a fixed voltage difference of 5 V is ensured and the resolution of the A-D conversion is equal to 10 bit.

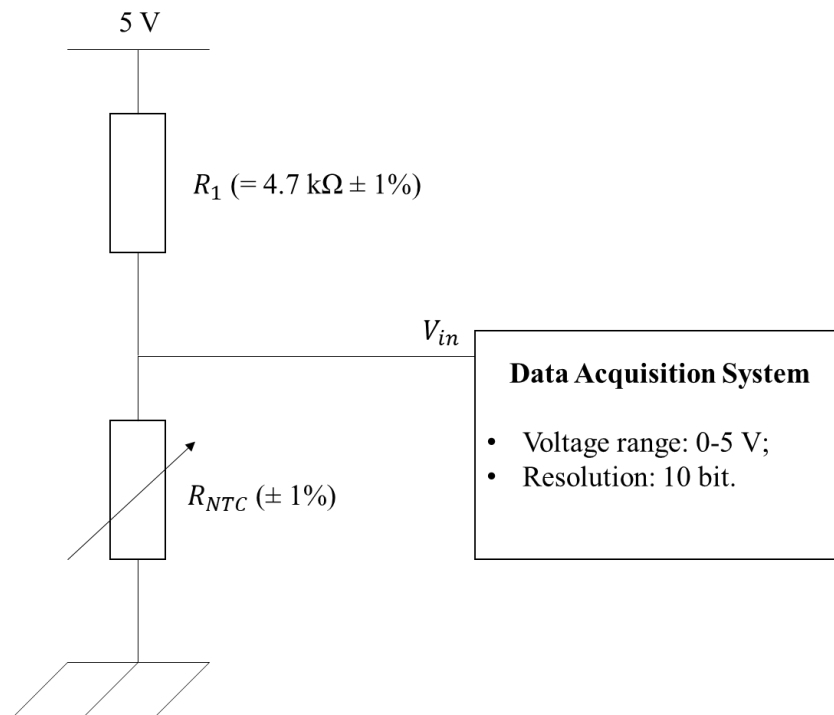


Figure B.1 – Electrical circuit of the NTC sensor.

Basically, the influence variables are summarized as:

- A/D conversion.
- Electrical resistance of the sensor;
- Electrical resistance of the resistance of the electrical circuit.

Considering a very high resistance of the Data Acquisition System, the electrical current passing through it is negligible and the input voltage V_{in} is defined as

$$V_{in} = 5 \cdot \frac{R_{NTC}}{R_{NTC} + R_1} \quad (B.5)$$

where R_{NTC} is the electrical resistance of the temperature sensor and it is measured in $k\Omega$. The fixed error of temperature B_T is simplified as

$$\begin{aligned} B_T &= \pm \sqrt{\left(\frac{\partial T}{\partial V_{in}} \cdot B_{V_{in}}\right)^2 + \left(\frac{\partial T}{\partial R_{NTC}} \cdot B_{R_{NTC}}\right)^2 + \left(\frac{\partial T}{\partial R_1} \cdot B_{R_1}\right)^2} = \\ &= \pm \sqrt{\left(\frac{\partial T}{\partial R_{NTC}} \cdot \frac{\partial R_{NTC}}{\partial V_{in}} \cdot B_{V_{in}}\right)^2 + \left(\frac{\partial T}{\partial R_{NTC}} \cdot B_{R_{NTC}}\right)^2 + \left(\frac{\partial T}{\partial V_{in}} \cdot \frac{\partial V_{in}}{\partial R_1} \cdot B_{R_1}\right)^2} \end{aligned} \quad (B.6)$$

The systematic uncertainty of the NTC sensor $B_{R_{NTC}}$ varies with its value, due to the non-linearity of the sensor whereas the values related to B_{R_1} and $B_{V_{in}}$ are fixed. The systematic uncertainty of the A/D converter is calculated as

$$B_{V_{in}} = \pm \frac{\text{Resolution}}{2} = \pm \frac{\text{Voltage range}}{2^{\text{number of bits}}} = \pm \frac{5}{2^{10}} = \pm \frac{5}{2^{11}}$$

The values of $B_{V_{in}}$, $B_{R_{NTC}}$ and B_{R_1} are presented in Table B.1.

Table B.1 – Systematic uncertainties of influence variables of temperature

$ B_{V_{in}} $ [V]	2.44 E-3
$ B_{R_{NTC}} $ [$k\Omega$]	$0.01 \cdot R_{NTC}$
$ B_{R_1} $ [$k\Omega$]	4.70 E-2

The sensibility coefficients which quantify the influence of each variable in temperature are simplified as

$$\frac{\partial T}{\partial V_{in}} = \frac{\partial T}{\partial R_{NTC}} \frac{\partial R_{NTC}}{\partial V_{in}} = \frac{\frac{-1}{\beta \cdot R_0}}{\left[\frac{\ln\left(\frac{R_{NTC}}{R_0}\right)}{\beta} + \frac{1}{T_0 + 273.15} \right]^2} \frac{4.7 \cdot 5}{(5 - V_{in})^2} \quad (\text{B. 7})$$

$$\frac{\partial V_{in}}{\partial R_1} = \frac{-5 \cdot R_{NTC}}{(R_{NTC} + R_1)^2} \quad (\text{B. 8})$$

Figure B.2 shows the evolution of the fixed error of temperature values B_T , as a function of the measured temperature for each sensor. It is possible to verify that the error decreases while the measured temperature is increasing.

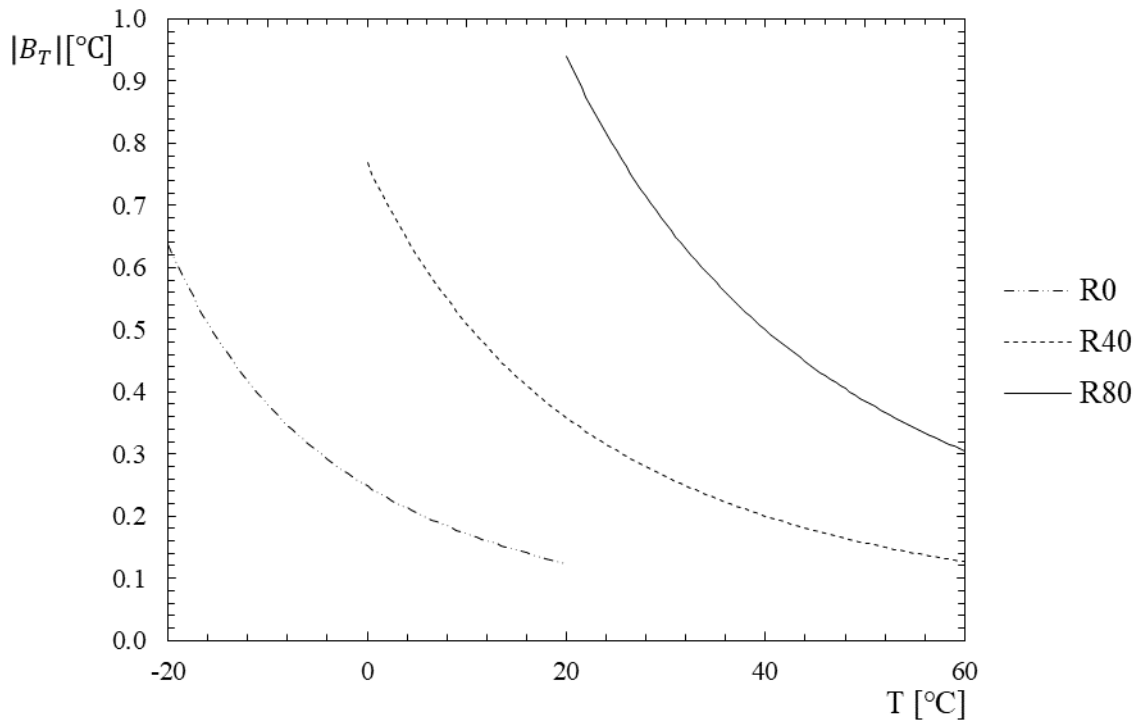


Figure B.2 – Systematic uncertainty of temperature as a function of measured temperature.

Uncertainty in the measurements of volume flow rate

The analysis of the uncertainty on the values of volume flow rate is similar with the approach presented for temperature. Thus, the influence variables are presented:

- Flow meter;
- Variation of temperature;
- Variation of operating point;
- Difference of pressure measurement device.

Considering the lack of available information about the flow meter, the uncertainty of this device is neglected, but it is assumed that this error may represent a considerable difference. The additional pressure drop is also neglected when compared with the overall pressure drop, which could cause a variation of the operating point and, consequently, the volume flow rate would change, as well as the influence of the difference of temperature between the airflow after the condenser and its reference (20 °C). Therefore, the fixed error on the measurement of volume flow rate is only analysed in the device used to measure the difference of pressure by checking its resolution. The systematic uncertainty is then defined as

$$B_{\dot{V}} = \pm \left| \frac{\partial \dot{V}}{\partial \Delta P} \cdot B_{\Delta P} \right| \quad (\text{B. 9})$$

Considering a resolution of 0.1 Pa and a digital device, its systematic uncertainty is equal to the resolution and the variation of the fixed error of the volume flow rate is plotted as a function of the difference of pressure in Figure B.3. The term $\frac{\partial \dot{V}}{\partial \Delta P}$ is obtained by derivation of the equation defined in Figure 5.4.

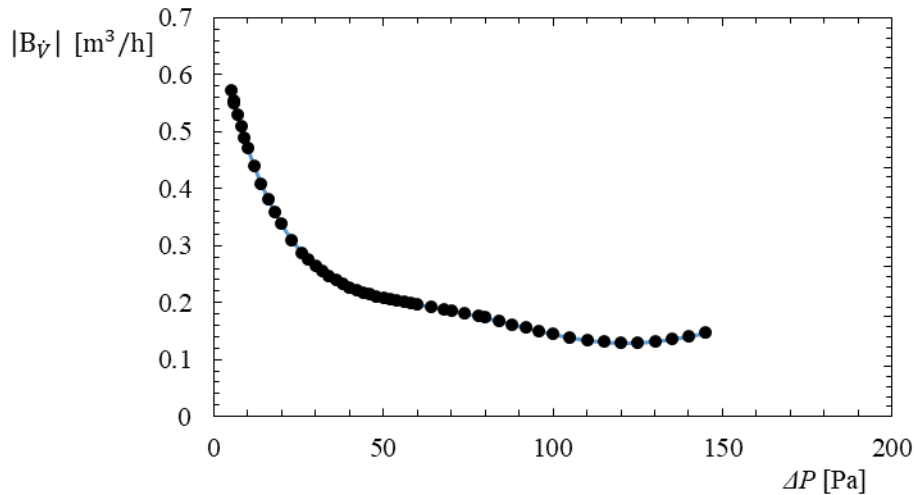


Figure B.3 – Systematic uncertainty of volume flow rate as a function of the difference of pressure.

Output Variables

After defining the uncertainties linked to the input variables, the quantification of its influence on output variables becomes an important step to evaluate the test results. Thus, the sensible effectiveness of the HRV and of the evaporator are analysed as well as the power output and the overall coefficient of performance.

Sensible Effectiveness of the HRV System

The sensible effectiveness of the HRV system is defined in Section 3.3.1 by equation 2.8. In order to simplify the uncertainty analysis of this variable, the expression is simplified as

$$\varepsilon_{HRV} = \frac{\dot{m}_E \cdot c_{p,E} \cdot (T_{E1} - T_{E2})}{\dot{m}_F \cdot c_{p,F} \cdot (T_{E1} - T_{F1})} = \frac{\dot{V}_E \cdot \rho_E \cdot c_{p,E} \cdot (T_{E1} - T_{E2})}{\dot{V}_F \cdot \rho_F \cdot c_{p,F} \cdot (T_{E1} - T_{F1})} \quad (B.10)$$

The error caused in the calculations of density and specific heat at constant pressure are neglected. The influence variables that are taken into account within this analysis are:

- Air volume flow rate;
- Exhaust and fresh air temperatures.

Therefore, the global uncertainty of the sensible effectiveness of the HRV system is written as

$$U_{\varepsilon_{HRV}} = \pm \sqrt{(U_{\dot{V}_E, \varepsilon_{HRV}})^2 + (U_{\dot{V}_F, \varepsilon_{HRV}})^2 + (U_{T_{E1}, \varepsilon_{HRV}})^2 + (U_{T_{E2}, \varepsilon_{HRV}})^2 + (U_{T_{F1}, \varepsilon_{HRV}})^2} \quad (B.11)$$

where $U_{i, \varepsilon_{HRV}}$ is the influence of variable i on global uncertainty of the output variable ε_{HRV} .

The terms of equation B.11 are now defined as a function of the equation B.10

$$U_{\dot{V}_E, \varepsilon_{HRV}} = \frac{\partial \varepsilon_{HRV}}{\partial \dot{V}_E} U_{\dot{V}_E} = \frac{\rho_E \cdot c_{p,E} \cdot (T_{E1} - T_{E2})}{\dot{V}_F \cdot \rho_F \cdot c_{p,F} \cdot (T_{E1} - T_{F1})} \cdot U_{\dot{V}_E} \quad (B.12)$$

$$U_{\dot{V}_F, \varepsilon_{HRV}} = \frac{\partial \varepsilon_{HRV}}{\partial \dot{V}_F} B_{\dot{V}_F} = \frac{\dot{V}_E \cdot \rho_E \cdot c_{p,E} \cdot (T_{E1} - T_{E2})}{\rho_F \cdot c_{p,F} \cdot (T_{E1} - T_{F1})} \cdot \frac{-1}{(\dot{V}_F)^2} \cdot B_{\dot{V}_F} \quad (B.13)$$

$$U_{T_{E1}, \varepsilon_{HRV}} = \frac{\partial \varepsilon_{HRV}}{\partial T_{E1}} B_{T_{E1}} = \frac{\dot{V}_E \cdot \rho_E \cdot c_{p,E}}{\dot{V}_F \cdot \rho_{F3} \cdot c_{p,F}} \cdot \frac{(T_{E2} - T_{F1})}{(T_{E1} - T_{F1})^2} \cdot B_{T_{E1}} \quad (B.14)$$

$$U_{T_{E2}, \varepsilon_{HRV}} = \frac{\partial \varepsilon_{HRV}}{\partial T_{E2}} B_{T_{E2}} = -\frac{\dot{V}_E \cdot \rho_E \cdot c_{p,E}}{\dot{V}_F \cdot \rho_F \cdot c_{p,F} \cdot (T_{E1} - T_{F1})} \quad (B.15)$$

$$U_{T_{F1}, \varepsilon_{HRV}} = \frac{\partial \varepsilon_{HRV}}{\partial T_{F1}} B_{T_{F1}} = \frac{\dot{V}_E \cdot \rho_E \cdot c_{p,E} \cdot (T_{E1} - T_{E2})}{\dot{V}_F \cdot \rho_{F3} \cdot c_{p,F}} \cdot \frac{1}{(T_{E1} - T_{F1})^2} \cdot B_{T_{F1}} \quad (B.16)$$

Sensible Effectiveness of the Evaporator

Similarly, the uncertainty analysis of the evaporator is based on the approach defined in Section 3.3.2. In terms of uncertainty analysis, the equation to obtain the sensible effectiveness of the evaporator is simplified as

$$\varepsilon_{evap} \approx \frac{T_{E2} - T_{E3}}{T_{E2} - T_{evap}} \quad (B.17)$$

Thus, the global uncertainty of the sensible effectiveness of the evaporator is defined as

$$\begin{aligned}
 U_{\varepsilon_{evap}} &= \pm \sqrt{\left(\frac{\partial \varepsilon_{evap}}{\partial T_{E2}} \cdot U_{T_{E2}}\right)^2 + \left(\frac{\partial \varepsilon_{evap}}{\partial T_{E3}} \cdot U_{T_{E3}}\right)^2 + \left(\frac{\partial \varepsilon_{evap}}{\partial T_{evap}} \cdot U_{T_{evap}}\right)^2} = \\
 &= \pm \sqrt{\left(\frac{T_{E3} - T_{evap}}{(T_{E2} - T_{evap})^2} \cdot U_{T_{E2}}\right)^2 + \left(\frac{-1}{T_{E2} - T_{evap}} \cdot U_{T_{E3}}\right)^2 + \left(\frac{T_{E2} - T_{E3}}{(T_{E2} - T_{evap})^2} \cdot U_{T_{evap}}\right)^2} \quad (B.18)
 \end{aligned}$$

Power Output

Regarding the analysis of the power output, its value is defined as

$$\text{Power Output} = \dot{m}_F \cdot c_{p,F} \cdot (T_{F3} - T_{F1}) = \dot{V}_F \cdot \rho_F \cdot c_{p,F} \cdot (T_{F3} - T_{F1}) \quad (B.19)$$

Therefore, the global uncertainty of the power output may be expressed as a function of the global uncertainties of the temperature and volume flow rate as

$$\begin{aligned}
 U_{P_o} &= \pm \sqrt{\left(\frac{\partial P_o}{\partial \dot{V}_F} U_{\dot{V}_F}\right)^2 + \left(\frac{\partial P_o}{\partial T_{F3}} U_{T_{F3}}\right)^2 + \left(\frac{\partial P_o}{\partial T_{F1}} U_{T_{F1}}\right)^2} = \\
 &= \sqrt{(\rho_F \cdot c_{p,F} \cdot (T_{F3} - T_{F1}) U_{\dot{V}_F})^2 + (\dot{V}_F \cdot \rho_F \cdot c_{p,F} \cdot U_{T_{F3}})^2 + (-\dot{V}_F \cdot \rho_F \cdot c_{p,F} \cdot U_{T_{F1}})^2} \quad (B.20)
 \end{aligned}$$

Coefficient of Performance

Considering the analysis of the coefficient of performance, its value is written as a function of the power input and output values as

$$COP = \frac{\text{Power Output}}{\text{Power Input}} = \frac{P_o}{P_l} \quad (B.21)$$

Similarly, the global uncertainty is written as function of the same variables

$$\begin{aligned}
 U_{COP} &= \pm \sqrt{\left(\frac{\partial COP}{\partial P_o} \cdot U_{P_o}\right)^2 + \left(\frac{\partial COP}{\partial P_l} \cdot U_{P_l}\right)^2} = \\
 &= \pm \sqrt{\left(\frac{\partial COP}{\partial P_o} \cdot U_{P_o}\right)^2 + \left(\frac{\partial COP}{\partial P_l} \cdot U_{P_l}\right)^2} = \sqrt{\left(\frac{1}{P_l} \cdot U_{P_o}\right)^2 + \left(\frac{-P_o}{P_l^2} \cdot U_{P_l}\right)^2} \quad (B.22)
 \end{aligned}$$

Appendix C

Test results

In this appendix, all test results are presented for the different test points discussed in Section 5.6. In Table C.1, Table C.2 and Table C.3 the test results are presented for outdoor air temperatures approximately equal to 2 °C, 7 °C and 12 °C, respectively. The values of relative humidity of both airstreams are not measured and it is assumed that these variables are equal to 50 % and 85 % for high and low temperature airstream sources, respectively.

Table C.1 – Test results for outdoor air temperature equal to 2 °C

\dot{V} [m ³ /h]	\dot{V}_{E3} [m ³ /h]	\dot{V}_{F3} [m ³ /h]	T_{E1} [°C]	T_{E2} [°C]	T_{E3} [°C]	T_{F1} [°C]	T_{F2} [°C]	T_{F3} [°C]	T_E [°C]	T_C [°C]	Work [W]
250	248.3	250.3	20.4	8.4	3.6	1.4	16.9	32.7	1.0	31.4	327.8
270	265.8	269.6	21.4	8.6	4.1	1.9	17.6	32.1	1.1	30.9	325.4
285	284.6	284.6	21.4	9.0	5.0	2.3	17.8	32.7	2.0	31.4	328.5
300	297.5	299.6	21.1	8.2	4.8	1.2	17.2	31.5	1.6	30.2	322.5

Table C.2 – Test results for outdoor air temperature equal to 7 °C

\dot{V} [m ³ /h]	\dot{V}_{E3} [m ³ /h]	\dot{V}_{F3} [m ³ /h]	T_{E1} [°C]	T_{E2} [°C]	T_{E3} [°C]	T_{F1} [°C]	T_{F2} [°C]	T_{F3} [°C]	T_E [°C]	T_C [°C]	Work [W]
160	158.1	162.1	20.2	11.2	1.7	7.2	17.8	38.2	-0.2	36.7	353.3
190	190.5	190.8	20.2	11.1	2.9	7.2	17.8	37.9	0.5	36.4	352.2
220	217.4	219.0	21.6	11.5	5.1	6.6	18.8	37.6	2.5	35.0	346.9
250	247.7	248.9	20.8	11.5	5.3	7.4	18.1	33.8	2.1	32.6	334.9
280	275.6	280.2	21.2	11.8	7.2	6.4	18.6	34.4	3.8	32.4	335.0
300	298.2	300.8	21.7	11.9	7.6	6.5	18.9	33.7	3.7	31.8	331.5

Appendix C

Table C.3 – Test results for outdoor air temperature equal to 12 °C

\dot{V}	\dot{V}_{E3}	\dot{V}_{F3}	T_{E1}	T_{E2}	T_{E3}	T_{F1}	T_{F2}	T_{F3}	T_E	T_C	Work
[m ³ /h]	[m ³ /h]	[m ³ /h]	[°C]	[°C]	[°C]	[°C]	[°C]	[°C]	[°C]	[°C]	[W]
120	119.4	119.8	20.1	13.7	3.0	11.9	18.5	44.1	1.3	43.1	385.9
150	150.4	151.1	21.0	13.7	3.2	11.6	18.8	41.2	1.4	39.3	367.2
180	180.6	181.0	20.7	14.0	4.8	11.7	18.9	40.4	3.0	38.3	364.2
210	207.1	209.1	20.7	14.0	5.6	11.8	18.9	39.0	3.2	36.7	355.9
240	236.1	238.2	21.2	14.2	5.9	11.5	19.3	36.5	3.1	35.0	347.4
270	265.2	268.6	21.2	14.2	7.5	11.8	19.2	36.3	4.9	33.9	343.0
300	295.6	298.3	21.1	14.1	8.1	11.6	19.2	34.8	5.1	32.7	337.2

Similarly, the random uncertainty linked to each test point is presented in Table C.4, Table C.5 and Table C.6 for outdoor air temperatures equal to 2 °C, 7 °C and 12 °C, respectively.

Table C.4 – Random uncertainties of the measurements for outdoor air temperature equal to 2 °C

\dot{V}	$ P_{\dot{V}_{E3}} $	$ P_{\dot{V}_{F3}} $	$ P_{T_{E1}} $	$ P_{T_{E2}} $	$ P_{T_{E3}} $	$ P_{T_{F1}} $	$ P_{T_{F2}} $	$ P_{T_{F3}} $	$ P_{T_E} $	$ P_{T_C} $	$ P_{Work} $
[m ³ /h]	[m ³ /h]	[m ³ /h]	[°C]	[°C]	[°C]	[°C]	[°C]	[°C]	[°C]	[°C]	[W]
250	3.8	3.0	0.3	0.2	0.1	0.3	0.1	0.2	0.4	0.2	1.6
270	3.6	4.1	0.1	0.0	0.1	0.1	0.0	0.2	0.2	0.2	1.0
285	4.0	3.3	0.1	0.3	0.3	0.3	0.2	0.5	0.2	0.4	2.1
300	4.5	4.6	0.4	0.3	0.4	0.4	0.4	0.5	0.2	0.5	2.6

Appendix C

Table C.5 – Random uncertainties of the measurements for outdoor air temperature equal to 7 °C

\dot{V}	$ P_{\dot{V}_{E3}} $	$ P_{\dot{V}_{F3}} $	$ P_{T_{E1}} $	$ P_{T_{E2}} $	$ P_{T_{E3}} $	$ P_{T_{F1}} $	$ P_{T_{F2}} $	$ P_{T_{F3}} $	$ P_{T_E} $	$ P_{T_C} $	$ P_{Work} $
[m ³ /h]	[m ³ /h]	[m ³ /h]	[°C]	[°C]	[°C]	[°C]	[°C]	[°C]	[°C]	[°C]	[W]
160	2.7	3.4	0.1	0.1	0.1	0.0	0.1	0.1	0.4	0.2	1.3
190	4.4	3.1	0.2	0.0	0.9	0.1	0.1	0.9	0.7	0.8	3.6
220	4.2	3.3	0.2	0.2	0.2	0.1	0.1	0.4	0.1	0.3	2.4
250	4.8	3.6	0.3	0.3	0.4	0.2	0.2	0.7	0.3	0.7	3.8
280	4.1	4.7	0.3	0.3	0.3	0.3	0.3	0.5	0.2	0.4	2.2
300	6.2	5.7	0.3	0.1	0.1	0.3	0.1	0.2	0.1	0.2	1.0

Table C.6 – Random uncertainties of the measurements for outdoor air temperature equal to 12 °C

\dot{V}	$ P_{\dot{V}_{E3}} $	$ P_{\dot{V}_{F3}} $	$ P_{T_{E1}} $	$ P_{T_{E2}} $	$ P_{T_{E3}} $	$ P_{T_{F1}} $	$ P_{T_{F2}} $	$ P_{T_{F3}} $	$ P_{T_E} $	$ P_{T_C} $	$ P_{Work} $
[m ³ /h]	[m ³ /h]	[m ³ /h]	[°C]	[°C]	[°C]	[°C]	[°C]	[°C]	[°C]	[°C]	[W]
120	2.5	2.2	0.0	0.0	0.0	0.0	0.1	0.0	0.0	0.0	0.6
150	2.2	1.9	0.2	0.1	0.2	0.1	0.2	0.5	0.2	0.5	3.2
180	2.6	2.3	0.1	0.0	0.1	0.1	0.0	0.2	0.1	0.1	0.8
210	2.5	3.4	0.2	0.1	0.2	0.1	0.1	0.3	0.3	0.3	1.6
240	2.4	2.7	0.2	0.1	0.1	0.2	0.1	0.2	0.1	0.2	1.6
270	5.2	4.8	0.1	0.1	0.1	0.1	0.1	0.2	0.2	0.1	0.0
300	1.7	3.1	0.1	0.1	0.2	0.1	0.1	0.2	0.2	0.2	1.3